INVESTIGATING THE BEHAVIOUR OF AIR-SILICONE OIL FLOWS IN VERTICAL AND HORIZONTAL PIPES FOR EFFECTIVE GAS-LIQUID TRANSPORT

A Thesis Presented to the Department of Petroleum Engineering

African University of Science and Technology, Abuja

In partial fulfilment of the requirements for the award

MASTER OF SCIENCE

By

KWATIA CATHERINE AYIMAH

Supervised by

Dr. Mukhtar Abdulkadir

African University of Science and Technology
www.aust.edu.ng
P.M.B 681, Garki, Abuja F.C.T
Nigeria

June, 2016

CERTIFICATION

INVESTIGATING THE BEHAVIOUR OF AIR–SILICONE OIL FLOWS IN VERTICAL AND HORIZONTAL PIPES FOR EFFECTIVE GAS–LIQUID TRANSPORT

By

Kwatia Catherine Ayimah

A THESIS APPROVED BY THE PETROLEUM ENGINEERING DEPARTMENT

RECOMMENDED:

_____

Supervisor, Dr. Mukhtar Abdulkadir

_____

Head, Department of Petroleum Engineering

APPROVED:

_____

Chief Academic Officer

_____

Date

ABSTRACT

The concurrent flow of gas/liquid in pipes poses a great challenge due to the difficulty associated with the flow of fluid. The flow is characterized by the existence of flow regimes which can be identified by the geometrical arrangement of the phases in a pipe, with Churn flow being the least understood flow pattern in vertical pipes because of the controversies associated with its existence, therefore making it difficult to be predicted. This work aims at investigating the behavior of air–silicone oil flows in vertical and horizontal pipes for effective gas–liquid transportation. To help predict the various flows that exist in these pipes, a drift-flux model was developed for the efficient calculation of void fraction. This model is often used to characterize and predict flow regimes for lots of geometries. The model was developed to calculate void fraction for the accurate prediction of flow regimes that were observed in this work. The various flow patterns in existence were identified, and the model generated for each of them by employing Zuber and Findlay's correlation. Afterwards, the parameters obtained from the drift-flux model, C_o (distribution parameter) and V_d (drift velocity) were fitted as linear functions, and their values were obtained from the slope and the intercept respectively. The developed model had better results for the void fraction as compared to the existing correlations investigated.

Keywords: Void fraction, drift flux, churn flow, radial phase distribution, flow patterns, flow map.

ACKNOWLEDGEMENT

To God be all the glory and honor for bringing me this far. He showed mercy and gave me life to this point. I couldn't have gone through this Master's program without Him; He made all things possible and beautiful in His own time.

My sincere gratitude goes to my supervisor, Dr. Mukhtar Abdulkadir for his patience, advice, understanding and words of encouragement. I must say, his guidance was exceptional to the success of this work. I say thumbs up to him for being the BEST. I thank all my lecturers, especially, Dr. Alpheus Igbokoyi, I couldn't have made it without you. God richly bless you for being a father to me.

I also want to show my appreciation to my dearest friend and brother whom I met on this campus, Mr. Bruno Senakpon Dandogbessi. I ask for God's favor to locate you wherever you find yourself and His unending blessings to come upon you for the love, care and support you gave me which enabled me to go through this program successfully.

To my boss, Mr. Emmanuel Lartey, Mr. Paul Dickson Udebhulu and the Holy Ghost Prayer Ministry, I say God bless you all.

Again, I want to appreciate my classmates, especially Chuks, Obed, Evans and Bayo for their advice and encouragement.

I can't end without saying, "Eshe" to Dr Akeem Arinkoola Olantunde, you've indeed been a blessing to me, God richly bless you.

A very big thanks to my sponsors, African Capacity Building Fund (ACBF), without you there would not have been an MSc for me at AUST. God bless this foundation.

Lastly, I thank my parents, especially my mum for her love, care and support. I say "Onyankopon nhyira mo". Special mention to my siblings George Kwatia Ansah, Naomi Tetteh and Angela Nanayaa Adubea, for their support and prayers; I ask for God's blessings for all of you.

DEDICATION

This work is dedicated to God Almighty for His unending love and mercy, my family, Madam Beatrice Larbi, Mr. Michael Kwatia Ansah, George Kwatia Ansah, Naomi Tetteh and Angela Nanayaa Adubea, for their love, care, support and encouragement throughout my program.

TABLE OF CONTENTS

LIST OF FIGURES

LIST OF TABLES

CHAPTER 1

1.1 Introduction

The simultaneous flow of fluids is difficult in a safe and controlled way, with the exception that various behaviors of the flow can be predicted with adequate reliability. It deals with the concurrent flow of fluids within different phases (i.e. gas, liquid and solid) or the different chemical properties but in the same phase, for example gas-liquid, gas-solid, liquid-solid, liquid-liquid and gas-liquid-solid (Abdulkadir, 2015). Multiphase flows are encountered in industries like; the petroleum, chemical, and nuclear industries. The transportation of gas- liquid two-phase flow in the petroleum industry over long distance is quite common. This simultaneous flow is encountered in instances like the flow of oil from the reservoir to the separator, and to the process facilities. As pressure decreases, gas starts to evolve, thereby creating a two-phase flow in the pipeline. Various difficulties are encountered in the flow of these fluids, some of which are phase velocity differences and the existence of several flow regimes. These flow regimes include; bubbly, slug, churn, plug, and stratified, among many others. The existence of these flow regimes in transportation lines poses certain challenges to the industry because they increase the pressure drop, heat transfer, mass and corrosion rate in the pipeline. Since the accurate prediction of these flow patterns is essential to the success of designing multiphase flow systems in vertical and horizontal flows, there is therefore, need to investigate the behavior of the fluids in pipes of various inclinations, for effective transportation in the industry.

1.2 Critics of Churn Flow

One may wish to know the reason for this particular subheading, the critics of churn flow. The topic is discussed because of the various schools of thoughts and ideologies from different research about the existence of churn flow regime. The question is, does Churn flow exist as a distinctive flow pattern or, it is just an extension of slug flow? To address this, this work is yet to find out as Mao and Dukler, and Hewitt and Jayanti presented different ideas about the existence of this particular flow.

According to Mao and Dukler (1993) in their paper, “The Myth of Churn Flow?” they presented evidence that proved that churn flow pattern is a simple and continuous

extension of the condition of slug flow and that no transition actually existed. Therefore it is not a distinctive and separate flow pattern on its own. In view of this, they presented two different pieces of evidence to buttress their point. These are visual evidence and instrumental evidence where experiments were performed to support their findings.

1.2.1 Visual Evidence

This evidence is no different from what other researchers observed in transparent pipes. Based on this, one can conclude that their observations proved the existence of churn flow as a unique and separate pattern that exists as a transition from, slug flow to annular flow.

According to Mao and Dukler, stable slug flow is an upward motion of a quasi-periodic arrangement of alternating Taylor bubbles and liquid slugs at a constant speed of propagation, and that the length of the Taylor bubbles and the liquid slugs remain the same as they rise. The velocity associated with the bubbles and liquid slugs is uniformly upward and the same as that which exists in front of both the slug and bubble. As the gas rate increases, the flow becomes chaotic, and the size of the liquid slug and Taylor bubbles increase forming lumps of bubbles as they move up and down the pipe. The flow then becomes oscillatory and displays irregular periods. Again, the main characteristic of slug flow is the falling of the liquid film around the Taylor bubbles and it disappears. All these observations show characteristic features of churn flow, thereby proving that it exists as a unique flow pattern.

1.2.2 Instrumental Evidence

In instrumental evidence, three different experiments were carried out to provide data for the work by using a 50.6 mm diameter vertical pipe. These data included the axial profile of the void fraction in the liquid slug, the thickness profile of the liquid film around the Taylor bubble, the axial profile of the magnitude and the direction of the shear stress along the bubble and slug, and the velocity propagation of the front and back of the bubbles and slugs.

From the first experiment conducted using an RF probe at three gas flow rates, three gas

velocities and a constant liquid superficial velocity, it concluded that; the lowest gas velocity, 0.76 m/s showed traces of full slug flow. The second experiment of 1.41 m/s showed slug flow with some up and down motion of the slugs, while the highest velocity 3.42 m/s, showed a churn flow with all the chaotic behaviors. From the second experiment, the velocity of 200 bubbles and slugs was determined by cross-correlation of two axial conductance probe positioned parallel to each other. From this, the percentage of slugs moving downward was determined. It was concluded that, very few slugs moved downward to be able to characterize it as churn flow, and that the percentage was not too different from what was observed to be fully slug flow. The last experiment was based on using a model to calculate the characteristic of slug flow. The experiment was done by averaging the void fraction over a unit cell containing liquid slugs and Taylor bubbles. The experiment was conducted using different flow rate pairs, 24 for slug flow and 18 for churn flow proved that for the 24 flow rate pairs, the calculated and experimental void fraction was 7% in agreement; the error estimated being 6%, and the standard deviation was 3.1%. The standard deviation for the 18 runs was 5.3%. With these values, they concluded that since the agreement between the churn flow model and slug flow model for void prediction was not too different, then churn flow is not a distinctive flow pattern. From these three experiments, they finally concluded that churn flow does not exist but it is just an extension of slug flow, and their initial evidence of the existence of churn as a distinctive model was a mistake.

Hewitt and Jayanti (1993), in their paper, “To Churn or Not to Churn”, raised an argument against Mao and Dukler concerning their findings. Hewitt and Jayanti disproved the findings based on the fact that, experiments were carried out at pressures close to atmospheric pressure. They came up with the fact that, the term churn has three uses and that the third type which is the distinctive flow pattern is characterized by the presence of flooding type waves throughout the flow regime. From this, they concluded that perhaps the gas velocity that was considered by Mao and Dukler, which is the 3.42 m/s was not high enough to get to the transition state between slug and annular since the flooding type waves would not have taken place. In this perspective, the 3.42 m/s gas velocity was taken as the second type of churn flow, which is the slug extension that was refferred to by Mao and Dukler. Hewitt and Jayanti stated that the main purpose of designating a flow regime is to be able to develop a model that can accurately predict a particular flow regime with a peculiar character, thereby reducing the number of flow patterns. In line with this, certain characteristics were listed which were only identifiable

with churn flow and not annular or slug flow. These characteristics include; the flooding wave which is a predominant phenomenon associated with churn flow pattern and the periodic reversals of the liquid film; the increase in the entrainment fraction by the flooding waves, and droplet deposition dominated by radial velocity imparted at the point of the droplet creation. The characteristics, as presented above, are significantly different from that of annular flow or slug flow. Since the characteristics of these two flow patterns are different, churn can be treated as a distinctive flow pattern. Again this flow pattern is noted to cover a wide range of flow velocity. Also, the transition of slug to churn exists at a gas velocity of 3.5 m/s and that this flow persists to velocities from 10-15 m/s. Based on these findings, they concluded that Churn flow exists as a distinctive pattern and not an extension of slug flow. It is also important to consider higher velocities of 10-15 m/s since most of the industrial equipment operates within these velocities.

1.3 Problem Statement

The success and safe design of multiphase flow systems depend on the accurate prediction of the various flow regimes that exist within the flow system. This is because, these regimes increase the rate of heat transfer, pressure drop and the corrosion rate of the system. These challenges intrigued a research in this area. To help solve this problem, there is a need for accurate determination of the void fraction which helps in the characterization and prediction of the flow regimes existing at a particular point in the flow system. Although numerous works have been done in this area, the results obtained still require further scrutiny since they reported poorly especially for churn flow. As the name implies, churn flow is a highly disturbed flow of liquid and gas in which the liquid motion is oscillatory, going up and down alternating, although not in a periodic and regular manner (. The net flow of liquid is generally in the direction of the flow of gas, although it may be zero or even negative. This flow regime is normally identified between the slug and annular flow regimes in vertical or near vertical upward flow. However, it occurs at low liquid flow rates, where an uninterrupted change to an annular flow pattern may occur, either from slug flow or bubbly flow regimes.

Churn flow is rare amid the flow regimes in that, several schools of thought exist regarding the mechanism of transition to this flow regime. It is also rather challenging to

predict its existence. For example, McQuillan and Whalley (1985) reported only a 36% success rate in predicting it, whereas other flow regimes were predicted with an accuracy of up to 80%. Others, for example, Mishima and Ishii (1984), and Brauner and Barnea (1986) did not adopt such an approach to measure the effectiveness of their models, but even in their results, several instances of inappropriate prediction of churn flow can be found, and the success rate was also rather poor. It is possible that this poor argument is as a result of one or both of the following:

- The predictive methods do not model the underlying mechanisms to a satisfactory degree of complexity;
- There may be more than one mechanism, over a range of flow conditions, governing this transition.

Due to the inappropriate prediction of the flow regimes, there is the need for further investigation into the possibilities leading to the occurrence of the various flow regimes in both, horizontal and vertical pipes using unpublished experimental results obtained at the University of Nottingham, United Kingdom.

1.4 Objectives of Research

The objectives of this research are threefold:

- To obtain void fraction data from wire mesh sensor (WMS) (67 mm internal diameter and 6 m long pipe) at gas superficial velocities up to 4.7 m/s using air–silicone oil as the model fluid from Nottingham University for the following;
  - To determine the effect of gas and liquid superficial velocities on void fraction.
  - To determine the effect of inclination angle on void fraction.
  - To identify the radial phase distribution of the flow.
- To develop a drift-flux correlation that is capable of correctly predicting the void fraction for churn flows in vertical pipes.
- Finally, flow regimes identification will be performed using the newly collected data to confirm the range of flow conditions which represent churn flow.

1.5 Organization of the Research

The report is structured in this format;

- Chapter one; introduction of the work, defining the problem, state the aims and objectives, the methodology employed to carry out the work and showing how the entire work will be structured.
- Chapter two; is the literature review. Previous work or research done on gas/liquid flow patterns in vertical pipes, transition of flow pattern, flow pattern Maps, identification in vertical and horizontal pipes for two-phase flow, and factors affecting the formation of churn flow,
- Data acquisition and the methodology employed to do this work is captured in Chapter three.
- Chapter four; the results and discussions. This chapter details the various results obtained and the analysis performed on the results in achieving the objectives set for the work.
- Chapter five will conclude the work and give Recommendations of further study if any.

CHAPTER 2

LITERATURE REVIEW

2.1 Gas-Liquid Flow Pattern

Two-phase flows through vertical, horizontal or inclined pipes adopt flow patterns that vary depending on the pipe geometry and orientation. Various works have been conducted to understand and determine the behavior of the various flow regimes and to develop models to aid the prediction of these regimes in pipelines.

Most recently, Schlegel et al. used neural networks for flow regime identification in nuclear reactor safety for the prediction of Boiling Water Reactor (BWR) behavior, and safety analysis in Pressurized Water Reactors (PWRs). Again, Computational Fluid Dynamics (CFD) codes such as CFX and FLUENT have been developed and applied in the simulation and prediction of multiphase flows. This work will focus on flow in vertical pipes with little emphasis on the horizontal pipe.

2.2 Vertical Gas/Liquid Flow Regimes

A flow pattern is the geometric distribution of the two phases in a pipe. Starting with a low upward gas flow-rate in a vertical pipe, and increasing the gas flow rate gradually, while keeping constant the liquid flow-rate, several flow regimes are encountered, these are; bubbly flow, slug flow, churn and annular flow as shown in **Figure 2**. The change of flow patterns occurs when the conditions of flow are altered. If for instance, a system starts with a single phase liquid flow through pumping liquid into a vertical pipe and then gas is injected into the lower end of the pipe, bubble flow occurs. Increasing the gas flow rate and maintaining the liquid flow rate changes the flow pattern into a slug flow. Continuous regulation of the gas and liquid flow rates result in different flow patterns.

2.2.1 Bubbly Flow

This flow is identified by a liquid continuum phase with dispersed bubbles of gas. The bubbles move upward with a velocity greater than the adjacent liquid, and the relative slip causes an agitation of the basic flow pattern and results in a wake behind the bubble (Zhu, 2003). In bubbly flow, gas bubbles vary in size and shape, and they are generally not- uniform. However, they are relatively small compared to the diameter of the tube in which they are formed. These bubbles rise within the liquid due to buoyancy. They gather together at the center of the pipe in some instances, while they are distributed near the wall of the pipe in other cases (Abolore, 2014). According to Ghiaasiaan (2008), the bubbles have little interaction at very low gas flows but increase in number as flow rate increases. As the gas flow gets higher, the bubbles coalesce and break up. Recent works show that this flow regime does not occur in large pipe diameters (150 and 200 mm), where there is a direct transition from bubble to churn flow (Azzopardi, 2006).

2.2.2 Slug Flow

When the bubbles coalesce, they form larger bubbles with hemispherical caps known as Taylor bubbles. These bubbles are separated from each other by smaller liquid slugs (Ghiaasiaan, 2008). A Taylor bubble has a constant pressure surface. It is a cylindrical shape bounded on top by a spherical cap or a bullet shaped nose, and a distorted flat tail at the bottom. There is a large axial variation in the void fraction between the Taylor bubbles and the liquid slugs. The flow is similar to the annular regime at a certain level across the Taylor bubble and changes to dispersed bubbly flow when it is across the liquid slug. As the void fraction increases, the Taylor bubbles are elongated and line up closely to the tail of the preceding bubble touching the nose of the downstream bubble. In this instance, the liquid slug between the bubbles become unstable and cannot sustain their shape due to the strong wake behind the bubbles (Zhu, 2003).

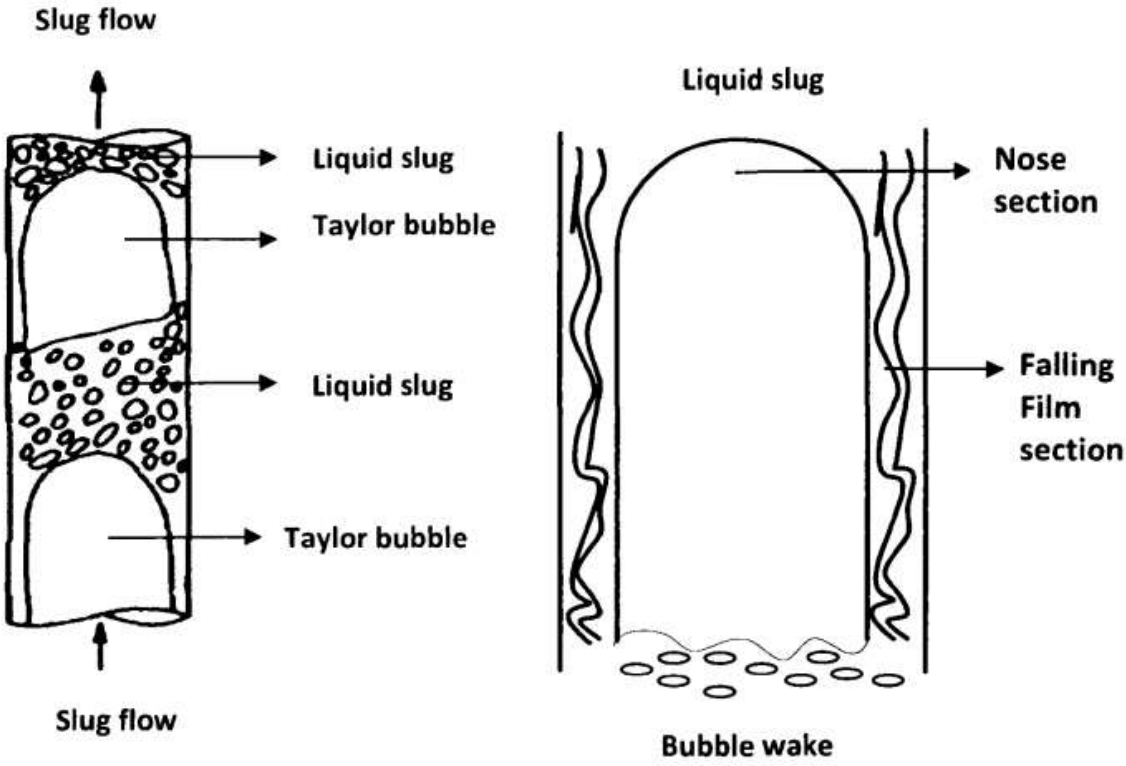

Figure 2.1: (a) A Cross Section of a Typical Slug Flow

(b) Taylor Bubble Showing the Nose and the Falling Film Sections (Abolore, 2014)

2.2.3 Churn Flow

Churn flow is slightly similar to slug flow, but much more chaotic, bubbly and disordered (Zhu, 2003). The main differences between the slug and churn flow are that slugs become narrower and more irregular, the continuity of the liquid in the slug is continually destroyed by regions of high gas concentration, and finally, the thin falling film of liquid surrounding slugs cannot be observed. Increasing the gas flow rate increases the size of the Taylor bubbles. As these bubbles get to the upper section of the channel, they become unstable and break down into smaller Taylor bubbles which oscillate up and down the pipeline. Typical churn flow is characterized by this oscillatory or alternating direction of motion of the liquid slug as well as the liquid film on the pipe wall. At the lower end of the range, it may be regarded as a breaking up of plug flow with intermittent connection across the tube by the liquid phase; but when the range of gas flow rates is high, it may be regarded as a debauched form of annular flow with the course of the film flow varying, and large waves forming on the interface (Azzopardi,

2006). This is a different interpretation of churn flow and represents the irregular region near the entrance of a long channel where eventually, a slug flow pattern will develop.

2.2.4 Annular Flow

Annular flow regime is identified by a layer of liquid on the walls of the tube and entrained bubbles of liquid in the gas core. The liquid phase moves upwards partly as a wavy liquid film and partially in the form of droplets in the gas core. Annular flow develops from churn flow when the gas flow rate is increased, such that there is a coalescence of bubbles into larger ones that fill the entire diameter of the pipe with liquid film along the walls of the pipe. Under certain conditions, gas bubbles can be entrained within the film. At high liquid flow rates, the liquid droplets become concentrations and coalesce into wisps. This is identified as a wispy annular flow in some flow pattern maps.

2.2.5 Wispy-Annular Flow

Increasing the liquid flow rate results in droplet concentration in the gas core of annular flow increases and eventually, droplet coalescence occurs leading to large lumps or streaks as wispy liquid occurring in the gas core. This flow can be identified as flows with high mass velocity (Agrawal, 2010). The first authors to first identify this unusual flow pattern were Bennett et al. (1965). Hewitt and Roberts (1969) classified this as a separate flow pattern while other flow maps rarely mention it. For instance, Hawkes et al. (2000) suggested that the observed wisps may have arisen from the agglomeration of liquid droplets within the gas core. Under certain circumstances, bubbles of gas may be entrained in the liquid film (Abolore, 2014).

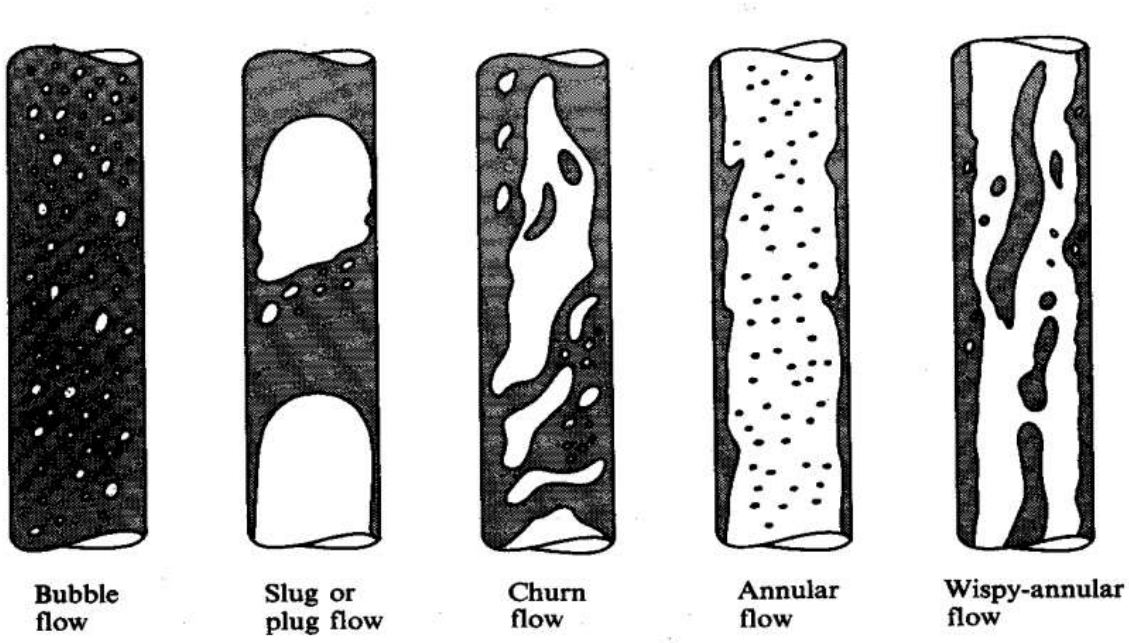

Figure 2.2: Vertical gas-liquid flow patterns (Kumar, 2010), (gas in white, liquid in grey),

2.3 Horizontal Flow Regime

The flow patterns in horizontal pipes are similar to the ones available in vertical flows. Gravity influence acts on the fluid distribution to separate the liquid to the bottom of the tube and the gas to the top. The figure below shows the flow regimes available in horizontal pipes. These flow patterns are:

2.3.1 Bubbly flow

The gas bubbles are dispersed in liquid with highly concentrated bubbles in the upper-end of the tube due to buoyancy. As the gas velocity increases, the bubbles collide and coalesce into larger sizes. They move away and are dispersed in the liquid continuous phase.

2.3.2 Stratified flow

This particular flow regime occurs at low liquid and gas flow rates, complete separation of the two phases occurs. Since the gas is less dense, it stays at the top and the denser phase being the liquid at the bottom of the tube, such that the horizontal

interface between them is undisturbed. This causes a separation between the liquid and the gas in this regime. For gas-liquid flows, the difference in densities of the two fluids is large and the flow ranges over which stratified flow is found, is correspondingly larger.

2.3.3 Plug flow

These are liquid plugs separated by elongated gas bubbles. These bubbles are smaller than the tube diameter such that the liquid phase is separated and found below them. This particular flow regime is also known as the elongated bubble flow.

2.3.4 Stratified-wavy flow

Once the gas flow rate in a stratified flow is increased, the gas velocity tends to increase such that waves are formed on the interface of these fluids. The waves move in the direction of flow with amplitude notable and dependent on the velocity of both phases. As the waves rise up the walls of the pipe, thin films of liquid are left on the wall.

2.3.5 Slug flow

Slug flow occurs in plug flow at higher gas flow rates. In this case, the gas velocities increase as the flow rate increases. This causes the elongated bubbles to increase in size to fill almost the entire diameter of the tube.

2.3.6 Annular flow

At higher gas flow rates, the liquid forms a thin film along the walls of the tube, similar to that in vertical flow. However, the liquid film at the bottom is thicker than at the top. The disturbance between the two phases causes droplets to disperse in the core of the gas core.

2.3.7 Mist flow

As the gas velocities increase in annular flow, the liquid films along the wall are stripped and coalesce into wisps in the gas core.

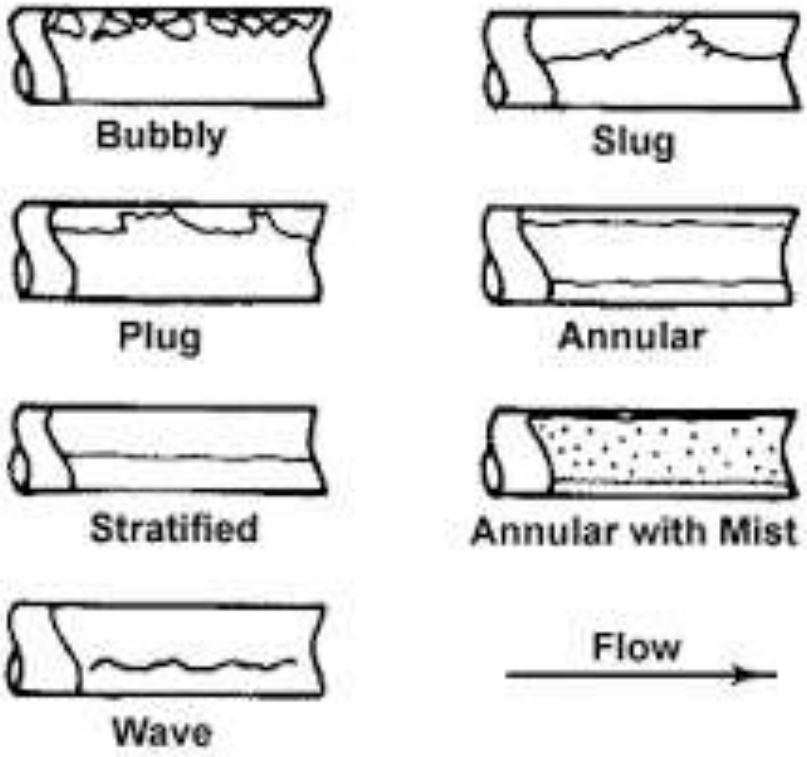

Figure 2.3: Horizontal gas-liquid flow patterns (Thome, 2010)

2.4 Structuring Flow Pattern

To easily identify the aforementioned flow regimes, several researchers developed maps and correlations. The easiest and simplest being the maps. To predict a particular flow pattern, the boundaries in which the flow pattern dominates is drawn and located knowing the mass, flux, liquid and gas superficial velocities. Flow pattern maps can be graphically categorized for both vertical and horizontal multiphase flows. Once all pattern boundaries observed are mapped, a clear overview of the behavior can be observed as a function of flow conditions. **Figure 4** shows a horizontal gas/liquid flow pattern map from Baker (1957), while **Figure 5** shows an upward vertical gas/liquid flow pattern map from Hewitt & Roberts (1969). There are two main types, which are theoretical and experimental flow pattern maps.

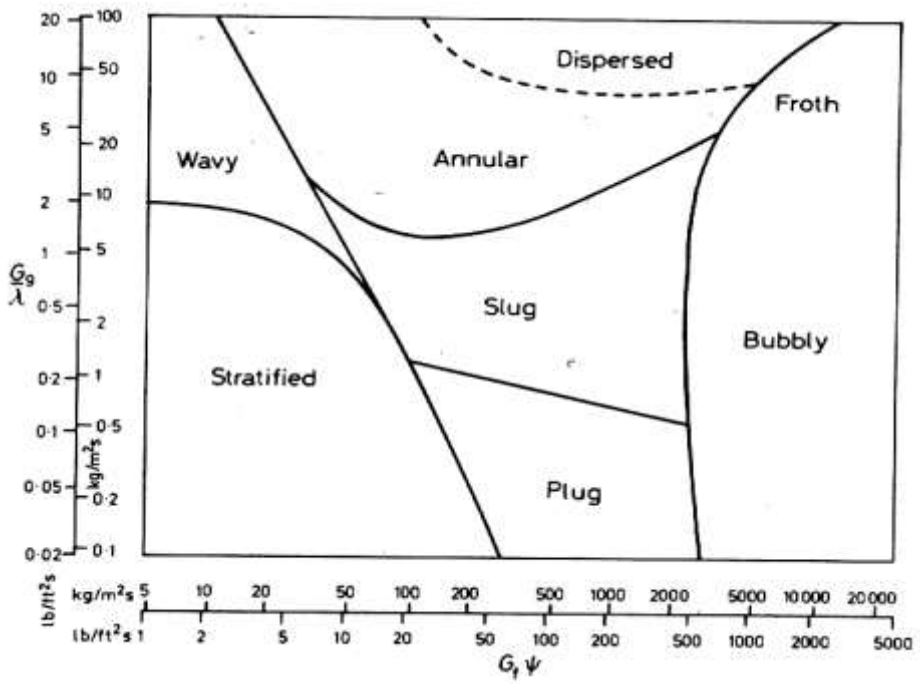

Figure 2.4: Baker's horizontal flow pattern map (Baker, 1954)

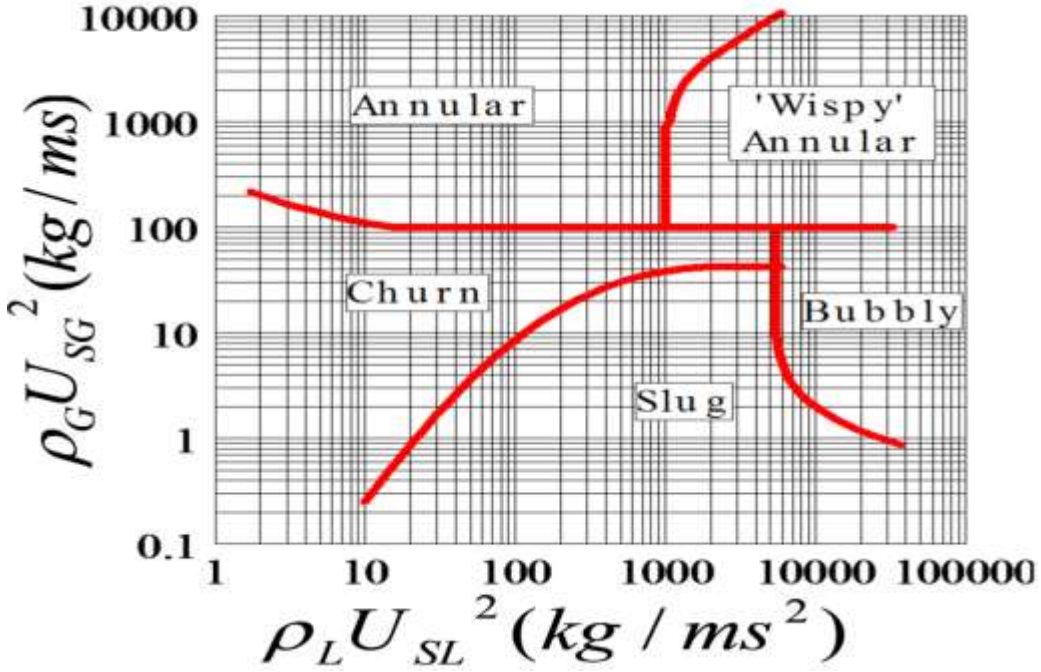

Figure 2.5: Hewitt and Robert (1969)'s vertical flow pattern map

2.4.1 Experimental Flow Pattern Maps.

To easily represent a two-phase flow data for a particular flow pattern, the two fluid pairs, and the geometry can be denoted graphically to develop the map. Taitel et al. (1980) came up with various coordinate systems and showed that the different flow regimes transitions couldnot all be represented by one coordinate pair. Hence different methods were adopted to overcome this problem, McQuillan, and Whalley (1985).

2.4.2. Theoretical flow pattern maps.

Taitel et al. (1980) presented an alternative to the experimental approach of obtaining flow pattern maps. The conditions necessary for the occurrence of each flow patterns were considered and the mechanisms by which each transition occured postulated. They then modeled these changes and produced various equations to enable the flow pattern boundaries to be calculated once the fluid properties and pipe geometry was known. These maps were then compared with existing experimental maps and experimental data with air-water mixture by the authors. An agreement was obtained from the comparison. This approach of flow regime prediction was also used by Mishima & Ishii (1984).

2.5 Flow Pattern Transition

To correctly develop a model that will predict the flow pattern existing at a particular flow condition, there is a need to have adequate knowledge about the various flow patterns in existence, and their transitions from one pattern to the other. This is because, the interaction between the bubbles resulting in the breakup and coalescence, and interactions between the pipes, makes it difficult to determine and describe the flow pattern existing at a time. Initially, the gas bubbles are smaller and widely distributed in the liquid phase. The bubbles at this stage are rounded and tend to move upward along the pipe. As the gas velocity increases, the bubble size also tends to increase, they then coalesce and form larger bubbles. As they move upwards in the channel, they become unstable due to the interaction between the pipe walls, resultantly they break up forming numerous large bubbles which move up and down the channel. The bubbles at a point in time become very large, filling the entire channel with films of liquid formed in between the pipe and the bubble.

2.5.1 Bubble to slug flow transition

The relationship between bubble coalescence caused by agglomeration and break-up by turbulence is key to the transition from bubblyto slug flow. Radovcich and Moissis (1962) investigated the frequency of bubble collision and found out that, a rapid increase occurs at a void fraction of ε > 0.2. Taitel et al. (1980) employed the critical void fraction, which they suggested at ε = 0.25, for the transition from bubble to slug flow regime. The transition equation is given by using the terminal velocity of a large bubble, U_o,

$$U_{sl} = \frac{1-\varepsilon}{\varepsilon} U_{sg} - (1-\varepsilon)U_o \quad \text{..... (2.1)}$$

Harmathy in 1960 proposed a correlation for the calculation for Uo and is given by the relation below;

$$U_o = 1.53 \left[\frac{(\rho_l - \rho_g) g \sigma}{\rho_l^2}\right]^{0.25} \quad \text{..... (2.2)}$$

Song et al. (1995) used a 25mm diameter pipe to propose the following correlation for bubble flow,

$$\varepsilon = 0.55 - 2.37 \left(\frac{D_b}{D_l}\right) \quad \text{..... (2.3)}$$

Azzopardi (2006) carried out research on the flow regime transitions for a larger diameter pipe using the data from 29 mm pipe by Cheng *et al*. (2002), and Guet *et al*. (2002) in a 72 mm pipe. Also, researchers like Cai *et al*. (1999) carried out an investigation of flow regimes in 100mm pipe and Shen et al. (2014) in his paper, 'Flow Characteristics and Void Fraction Prediction in Large Diameter Pipes'.

2.5.2 Transition from Slug to Churn Flow

Churn flow occurs as a result of the breakdown of slug flow into smaller Taylor bubbles. According to Jayanti and Hewitt (1992), there are four basic mechanisms that cause the transition from slug to churn flow, These are the entrance effect, flooding, wake effect and the bubble coalescence.

2.5.2.1 Entrance effect

It is the formation process of stable slug further downstream in the pipe. In this mechanism, churn flow is considered as a transition to stable slug flow. Short liquid slugs and Taylor bubbles are formed by the gas and liquid at the inlet of the pipe. When the pipe is long enough, the collapse and merging of successive slugs result in the formation of stable liquid slugs. As the gas flow rate increases, the slugs become unstable, breakup and coalesce into smaller Taylor bubbles. The small Taylor bubbles formed move up and down the pipe thereby forming the churn flow. An experimental study of the slug and churn flows has been conducted in laboratories in pipes of diameters, 0.025 and 0.05m. An expression was developed by Dukler and Taitel to evaluate the entrance length for churn flow, Le, above which churn flow exists.

$$\frac{L_e}{D} = 40.6\left(\frac{V_M}{\sqrt{gD}} + 0.22\right) \quad \text{(2.4)}$$

$V_M$is the mixture velocity, g is the gravitational acceleration and *D* is the pipe's inner diameter. If the real length of the pipe is less than the Le calculated from the above equation, then churn flow should be expected throughout the pipe, else slug flow will be observed if Le is less than the real length.

2.5.2.2 Flooding

It is the process whereby the liquid film around the Taylor bubble is broken down as a result of the formation of large interfacial waves. Wallis observed that the air velocity required to initiate flooding in a falling film of very small flow rate is approximately the same as the velocity of the slug to churn transition. Researchers like McQuillan and Whalley (1985) endorsed flooding as the basis for slug-churn flow transition, and there is experimental evidence from Wallis and Chaudry's et al. work in agreement with it. Hewitt and Wallis developed a semi-empirical expression to predict the flooding gas and liquid flow rates.

$$(V_{SG}^*)^{0.5} + (V_{SL}^*)^{0.5} = C \quad \text{(2.5)}$$

$$V_{SG}^{*} = V_{SG}\frac{\rho_G^{0.5}}{[gD(\rho_L-\rho_G)]^{0.5}} \quad \text{(2.6)}$$

$$V_{SL}^{*} = V_{SL}\frac{\rho_L^{0.5}}{[gD(\rho_L-\rho_G)]^{0.5}} \quad \text{(2.7)}$$

$$V_{BS} = \left(1-4\frac{\delta}{D}\right)[1.2V_M + 0.35\left(\frac{gD(\rho_L-\rho_G)}{\rho_L}\right)^{0.5} \quad \text{(2.8)}$$

$$V_{fs} = V_{BS} - V_M \quad \text{(2.9)}$$

Where δ is the liquid film thickness in the Taylor bubble region, calculated with Nusselt's expression for a laminar falling film (Nusselt, 1916)

$$\delta = \left[\frac{3V_{fs}D\mu_L}{4g(\rho_L-\rho_G)}\right]^{1/3} \quad \text{(2.10)}$$

μ_L is the dynamic viscosity of the liquid. The constant C in Eq. 2.5 was proposed by McQuillan & Whalley to be C = 1.

Jayanti & Hewitt used the same approach as McQuillan & Whalley. They realized two key weaknesses in the McQuillan & Whalley method. One was the assumption that the film around the Taylor bubble is laminar, and the Nusselt relation between the film thickness and film velocity employed in the study. They proposed to replace this by the empirical correlation given by Brotz, which was found to be valid over an extensive range of film Reynolds numbers. This expression can be written in terms of the superficial film flow rate as;

$$V_{fs} = 9.916(1-\alpha_b)\left[\frac{gD\Delta\rho(1-\sqrt{\alpha_b})}{\rho_L}\right]^{0.5} \quad \text{(2.11)}$$

Where $\alpha_b = 1-4\frac{\delta}{D}$ (2.12)

An empirical correlation, Eq. (10), was suggested by the authors to take account of the falling film length on the flooding velocity.

$$(V_{SG}{}^{*})^{0.5} + m(V_{fs}{}^{*})^{0.5} = 1 \quad \text{(2.13)}$$

Where the coefficient m is a function of L/D and is given by

$$m = 0.1928 + 0.01089\left(\frac{L}{D}\right) - 3.754 * 10^{-5}(\frac{L}{D})^2 \quad \text{(2.14)}$$

$$if\ \frac{L}{D} \leq 120 \qquad if\ (\frac{L}{D}) > 120 \qquad m = 0.96 \approx 1$$

2.5.2.3 Wake Effect

According to some researchers, the upward movement of the Taylor bubble destroys the liquid slugs. The liquid slugs are destroyed in the process of transition as they coalesce, and the Taylor bubbles become close to each other. This results in a strong wake effect which destroys the liquid slug between the Taylor bubbles. The void fraction that surrounds the Taylor bubble becomes equal to the average void fraction in the entire pipe. This is known as the wake effect.

$$\alpha_v = \frac{V_{SG}}{\left[C_o V_m + 0.35\sqrt{gD\frac{(\rho_L - \rho_G)}{\rho_L}}\right]} \quad \text{(2.15)}$$

$$\alpha_{TB} = 1 - 0.813\left\{(C_O - 1)V_m + 35\sqrt{\frac{gD(\rho_L - \rho_G)}{\rho_L}}\left[V_m + \frac{3}{4}\sqrt{\frac{gD(\rho_L - \rho_G)}{\rho_L}}\left(\frac{gD^3(\rho_L - \rho_G)\rho_L}{\mu_L^2}\right)^{\frac{1}{8}}\right]^{-1}\right\}. \quad \text{(2.16)}$$

Where ρ_G and ρ_L are the densities of the gas and the liquid phases, respectively, u_{GS} is the gas superficial velocity, μ_L is the liquid dynamic viscosity, and C_o is calculated by Eqs. (14) and (15), for round tubes and rectangular ducts, respectively

$$C_o = 1.20 - 0.2\sqrt{\frac{\rho_G}{\rho_L}} \quad \text{(2.17)}$$

$$C_o = 1.35 - 0.35\sqrt{\frac{\rho_G}{\rho_L}} \quad \text{(2.18)}$$

Chen and Brill (1997) proposed a new transition model based on the wake effect occurring at the tail of a typical Taylor bubble. The authors split the liquid slug into three regions: the wake, the intermediate, and the developed regions. As the gas flow rate increases, the effects of the wake region on the liquid slug dominates and affects the nose of the bubble right ahead. This might result in the collapse of the slug and consequentially in the transition to churn flow. Equation (16) represents the transition criteria proposed by the authors.

$$\beta_s \leq 0.15, \qquad \alpha_s \geq 0.52 \quad \text{(2.19)}$$

Where α_S is the void fraction in the slug while $\beta_S = L_s/L_u$ is the relative length of the liquid slug. Considering the gas as incompressible, the total volumetric flow rate of the mixture is constant at any cross section. Therefore

$$\alpha_{TB}V_{TB} - (1 - \alpha_{TB})V_f = V_{SG} + V_{SL} = V_M \quad \text{(2.20)}$$

V_{TB} is the gas velocity inside the Taylor bubble, respectively, u_F is the liquid film terminal velocity, V_{SG} is the gas superficial velocities, V_{SL} is the liquid superficial velocities, and V_M is the mixture velocity. A gas mass balance across the entire slug unit can be approximated by

$$V_{SG} = \alpha_{TB}(1 - \beta_s)V_{TB} + \alpha_S\beta_s(V_{SG} + V_{SL}) \quad \text{(2.21)}$$

2.5.1.4 Bubble Coalescence

The mechanism associates the slug-to-churn transition to the churning of liquid slugs. It supports the fact that, the gas in the liquid slugs is distributed due to turbulence, the bubbles collide and coalesce due to their proximity as the gas holdup in the slug increases above 0.52. The transition to churn flow should occur at a void fraction equal to 0.52, a figure 0.44 lesser than the maximum packaging fraction of 0.74. This shows that

collision between bubbles increases as bubbles get closer. Thus, the continuity of the liquid slug is hence destroyed. Chen and Brill (1997) used an earlier model developed by Barnea and Brauner (1985) to evaluate the void fraction in the slug, given by

$$\alpha_s = 0.058\left[d_c\left(\frac{2f_M V_M^3}{D}\right)^{0.4}\left(\frac{\rho_L}{\sigma}\right)^{0.6} - 0.725\right]^2 \quad \text{(2.22)}$$

Where σ is the surface tension and *dc* is the characteristic bubble size for vertical flow, given by

$$d_c = 2\left[\frac{0.4\sigma}{g(\rho_L - \rho_G)}\right]^{0.5} \quad \text{(2.23)}$$

And the friction factor, f_M, is defined as

$$f_M = \frac{2\tau_w}{\rho_L V_M^2} \quad \text{(2.24)}$$

Where, $\boldsymbol{\tau_w}$ is the wall shear stress. The friction factor and Reynolds number are given in the relationships below;

$$Re = \frac{\rho_L V_M D}{\mu_L} \quad \text{(2.25)}$$

$$f = \frac{16}{Re} \qquad \text{if Re < 2100} \quad \text{(2.26)}$$

$$f = \frac{0.046}{Re^{-0.2}} \qquad \text{if Re > 2100} \quad \text{(2.27)}$$

2.5.3 Churn to annular flow transition

The critical condition of a sufficiently high gas velocity to keep the entrained droplets suspended was suggested by Taitel et al. (1980). The conclusions drawn from the force balance for a droplet, is;

$$0.5C_D\frac{\pi D_d^2}{4}\rho_g u_g^2 = \frac{\pi D_d^3}{6} g\Delta\rho \quad \text{(2.28)}$$

Hinze (1955) proposed a correlation that could be used to predict the maximum stable drop size

$$D_d = \frac{We_c \sigma}{\rho_g u_g^2} \quad \text{(2.29)}$$

The last two equations are combined to predict the churn to annular transition by using critical Weber number, We_c, = 30 and Drag coefficient, Co = 0.4 as suggested by Turner et al. (1969) in the Kutateladze number which is given in equation

$$K_u = \frac{u_{sg}\sqrt{\rho_g}}{[\sigma g(\rho_l - \rho_g)]^{0.25}} = 3.1 \quad \text{(2.30)}$$

Two mechanisms were suggested by Barnea (1986) as being the cause for a churn-to-annular transition for all ranges of pipe inclinations. The mechanisms are instability of liquid film and the blockage at wave crest due to significant water accumulation.

2.6 Void Fraction

As discussed earlier, the present work will study and develop a drift flux model for churn flow prediction. There is the need to review some works done by other people concerning void fraction. Void fraction is the fraction of pipe volume occupied by the gas phase. This parameter is one of the important parameters used to characterize a flow pattern in two-phase flows. It is used for determining other parameters like two-phase flow viscosity, density, the relative average velocity of two-phases and for predicting flow pattern transitions, heat transfer, interfacial area calculation and determination of pressure drop. It can be measured using wire mesh sensors, quick-close valves, γ rays, x-rays, and microwave, among many others (Oteng, 2014). In considering void fraction, the time-average value (taken over a long period) is used, but it should be noted that the void fraction fluctuates with time, and instantaneous values are also of interest (Hewitt, 2010).

2.6.1 Concept of void fraction

As discussed earlier, it is one of the most important parameters used to characterize the two-phase flow. Void fractions are defined in several ways, for example, local void fraction, cross-sectional void fraction, and volumetric void fraction. The local and cross-sectional void fraction represent the void fraction at any given point in the pipe and its distribution across the pipe's cross section. The definition also reflects the method of measurement; i.e. void fraction is measured using a miniature probe and optical or electromechanical means. For a total pipe cross-sectional area; the void fraction is given by:

$$\varepsilon = \frac{A_G}{A} \quad \text{..... (2.31)}$$

Using the quick-closing valves method, the volumetric void fraction is defined in terms of volumes of gas and liquid phases trapped in a section of a pipe. This is given by:

$$\varepsilon = \frac{V_G}{V_G + V_L} \quad \text{..... (2.32)}$$

Liquid holdup is the remaining volume of space occupied by the liquid phase and is given by:

$$H_L = 1 - \varepsilon = \frac{A_L}{A} \quad \text{..... (2.33)}$$

Quality in two-phase flow is defined as the mass ratio of the gas phase to the total fluid mass in a particular pipe segment. It is expressed as mass and is a function of the phase density and void fraction.

$$\varepsilon = \frac{V_G}{V_G + V_L} \quad \text{..... (2.34)}$$

It is also important to consider the gas volumetric flow fraction denoted as β in the present study. It indicates the ratio of the gas volumetric flow rate over the mixture volumetric flow rate written as,

$$\beta = \frac{Q_G}{Q_G + Q_L} \quad \text{..... (2.35)}$$

Where Q_g and Q_l are the volumetric flow rates of gas and liquid phases, respectively.

2.6.2 Void fraction correlations

This section outlines some of the well-known correlations used to predict the void fraction. The void fraction correlations can be classified as empirical or semi-empirical. This section presents void fraction correlations based on the experimental data and hence categorized as empirical correlations.

Chisholm (1973) proposed a correlation to predict void fraction. This expression was based on α-β relationship and applicable to a range of β = 0.4 to 0.9. The equation was developed for vertical upward flow, but can successfully be used to predict the void fraction in the downward two-phase flow. It works well for downward flow because void fraction decreases for higher values of void fraction between the upward and downward flow. The relation is given as:

$$\alpha = \frac{\beta}{\beta + (1-\beta)^{0.5}} \quad \text{..... (2.36)}$$

Hughmark (1962) developed a correlation for the in-situ liquid volume fraction for vertical flow. Further studies by Dukler et al. proved that it could be applied to horizontal flow. The Hughmark correlation is

$$H_L = 0.82\left(\frac{U_{SG}}{U_{SG}+U_{SL}}\right) = 0.82\left(\frac{U_{SG}}{U_M}\right) \quad \text{..... (2.37)}$$

Clark and Flemmer (1985)

$$\varepsilon = \frac{U_{SG}}{1.17U_M + 1.53\left(g\sigma\left(\frac{\rho_L - \rho_G}{\rho_L^2}\right)\right)^{0.25}} \quad \text{..... (2.38)}$$

Cai et al. (1997)

$$\varepsilon = \frac{U_{SG}}{1.185U_M + 1.53\left(g\sigma\left(\frac{\rho_L - \rho_G}{\rho_L^2}\right)\right)^{0.25}} \quad \text{..... (2.39)}$$

2.7 Pressure Drop Prediction in Vertical Pipes

Prediction of pressure drop in multiphase flow channels is essential for the design of flow equipment. It allows sizing of the pump necessary for the operation of the flow system and enables operators to minimize the occurrence of some multiphase challenges like gas hydrate formation since this impedes on the flow efficiency. The total pressure drop considered in this pipe comprises of three distinct components.

$$\left(\frac{dP}{dz}\right)_{TP} = \left(\frac{dP}{dz}\right)_{fric} + \left(\frac{dP}{dz}\right)_{grav} + \left(\frac{dP}{dz}\right)_{acc} \quad \text{..... (2.40)}$$

Where $\left(\frac{dP}{dz}\right)_{grav} = \frac{g}{g_c}\rho \sin\theta$ is the component due to potential energy or elevation change, it is also referred to as the hydrostatic component.

$\left(\frac{dP}{dz}\right)_{grav} = \frac{fpV^2}{2g_cD}$ is the component due to frictional loss.

$\left(\frac{dP}{dz}\right)_{grav} = \frac{\rho v dv}{g_c dL}$ is the component due to kinetic energy change or convective acceleration. According to the definition of flow geometry, when the pipe is in the horizontal position, the angle and the sine of the angle is zero. This means that there is no elevation and hence the pressure drop and the pressure gradient equation becomes

$$\left(\frac{dP}{dz}\right)_{TP} = \left(\frac{dP}{dz}\right)_{fric} + \left(\frac{dP}{dz}\right)_{acc} \quad \text{..... (2.41)}$$

The pressure drop due to acceleration is often minimal and is mostly overlooked in design calculations.

2.8 Drift Flux Method

The drift flux model was first defined by Zuber and Findlay (1964) as a general method for the prediction of void fraction and was later developed by Wallis, Ishii, and other researchers. The model considers the relative motion between the two phases rather than the motion of individual phase and is convenient for analyzing the flow patterns in which the gravity, buoyancy, pressure and interaction between the two phases are influential, Wallis (1969).

Tengesdal et al in 1998 proposed a transition to churn on the drift flux concept. As the gas flow rate increases, there is also an increase in the void fraction, this resultantly causes a breakup of the slug resulting in a churn flow pattern. Global void was expressed from the slug flow as:

$$\alpha = \frac{V_{SG}}{1.2V_M + V_o} \quad \text{..... (2.42)}$$

Where V_0 is the rise velocity of the elongated bubble.

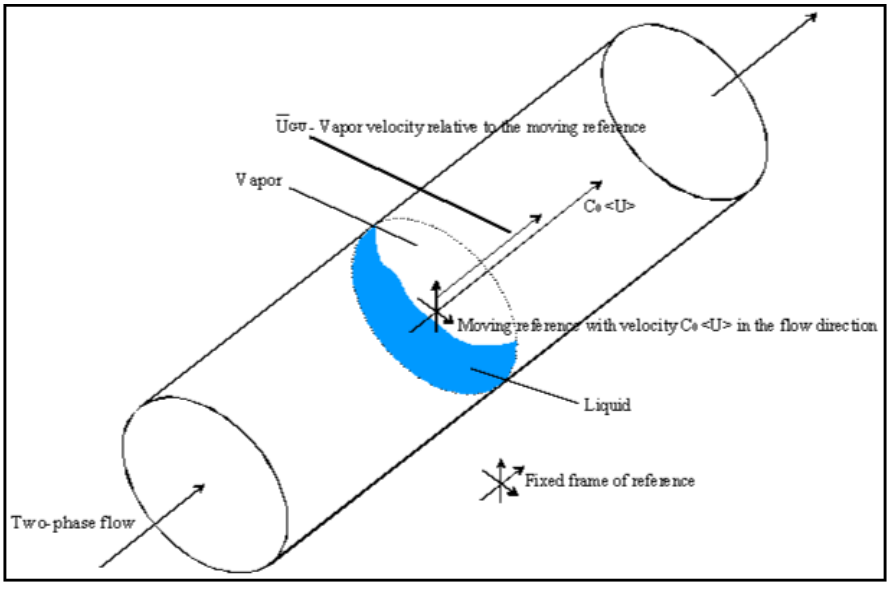

Figure 2.6: A Drift Flux Model (Thome, 2010)

Chokshi proposed that once the global void fraction is around 0.8, then a transition from slug to churn flow will be encountered. A global void fraction of 0.73 was also proposed by Garber and Varanosi based on Fernandes slug and churn flow data. Hewitt also came up with a void fraction of about 0.78. Since churn flow can be considered as a pseudo

single- phase flow, the gas holdup in the Taylor Bubble region is considered the global void fraction at the transition (Tengesdal et al., 1998). Tengesdal et al. used Hewitt's void fraction value of 0.78 since his experiment was carried out in a more stable and controlled environment. As a result, the above equation becomes:

$$V_{SG} = 12.1875(1.2V_{SL} + V_o) \quad \text{(2.43)}$$

Again Tengesdal et al considered the inclination angle that was proposed by Bendikson in the transition correlation and proposed a relation given below as;

$$V_{SG} = 12.1875\left[1.2V_{SL} + \left((0.35 * \sin\theta + 0.54 * \cos\theta)\sqrt{\frac{gD(\rho_L - \rho_G)}{\rho_L}}\right)\right] \quad \text{(2.44)}$$

2.8.1 Small pipes

Ishii (1977) is one of the first scientists who implemented the mechanistic theory of drift-flux model for small pipes. He developed a set of drift-flux models for small circular pipes as well as rectangular channels. These models are often used due to simplicity and accuracy across a wide range of conditions. For the distribution parameter, Ishii developed a simple correlation in upward two-phase flow, based on the density ratio of the two fluids and the Reynolds number, in a fully developed bubbly flow. After a numerous tests with a wide range of Reynolds numbers, his C_o value was approximated to 1.2 for an upward flow in a round pipe. A more complex equation was derived for the annular flow regime derived from the model of the drift term and the mean drift velocity:

$$\overline{V_{gJ}} = V_{gj} + (C_o - 1)j \quad \text{(2.45)}$$

$$C_o = 1 + \frac{1-\alpha}{\alpha + 4\sqrt{\rho_g/\rho_f}} \quad \text{(2.46)}$$

Eliminating the pressure gradient from the momentum equation in the first equation (because the model is designed for steady-state adiabatic flows), and introducing the general drift-flux formulation by Zuber yields a drift term for annular flow as presented below:

$$V_{gj} = 1 + \frac{1-\alpha}{\alpha+4\sqrt{\rho_g/\rho_f}}\sqrt{\frac{gD_h\Delta\rho(1-\alpha)}{0.015\rho_f}} \quad \text{..... (2.47)}$$

Drift term for the other flow regimes by taking into account the geometry, the body-force field, the shear stresses, and the interfacial momentum transfer based on the drag and lift equilibrium on the bubble system.

For Churn flow;

$$V_{gj} = \sqrt{2}\left(\frac{\sigma g\Delta\rho}{\rho_f^2}\right)^{0.25}(1-\alpha)^{0.25} \quad \text{.....(2.48)}$$

For Slug flow;

$$V_{gj} = 0.35\sqrt{\frac{gD_h\Delta\rho}{\rho_f}} \quad \text{.....(2.49)}$$

For Bubbly flow;

$$V_{gj} = \sqrt{2}\left(\frac{\sigma g\Delta\rho}{\rho_f^2}\right)^{0.25}(1-\alpha)^{0.75} \quad \text{.....(2.50)}$$

Again, an equation was developed by Ishii (1977) for boiling flow with the formulation of the distribution parameter, based on the number of nucleating sites, and dependent on the void fraction. This distribution parameter is applicable over a wide range of regimes because, in small pipes, the shape of the bubbles and the liquid film around gas slugs are similar among the flow regimes. Hence, the void fraction and velocity profiles will be similar.

$$C_o = \left(1.2 - 0.2\sqrt{\rho_g/\rho_f}\right)(1-e^{-18\alpha}) \quad \text{.....(2.51)}$$

Hibiki and Ishii (2002) obtained a drift term similar to that of Ishii (1977) but modified a distribution parameter that proposed that the prevailing element to determine the distribution parameter in vertical upward bubbly flow would be the bubble Sauter mean diameter. In the model below, the distribution parameter was taken without the diameter

correction.

$$\begin{cases} C_0 = \left(1.2 - 0.2\sqrt{\rho_g/\rho_f}\right)\left(1 - e^{-\frac{22d_s}{D}}\right) \\ V_{gj} = \sqrt{2}\left(\frac{\sigma g \Delta\rho}{\rho_f^2}\right)^{0.25}(1-\alpha)^{1.75} \end{cases} \quad \text{..... (2.52)}$$

2.8.2 Intermediate pipes

Schlegel et al. (2010) show that the series of intermediary pipes begins at a non-dimensional hydraulic diameter of 18.6 and ends at a value of 30. The transition from one regime to another, and from one diameter to another, was based on a linear interpolation. A drift-flux model was proposed to include the interpolation in the equation below. Λ is the weighting factor of the physical parameter or flow regime, the subscript A represents the left boundary of the domain, B is the right border of the domain while p denotes a parameter of the drift-flux model.

$$p_{A,B} = p_A \Lambda + p_B(1 - \Lambda) \quad \text{..... (2.53)}$$

There are different mechanisms governing the transition from one regime to another hence, the need for various predictive correlations.

Hasan et al. (2010) proposed a transition between flow regimes. Their model was based on exponential functions to obtain a continuous function over the entire range of transition. A function was provided for the calculation of the distribution parameter which interpolated the transition between the facility configurations. The transition between the bubbly and slug flow has been proposed by the following equation:

$$C_o = C_{o,b}\left(1 - e^{-\frac{0.1v_{bs}}{(jg - v_{bs})}}\right) + C_{o,s}\left(e^{-\frac{0.1v_{bs}}{(jg - v_{bs})}}\right) \quad \text{..... (2.54)}$$

C_o is the distribution parameter, $C_{o,b}$ is the dimensionless parameter for fully developed bubbly flow, and $C_{o,s}$ is the dimensionless parameter for fully developed slug flow and v_{bs} is the transition velocity.

2.8.3 Large pipes

Pipes with non-dimensional hydraulic size greater than 30 are considered as large pipes. In this case, Taylor bubbles contained in the entire pipe section cannot be sustained and therefore break up. For air-water flows at atmospheric conditions, this is about 10 cm. Three main peculiarities of the large pipes systems must be considered when developing a drift-flux model, they are reflected in these correlations:

1. The radial profile of void fraction in large pipes will be different from those of small pipes, in particular, it is flatter in large pipes;
2. The drift-flux velocity in large pipes systems increases due to the reduced influence of the pipe wall;
3. The recirculation patterns due to turbulence can modify the drift flux parameters because of the increased diffusion.

Hill, in 1976, developed the under listed correlations based on an experiment with a pipe 150 mm in diameter and 10.5 m tall.

$$\begin{cases} V_g = 1.2V_M + 0.24 & for\ V_{sl} > 0.3\ m/s \\ V_g = V_M + (0.24 + 4.0\alpha^{1.72})(1-\alpha) & for\ V_{sl} \leq 0.3 m/s \end{cases} \quad \ldots\ldots\ldots (2.55)$$

The unit of the parameters in these correlations should be m/s since the mixture volumetric flux in his experiment should be 6.2 m/s at maximum.

This model performs well for the experimental data obtained by Hill, but it is empirical and hence may not do well for conditions outside those seen in his experiments. Fluid properties are not explicitly taken into account, so the correlation may not work very well for systems other than air-water at atmospheric conditions.

Mishima and Ishii (1985) developed a model for large pipes with the drift-velocity that depended on the diameter, system pressure, gas flux and fluid physical properties. According to their model, the distribution parameter is the same as Ishii (1977),

$\mathrm{Co} = 1.2 - 0.2\sqrt{\rho_g/\rho_f}$, and drift velocity is defined as;

$$\begin{cases} V_{gj} = 0.0019 D_h^{*\,0.809} \left(\frac{\sigma g \Delta\rho}{\rho_f^2}\right)^{0.25} \left(\frac{\rho_g}{\rho_f}\right)^{-0.157} N_{\mu f}^{-0.562} \\ V_{gj} = 0.030 D_h^{*\,0.809} \left(\frac{\sigma g \Delta\rho}{\rho_f^2}\right)^{0.25} \left(\frac{\rho_g}{\rho_f}\right)^{-0.157} N_{\mu f}^{-0.562} \end{cases} \quad \text{..... (2.56)}$$

The first equation is for $D^*_h \leq 30$, and the second one for $D^*_h > 30$. Where the viscosity number is defined as;

$$N_{\mu f} = \frac{\mu f}{\left(\rho f \sigma \sqrt{\frac{\sigma}{g\Delta\rho}}\right)^{0.5}} \quad \text{..... (2.57)}$$

The above equations are valid for low viscous cases ($N\mu f \leq 2.25\times10^{-3}$). For the high viscous case the following equation can be used:

$$V_{gj} = 0.92 \left(\frac{\rho_g}{\rho_f}\right)^{-0.157} \quad \text{..... (2.58)}$$

This new criterion was compared to existing conditions and experimental data under steady-state and fully developed flow situations using relative velocity correlations. The criteria showed an agreement with data obtained for atmospheric air-water flows. The model was then compared further to data obtained from rectangular channels at high system pressures for steam-water systems. The outcome revealed that the current flow pattern transition criteria could cover a wide range of parameters as well as boiling flow. Hibiki and Ishii (2003) developed correlations for bubbly and cap bubbly flows in large diameter channels with gas holdup smaller than 0.3. They realized that the drift-flux parameters for bubbly flow in large pipes depended on the inlet conditions. If the inlet flow regime is bubbly flow with small and uniformly distributed bubbles, the distribution parameter is:

$$\begin{cases} C_o = exp\left[0.475 \left(\frac{j_g}{j}\right)^{1.69}\right]\left(1 - \sqrt{\frac{\rho_g}{\rho_f}}\right) + \sqrt{\frac{\rho_g}{\rho_f}} \\ C_o = \left[-2.88 \left(\frac{j_g}{j}\right) + 4.08\right]\left(1 - \sqrt{\frac{\rho_g}{\rho_f}}\right) + \sqrt{\frac{\rho_g}{\rho_f}} \end{cases} \quad \text{..... (2.59)}$$

With the first equation in the range of $0 \leq jg/j \leq 0.9$, and the latter for $0.9 < jg/j$. The following equations describe the drift term of this model.

$$\begin{cases} V_{gj} = \sqrt{2}\left(\frac{\sigma g \Delta\rho}{\rho_f^2}\right)^{0.25} (1-\alpha)^{1.75} N_{\mu f}^{-0.562} \\ V_{gj} = 0.0019 \min(D_h^*, 30)\left(\frac{\sigma g \Delta\rho}{\rho_f^2}\right)^{0.25} \left(\frac{\rho_g}{\rho_f}\right)^{-0.157} N_{\mu f}^{-0.562} \end{cases} \quad \text{..... (2.60)}$$

A closure relationship was developed by Choi et al. (2012) for drift-flux parameters that are applicable to an extensive range of conditions. This model was developed to estimate liquid holdup using a 76 mm diameter pipe. In comparison with the available correlations, their model performed better over an extensive range of situations. They realized no work had been done considering Re>1000. The Co within this range tended to vary from 1 to 1.2. However, unfortunately, there has not been a dataset of viscosity to validate the transition region between the two patterns. The disparity in the distribution parameter with Reynolds number resulted in the new closure relationship correlation merging, Fabre, and Line (1992). This is a function of Reynolds number and Ishii (1977), which is relatively simple and accurate, as given below:

$$C_o = \frac{2}{1+(\frac{Re}{1000})^2} + \frac{1.2-0.2\sqrt{\frac{\rho_G}{\rho_L}}(1-\exp(-18\alpha_G)}{1+(\frac{1000}{\mathrm{Re}})^2} \quad \text{..... (2.61)}$$

2.9 Factors Affecting the Formation of Flow Regimes

The formation of a particular flow pattern to some extent is dependent on various parameters. These parameters include; the gas and liquid flow rate, the void fraction, the physical properties of the phases, the geometry and inclination of the pipe and finally the gas and liquid velocities.

2.9.1 Mass Flow Rate

This Mass flow rate comprises both the liquid and gas flow rate. It is one of the determining factors of flow patterns in two-phase flow. It is the volume of oil and gas

that is introduced at the inlet and flowed through the pipe. As the gas flow rate increases, different flow patterns are observed. For example, when the gas flow rate iincreases in the presence of bubbly flow, slug flow is likely to be observed. Churn flow occurs when there is an increase in both the liquid and gas flow rate in the presence of a slug flow. The size of the Taylor bubbles increase and causes instability, which results in the breakup of these bubbles. The annular flow regime is entered as the gas flow rate is increased in the churn flow regime.

2.9.2 Physical Properties of the Phases

One of the factors that determine the flow regimes formation is the effect of fluid properties on the flow. A number of authors have studied this over the past 50 years. The studies on flow characteristics were carried out in vertical and horizontal pipes. The physical properties included viscosity, density and surface tension.

Davies and Taylor (1950) conducted one of the first researchwork to determine the viscous potential flow analysis of cap bubbles and discovered that, the terminal rise velocity was related to the curving radius of the cap bubble. They concluded that the behavior of Taylor bubbles would differ from a single bubble in static liquid due to disturbances caused by the bubbles in the liquid. The theoretical approach has hence been reduced to the Reynolds number regime.

2.9.3 Pipe Geometry

Pipe geometry concerns the shape, equivalent diameter of the pipe and inclination angle. The flow of fluids from the reservoir to the process facilities is through pipes. These pipes come in different shapes and diameters ranging from, microchannels to large diameter pipes. A considerable number of researchers have reported that the behavior of two-phase flow in vertical pipes and the characteristics of the flow depend on the pipe diameter. The pipe diameters may have an effect on the shape of the bubbles and limit their ability to flow inside the pipes. Thus, there is a link between the behavior of the bubbles and the diameter of the pipe. Pipes with non-dimensional hydraulic diameterare defined as:

$$D_H^* = \frac{D_H}{\sqrt{\sigma/g\Delta\rho}} \quad \text{..... (2.62)}$$

Pipe sizes smaller than 18.5 are considered to be small diameter pipes since stable Taylor bubbles are formed occupying almost the entire diameter of a pipe. On the other hand, if the non-dimensional diameter is equal to 40 then the pipe is considered a large diameter pipe. In this case, the Taylor bubbles formed in the entire pipe section can no longer be sustained. A non-dimensional pipe diameter ranging from 18.5–40 is considered a transition area between the two behaviors.

There are lots of challenges associated with the prediction of flows in large diameter pipes. Amongst such challenges is the surface instability generated at the upper portion of the pipe which results in the breakup of large Taylor cap bubbles into smaller bubbles. The breakup of the large Taylor bubbles results in small Taylor bubbles which have highly distorted surfaces. Thus, preventing the formation of stable slug bubbles. The instability and complexity of these affect all facets of hydrodynamics of the flow. This makes the prediction of this flow regime transition difficult.

Unlike small pipe diameters, large diameter pipes in two-phase systems are of importance due to the challenges encountered in their predictions; significant effort has already been made to develop the tools necessary to help in the prediction of the various flow patterns that exist in these pipe diameters.

2.9.4 Gas Velocity

One of the determining factors of flow patterns is the gas-liquid velocities that exist in transportation pipes and the superficial gas velocity. Gas and liquid are initially injected at the inlet in the two-phase vertical pipe at sufficient rates. Holding the liquid rate constant and increasing the gas rate results in an increase in the gas velocity. This, in turn, increases the bubble size and causes it to rise in the pipe. The increase in bubble size increases the drag force between the fluids.

In small diameter pipes, the increase in the gas velocity results in the formation of slug flow patterns which prevail as the gas bubbles flow upwards. The continual increase in velocity causes the bubbles to increase in size to almost the size of the diameter.

In large diameter pipes, as the liquid and gas velocities increase, a chaotic and bubbly

scene is observed. As the large bubbles move up the pipe, they become unstable at a point and breakdown. In this regime, the gas bubbles tend to create an oscillation motion in the pipe. The subsequent increase in the gas velocity increases the bubbles size to fill the entire column of the pipe, thus resulting in an annular flow.

2.10 The Wire Mesh Sensor

To study the flow behavior of the air-silicon oil mixture, the wire mesh sensor was employed. The sensor was used to determine the void fraction as the mixture flowed through the pipe. The wire mesh was used to determine the capacitance of the two fluids. It is the most convenient instrument used to determine the gas fraction distribution. Most recently, it has been extended to use capacitance measurements so that the instrument can be employed with non-conducting liquids such as organic chemicals or oils.

2.10.1 An Electrode Mesh

The wire mesh was originally developed by Prasser et al. (1998). Its principle is based on the conductivity measurement probe used by Taylor in 1954. The difference between Taylor's work and Prasser et al. is the fact that, Taylor's measurement is point based whereas Prasser et al. is plane or volume measurement. Prasser et al. (1998) developed it based on an older U.S. patent from Johnson (1987). The advantages of this instrument are the measurement of high void fractions, its applicability in opaque liquid and it is less expensive. It also has the capability of measuring high speed and transient flow with temporal resolution up to 5 kHz. Furthermore, the problem associated with measuring high thermal and mechanical load for nuclear reactor applications is overcome. Hence, the technique is known to be one of the best methods for gas-liquid flow measurement. It consists of two sets of wires stretched over the cross-section of a vessel to form a grid of electrodes (Da Silva et al., 2011). Each plane of parallel wires is separated 2 mm from each other. One set of the parallel wires serve as the transmitter and the other set the receiver components connected with the gas-liquid system. Hence, the capacitance between two fluids can be detected and converted to a void fraction.

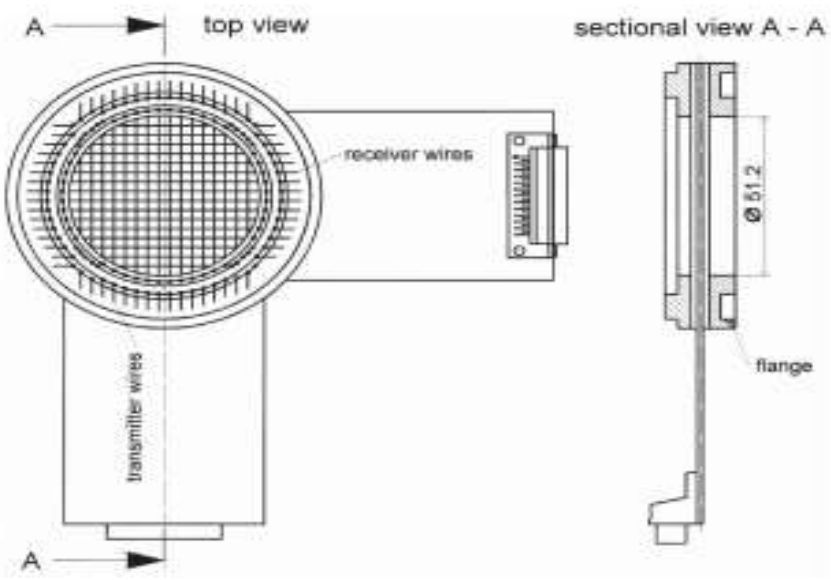

Figure 2.7: A schematic Representation of a Wire Mesh Sensor (Prasser et al., 1998)

2.10.2 The Measurement Principle

The instrument operates on a simple principle. The fluid to be measured is filled in the small diameter between two wires. Two planes of wire grids are placed at a short distance from each other and are positioned perpendicular to each other. A pulse of voltage is supplied to the transmitter. If the pulse supplied to one of the transmitters arrives at a receiver plane, it is supposed that the crossing point is occupied by the conducting phase (water). This measurement is then carried out for the remaining crossing points of the wires of the two planes. Finally, the holdup is obtained by subtracting the signals received at the receiver from the total signals sent out.

2.10.3 The Sensor

As discussed earlier, the sensor is able to measure the conductivity of a plane. The figure below is a diagram of the mesh system. Electrical pulses are transmitted through four wires in a plane which are located within a small distance below the top plane, perpendicular to the transmitter wires, separated 2mm apart. The top and bottom planes represent the transmitter planes. Each of the layers has eight wires of stainless steel with a 100 µm diameter and spaced 3.25 mm apart. The local capacitance in the gaps of the

crossing points is measured with the associated electronics applying a 5 MHz sinus signal at high recurrence level through a multiplexed approach. Each of the measured signals reflects the composition of the flow within its related sub-region, i.e. the crossing point serves as local phase gauge. The data obtained from the sensor thus represents the void fraction over the cross-section hence no need for reconstruction procedures for tomographic imaging systems. Each image can be measured with a resolution of 1 kHz frame rate. Hence, this technique permits the conception of cross-sectional phase distributions with a high resolution (Da Silva et al., 2011).

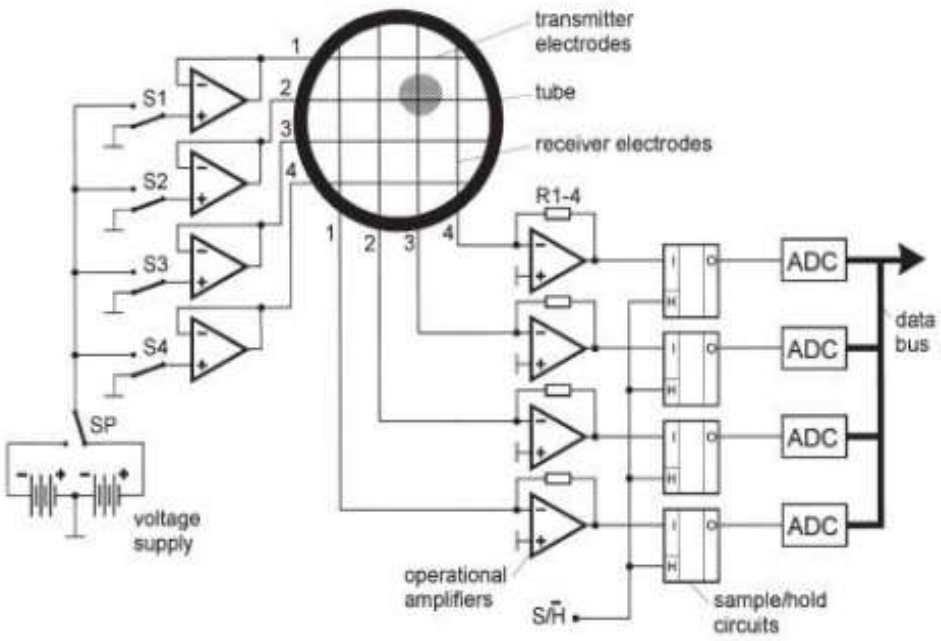

Figure 2.8: Simplified Electrical Wire Mesh Scheme (Prasser et al., 1998)

2.10.4 The Electronics

The pulses consist of alternating positive and negative signals of equal size to avoid electrolysis. Also, when a conductive fluid is present, the received signal shows transient behavior because of the capacitance of the wires. It is advisable to measure the received signal after the transient behavior is destroyed so that the effect above will be reduced. Again, the suppression of cross-talk was corrected by Presser et al. For a sharp resolution, it is vital that only the wire with a driven current transmit a signal. Since the wires are closely arranged, the tendency of the electrical field being obstructed from

generating signals in the other wires is high, therefore the need to construct the wire mesh is such that the wires have a significantly lower impedance than the fluid between them. This is because crosstalk results in blurring of the signal and it is undesirable. The mode of construction, therefore, will help minimize the effect since there is the absence of driving potential differences between the wires (Bulk, 2012).

2.10.5 Application of Wire Mesh Sensor

Wire Mesh Sensors were developed to increase frame rate, bubble size measurement, gas phase velocity measurement and for measurement at elevated pressures. Recent works show that sensors can be devised with up to 64 × 64 wires, wire diameters of about 0.05 mm, in a variety of diverse cross-section geometries and operating parameters. Wire-mesh sensors with high pressure can be used for temperatures and pressures up to 286 °C and 7 MPa, respectively. The interfering effect of wire-mesh sensors was investigated by high-speed camera measurements, and compared with fast x-ray tomography systems. The results showed that the sensor yields images of an undisturbed flow. The disadvantage of being intrusive is partially compensated by high temporal resolution. It is also less expensive, and simple when compared with other imaging systems.

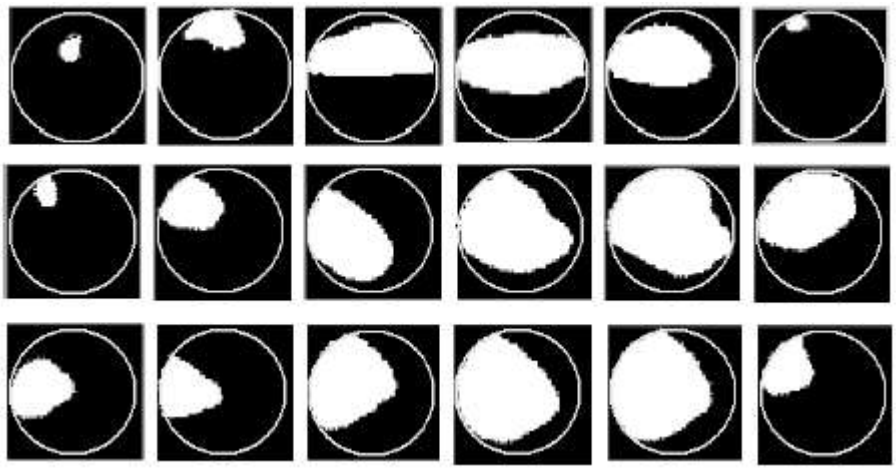

Figure 2.9: The measurement of a Gas Bubble with a Wire-Mesh in a Two-Phase Flow (Murai et al., 2005)

CHAPTER THREE

METHODOLOGY

3.1 Data Acquisition

The data was obtained from experiments carried out by Abdulkadir (2011). He worked on "Experimental and Computational Fluid Dynamics (CFD) Studies of Gas-Liquid Flow in Bends" using an inclinable rig (-5 ^{o} to 90 ^{o}) in the Chemical Engineering Laboratory of the University of Nottingham. The experimental facility was made up of a testing section made from transparent acrylic glass pipes of 67 mm diameter pipes and 6 m long. The fluid mixture considered was an air-silicone oil mixture using a state of the art instrument called a Wire Mesh Sensor (WMS).

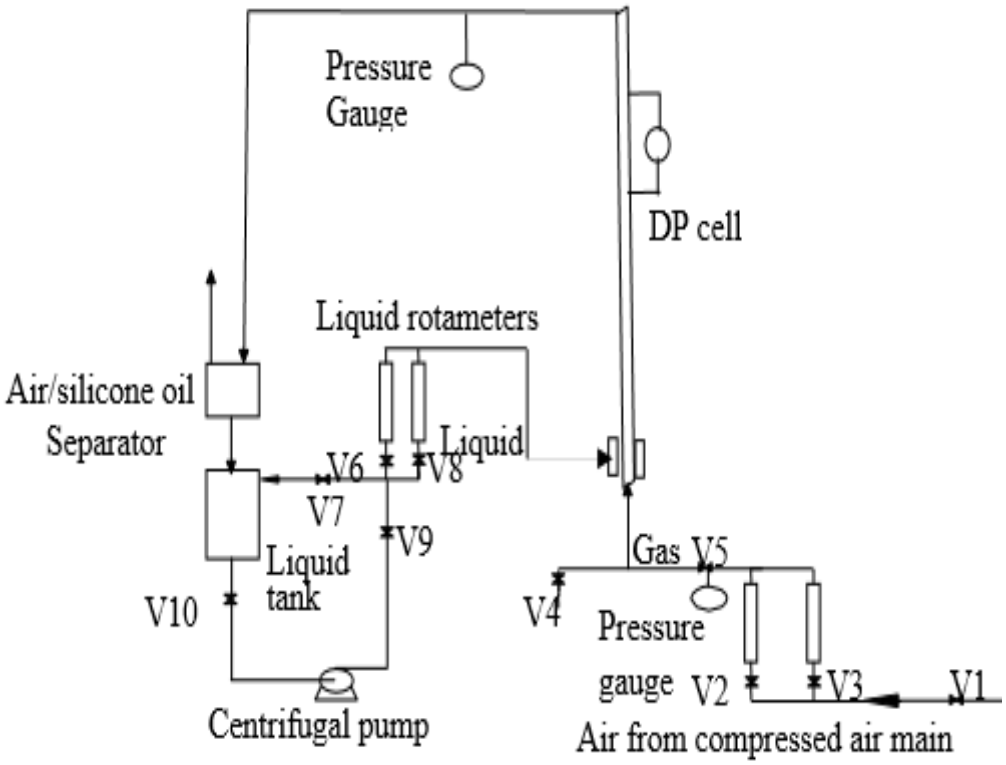

Figure 3.1: A Schematic Diagram of the Flow Facility (Abdulkadir et al., 2015)

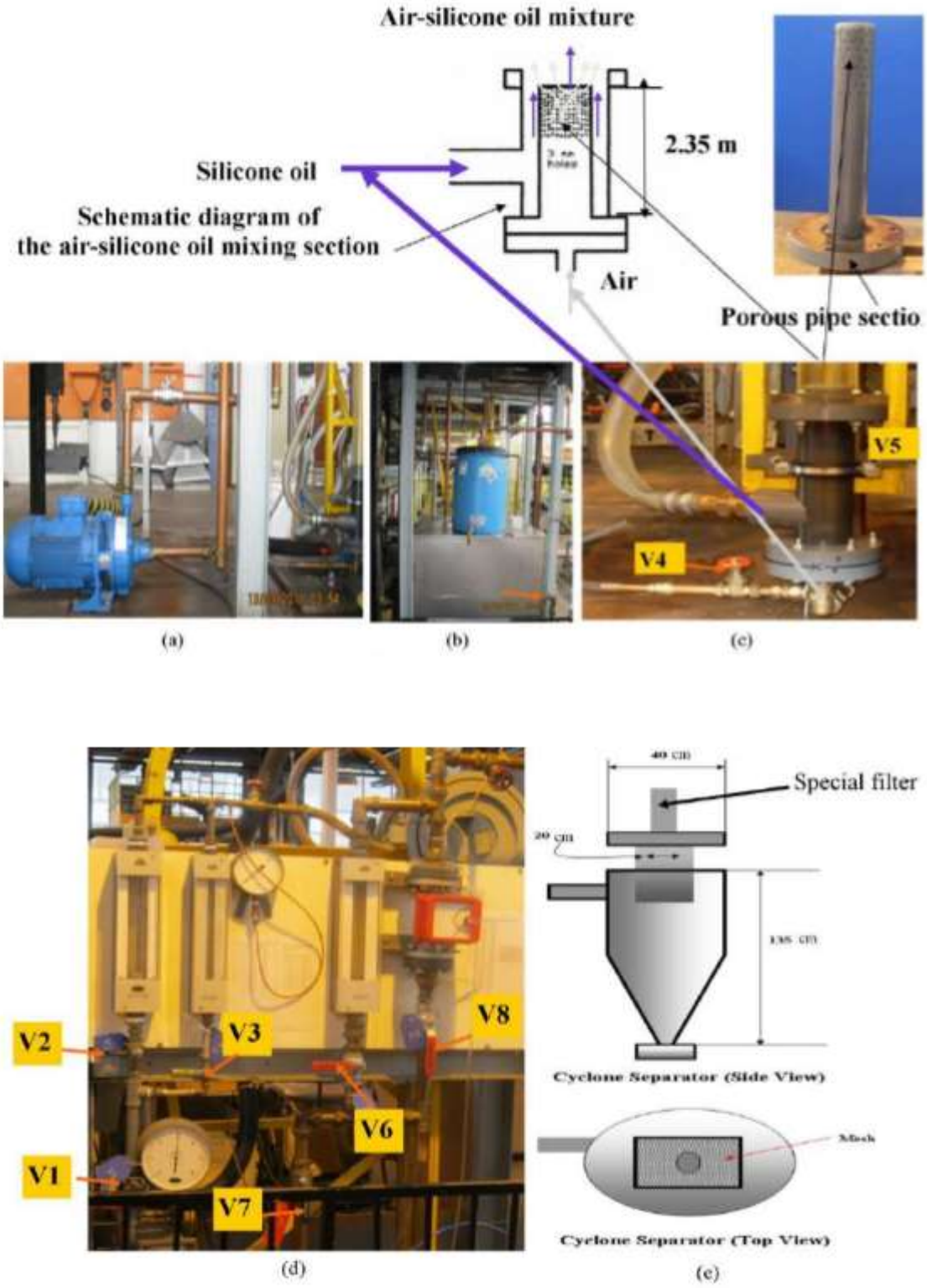

Figure 3.2: The components of the rig (a) liquid pump (b) liquid tank (c) air-silicone oil mixing section (d) rotameters and (e) cyclone separator (Abdulkadir, 2011)

Figure 3.3: Experimental flow facility, (Abdulkadir, 2011)

3.2 Analysis of Acquired Data

The wire mesh sensor was used in obtaining the cross-sectional mean void fractions. These data were analyzed to determine the contribution of gas superficial velocities (0.047- 4.727 m/s), at different liquid superficial velocities (0.047-0.378 m/s) on the void fraction, obtained for both the horizontal and vertical pipes. This was done by making a plot of void fraction against superficial velocity.

An analysis of the effect of inclination angle on the void fraction was performed by, plotting the void fraction against superficial velocity at different inclination angles. This was done to help investigate the impact of the inclination on the void fraction.

Also, the radial phase distribution of the fluids was determined. In this analysis, the void fraction was plotted against the dimensionless radial distance (r/R) to establish the phase distribution at different locations. The dimensionless radial distance was obtained by, dividing the distance at each cross point of the WMS by the radius of the pipe. The range was from 0 to 1, representing the center and wall of the pipe respectively.

Finally, void fraction comparison was made to determine the performance of each of the existing correlations by comparing the calculated void fractions with the experimental data. The comparison allowed the determination of the best correlation applicable to the dataset because all the correlations have their inherent limitations due to the conditions at which each of the data were collected. Eight correlations were analyzed, they included; Nicklin et al. (1962), Hughmark (1962), Greskovich and Cooper (1975), Clark and

Femmer (1985), Hassan and Kabir (1988), Kokal and Stanislav (1989), Hassan (1995), and Cai et al. (1997). The RMSE for the correlations were also calculated to determine the error margin of each of the correlation.

3.3 Identification of Flow Regime using the Flow Pattern Map

The easiest and simplest way of determining a flow regime is by the use of flow pattern maps. This work concentrates on the use of Shoham's (2006) flow pattern map to determine the various flow regimes for the dataset. This was achieved by superimposing Shoham's mechanistic model in V_{SL} against V_{SG} plot of the dataset, and setting the fluid properties, the pipe geometry and the interfacial boundary of the phases, after which the model was run to determine the flow regimes of the experimental dataset.

3.4 Development of Drift-Flux Model

The constitutive approach of drift flux model was adopted in developing this model. It is based on Zuber and Findlay's (1965) one-dimensional model. In this model, a plot of V_G against V_M gave a linear function with a high coefficient of correlation. The drift parameters, C_o, and V_d were then determined as the slope and intercept of the graphs respectively. These plots were made for the individual flow regimes to account for the different conditions governing the transition of each of the flow regimes. The constitutive equation employed for the model generation is given below:

$$V_G = C_o V_M + V_d \quad \text{.....} \quad (3.1)$$

3.5 Model Validation

The model generated was used to compute the void fraction. The drift parameters from five existing correlations were determined and used to calculate the void fraction. These values were then compared with the experimental void fraction to determine how best these correlations agree with the data. After the calculation of the void fractions, a cross plot was made. Again, the RMSE was calculated for the models to determine their

performances. The model was again validated with the other models to determine how best they agree with the proposed model. The equation used for the void fraction calculation is shown below:

$$\varepsilon = \frac{U_{SG}}{C_o U_M + V_d} \quad \text{..... (3.2)}$$

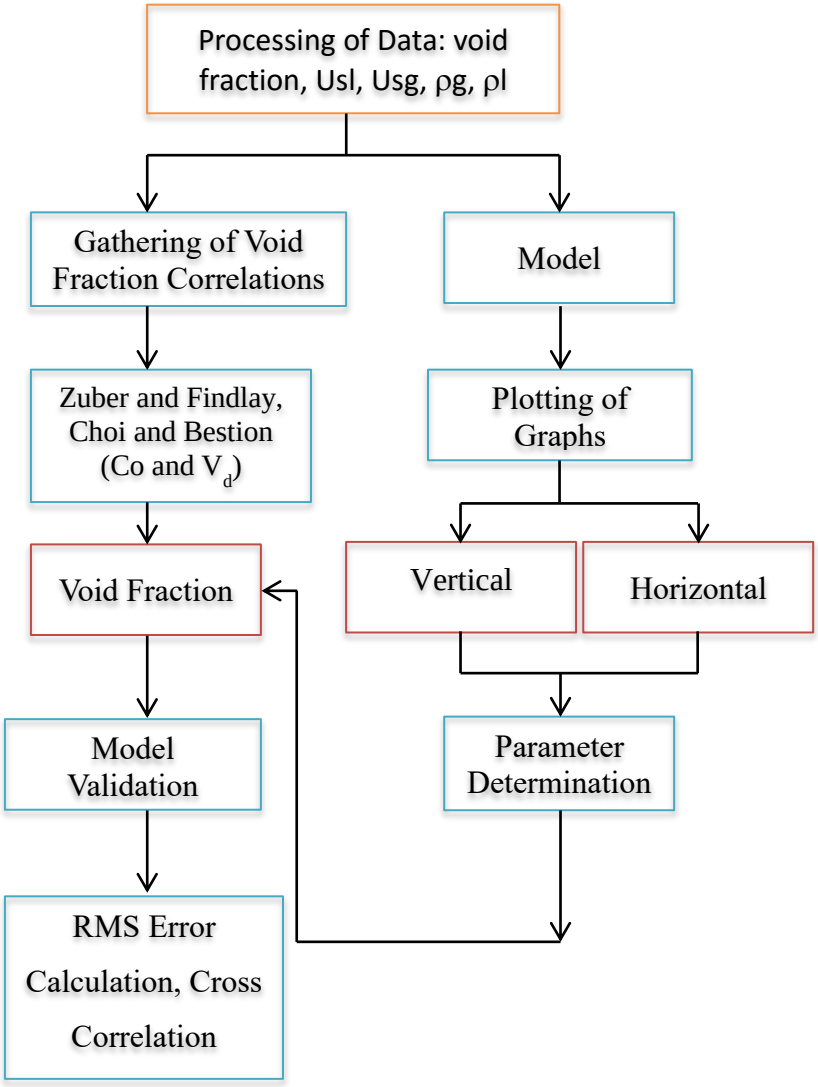

Figure 3.4: Flow Sheet of the Generated Drift Flux Model

CHAPTER 4

RESULTS AND DISCUSSIONS

4.1 The Effect of V_{SG} and V_{SL} on Void Fraction

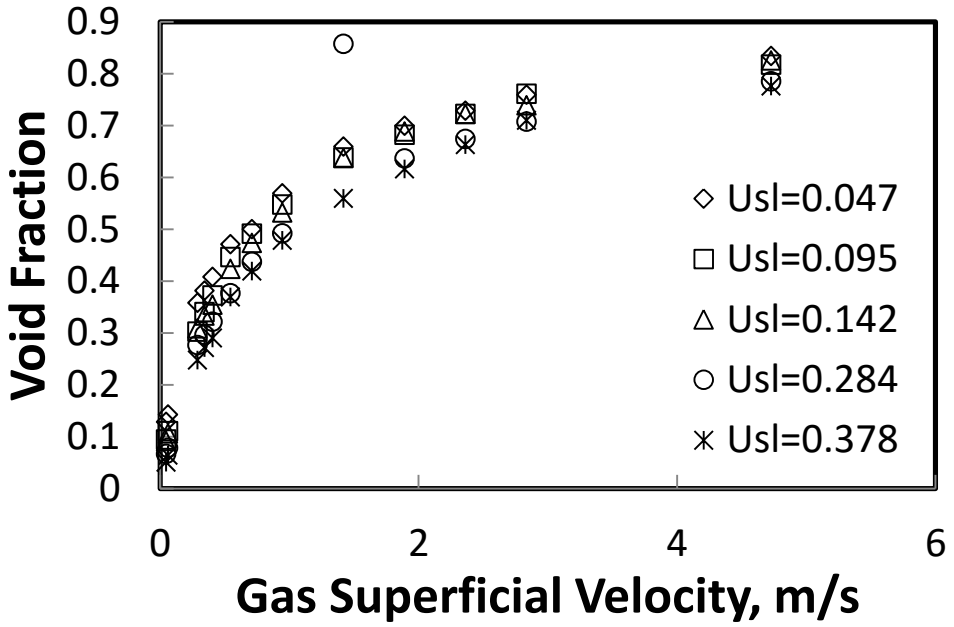

Figure 4.1: Cross-Sectional Void Fraction with Gas Superficial Velocity at Different Liquid Superficial Velocities for the Vertical Pipe

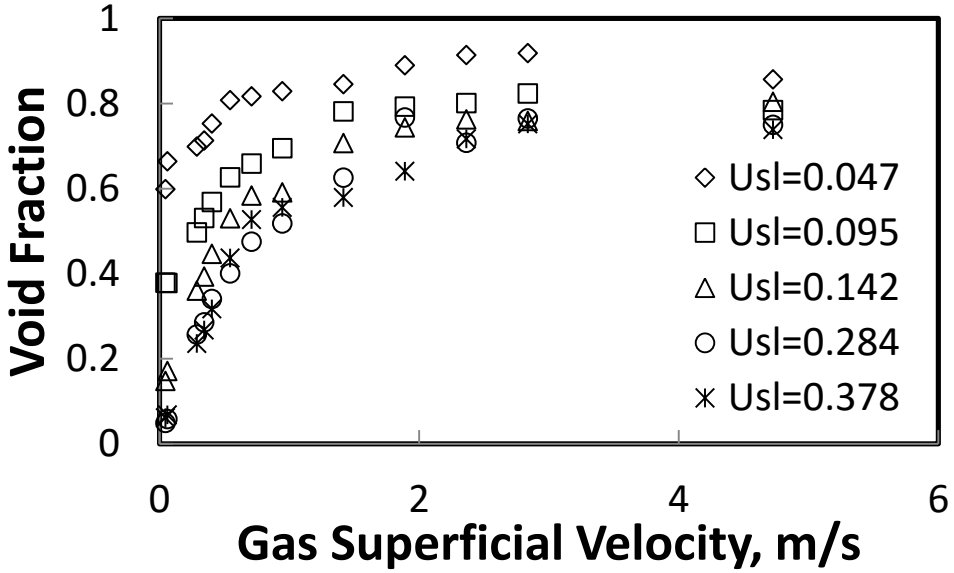

Figure 4.2: Cross-Sectional Void Fraction with Gas Superficial Velocity at Different Liquid Superficial Velocities for the Horizontal Pipe

Figure 4.1 and **4.2** present the plots of void fraction against gas superficial velocity and liquid velocities for both vertical and horizontal pipes respectively. The plots show that the void fraction increases with increasing gas superficial velocity, and reduces with increasing liquid superficial velocity. Hence, the void fraction is directly proportional to the gas superficial velocity and inversely proportional to the liquid superficial velocity. This is because increasing the gas flow rate causes a corresponding increase in the gas superficial velocity hence, resulting in an increase in the pipe volume occupied by the gas phase. This trend is in agreement with the work of Abdulkadir (2010, 2011 and 2015) and Safa *et al.* (2015).

4.2 The Effect of Inclination Angle on Void Fraction

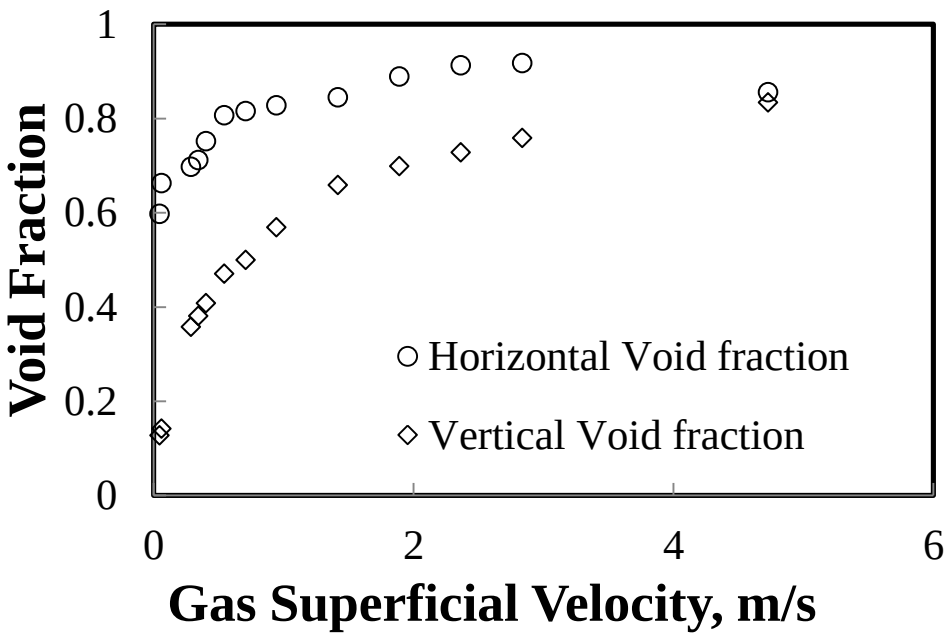

Figure 4.3: Effects of Inclination on Time Averaged Cross-Sectional Void Fraction versus Gas Superficial Velocity at Different Liquid Superficial Velocities for both Pipes

Figure 4.3 represents the effect of the angle of inclination on a void fraction. From the plot, it is seen that there is a general reduction in the void fraction as the angle of inclination is increased. This is because the liquid will naturally flow to the bottom under the influence of gravity and when the inclination angle increases, some part of the liquid will resist the gas flow, hence increasing the amount of water stored in the inclined tubes.

Therefore, the value of void fraction decreases when the inclination angle increases.

4.3 Identification of the Radial Phase Distribution

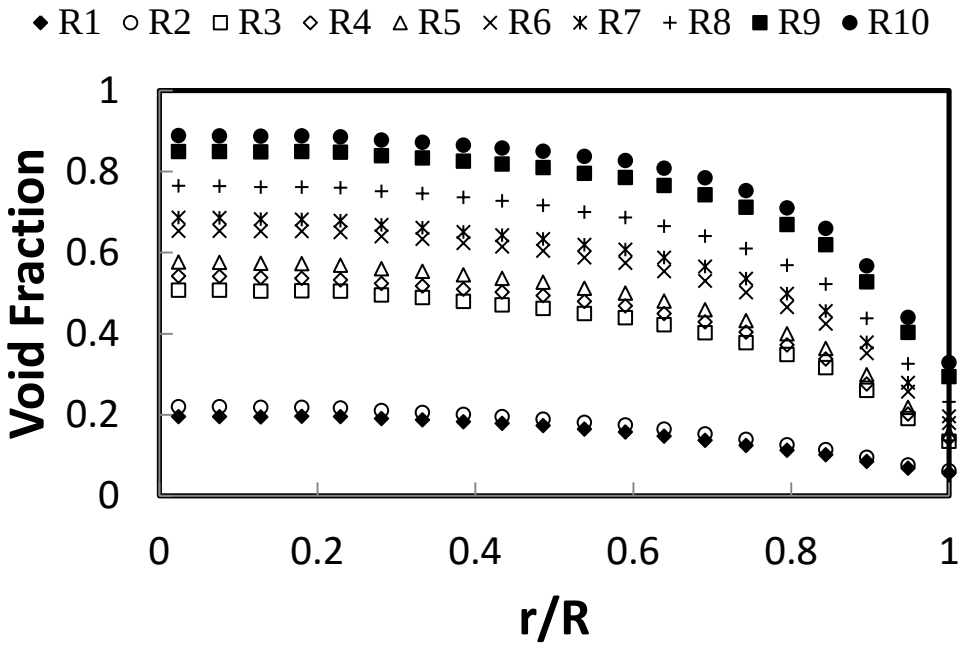

Figure 4.4: Radial Phase Distribution for the Vertical Pipe

Figure 4.4 and **4.5** show plots of void fraction against dimensionless radial distance. From both graphs, the bubbles were observed to be concentrated at the walls and at very low void fractions. That is, there was a wall peak at low void fractions. However, as the gas flow rate increases, there is a corresponding increment in the void fraction which causes the gas bubbles to fall off the walls towards the center of the pipe. This was because at low void fractions the lift forces existing bubbles to flow perpendicular to the direction of the flow thereby causing smaller bubbles to be concentrated on the walls. However, as the void fraction increases, the bubbles collide and coalesce into larger bubbles which cannot be held onto the walls of the pipe due to the existence of the wall lubrication force which tends to push the bubbles towards the center. This analysis is in agreement with the work of Uzochukwu (2013).

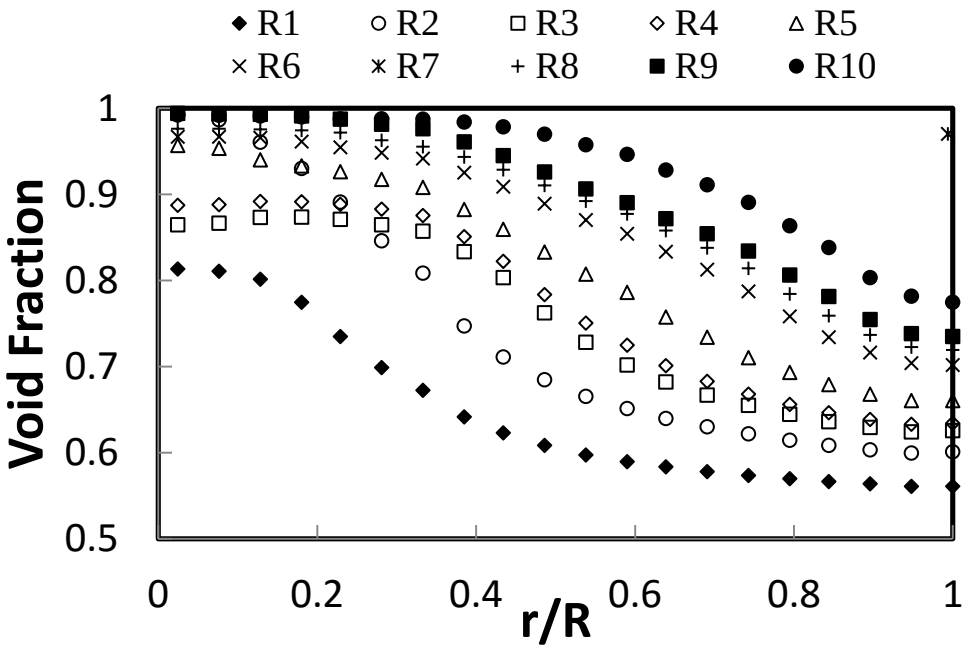

Figure 4.5: Radial Phase Distribution for the Horizontal Pipe

Further analysis of the radial phase distributions was carried out to obtain predicted radial void fraction values. The comparison of both experimental and predicted radial void fractions are shown in **Figure 4.6**. The equation used to predict the radial void fraction developed by Wu *et al.* (2001) is given as:

$$\alpha_r = \bar{\alpha}_g \left(\frac{n+2}{n+2-2_c}\right)\left(1 - c\left(\frac{r}{R}\right)^n\right) \quad \text{..... 4.1}$$

The parameters n and c of equation 4.1 take into consideration the steepness of the profile and void fraction close to the wall respectively. Wu *et al*. (2001) correlation was compared with the dataset obtained for this work. There was an agreement between the experimental and predicted radial void fraction, with the best fit obtained at a gas superficial velocity of

0.061 m/s. From the figures below, it can be seen that the error between the experimental and predicted radial void fraction increases as the gas superficial velocity increases. Thus, their equation may not be applicable in dataset having high gas superficial velocities. This finding is in agreement with the analysis made by Abdulkadir *et al*. (2015).

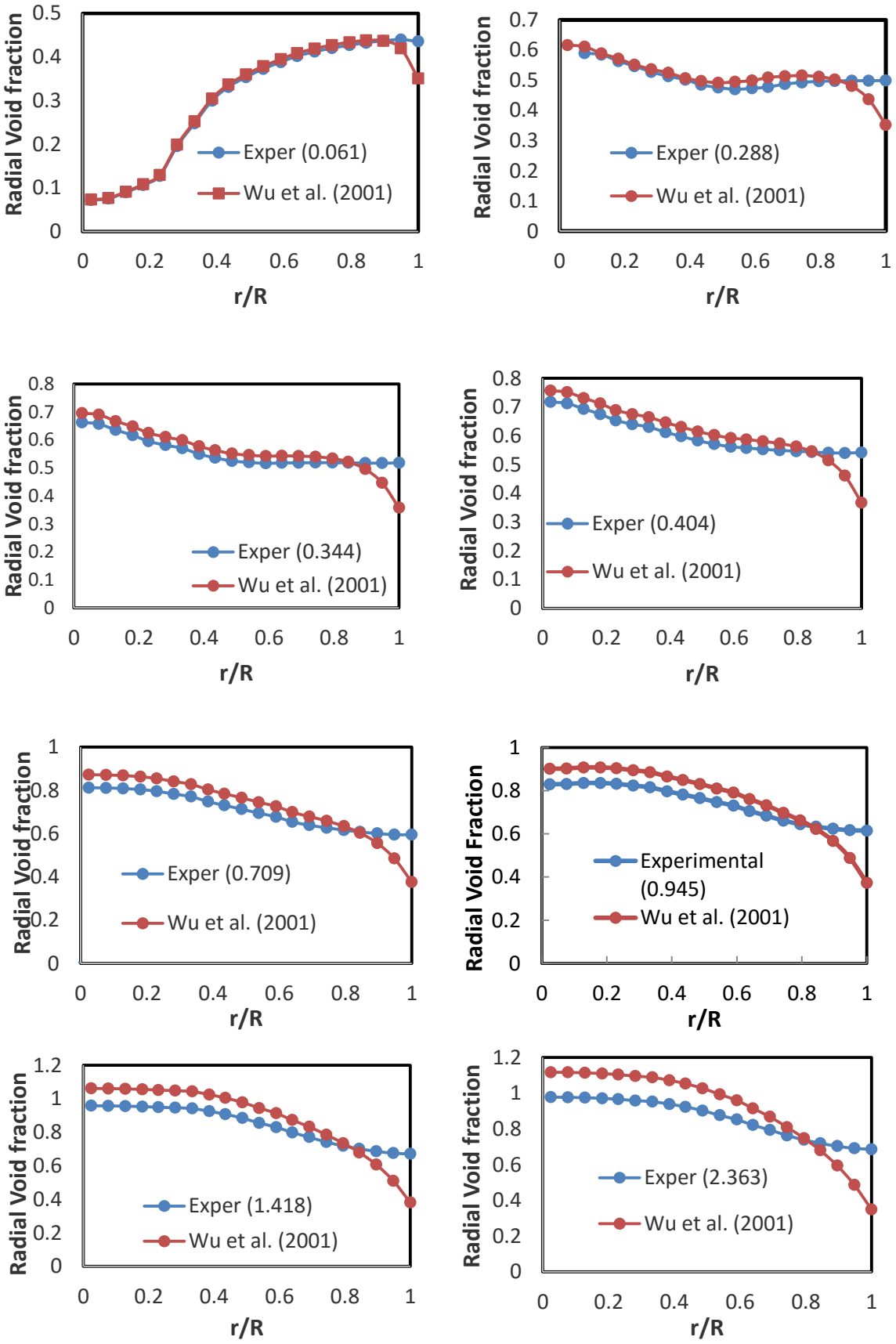

Figure 4.6: Comparison of Experimental Radial Void Fraction with Wu et al. (2001) Equations

4.4 Variation of the n and c Parameter with Gas Superficial Velocity

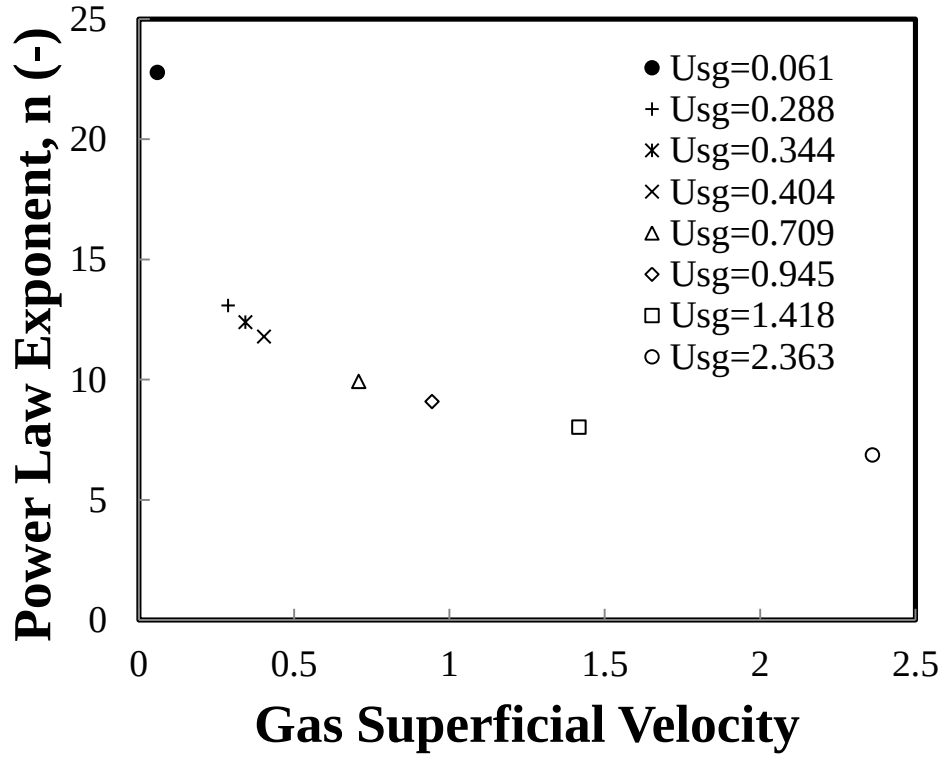

Figure 4.7: Power Law Exponent variations with Gas Superficial Velocity

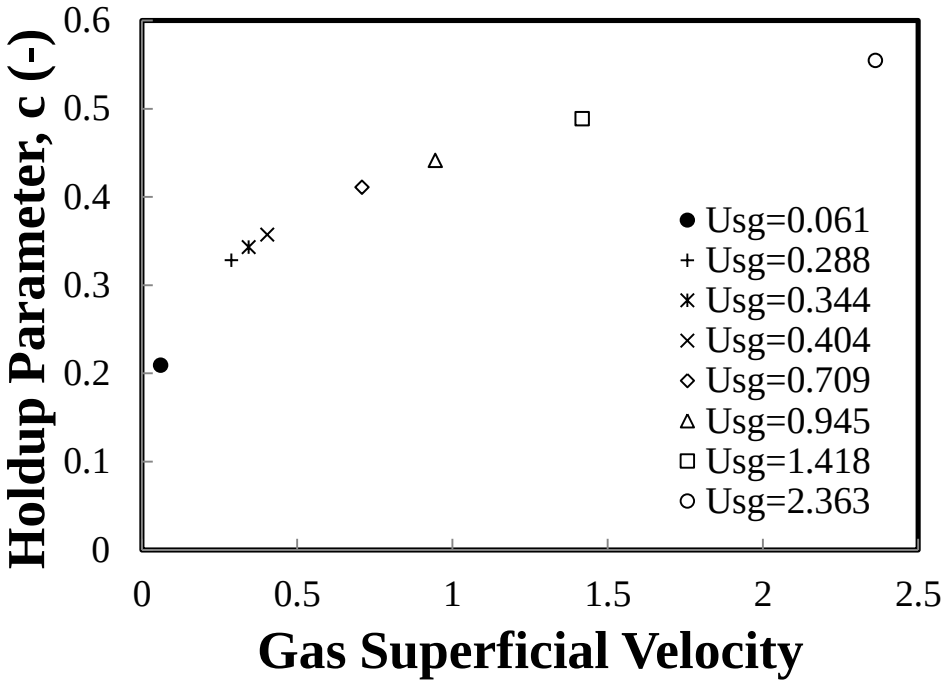

Figure 4.8: Holdup Parameter against Gas Superficial Velocity

The c-parameter defines the amount of gas near the wall. The parameter n and c were calculated and plotted against gas superficial velocity as shown in the figures above. From **Figure 4.7**, it can be seen that as the gas superficial velocity increases, the power exponent decreases. It can thus be concluded that the power exponent is inversely proportional to the gas superficial velocity. Again, the holdup parameter increases as the gas superficial velocity increases as shown in **Figure 4.8**. Hence, the holdup parameter is directly dependent on the gas superficial velocity and the amount of gas near the pipe wall increases with increment in gas superficial velocity. The power law exponent, n, and holdup parameter, c, is in agreement with the work of Abdulkadir et al. (2015), but not in agreement with the work of Uzochukwu (2013). This is because, Uzochukwu's work was performed using an air-water system and fluid properties like, fluid viscosity and density and these affect the values of c- and n-parameters.

4.5 Comparison of Void fraction Correlations

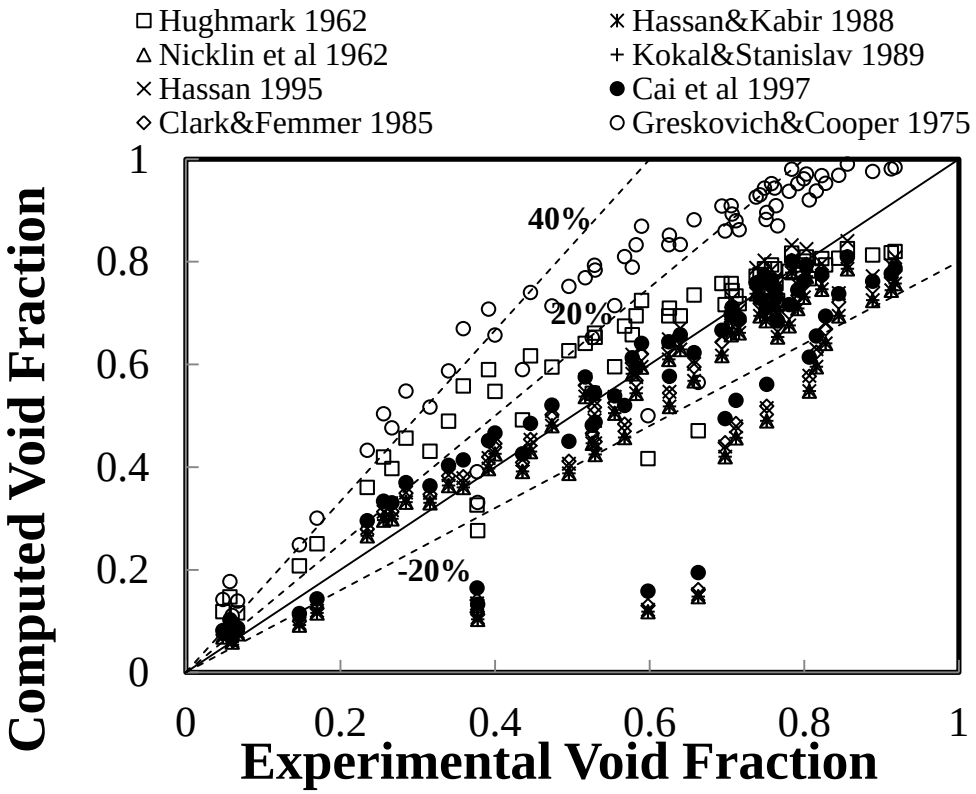

Figure 4.9: Experimental void fraction against empirical models for the Horizontal Pipe

Figures 4.9 and **4.10** are plots made to compare the experimental void fractions of the void fraction obtained from existing correlations for the horizontal and vertical pipes respectively.

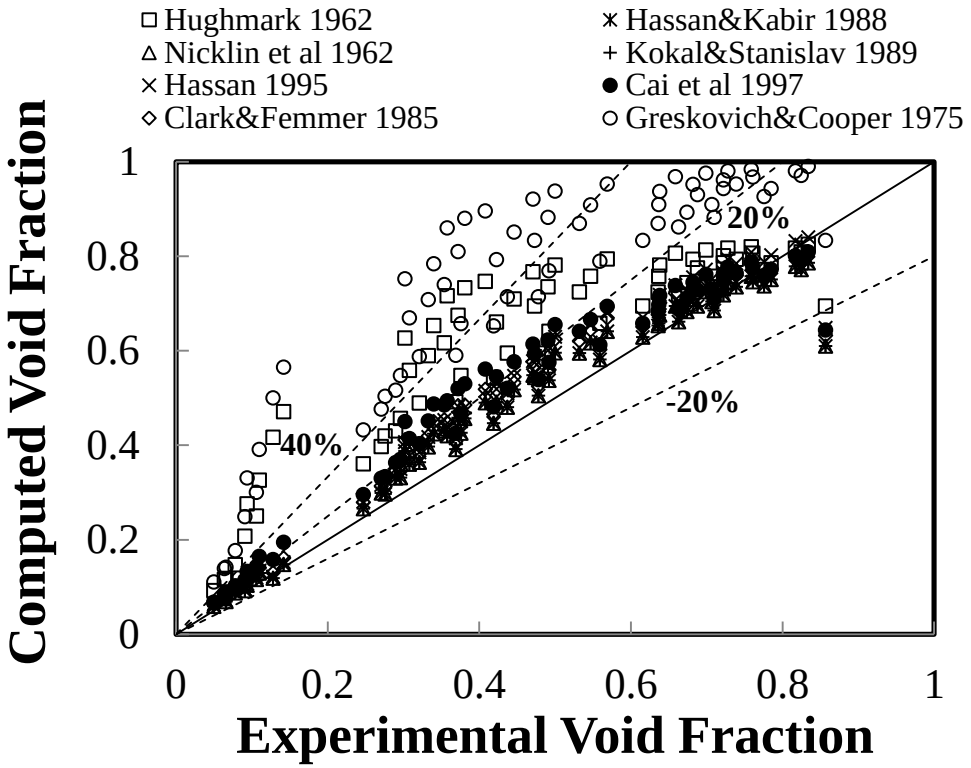

Figure 4.10: Experimental void fraction against empirical models for the Vertical Pipe

The average root mean square error is a statistical tool used to measure the data dispersion around zero deviation. The correlation used in the calculation of this error is given below as;

$$RMS = \sqrt{\frac{1}{n}\sum_{i=1}^{n}\left(\varepsilon_{measured} - \varepsilon_{predicted}\right)^2} \quad \text{..... (4.2)}$$

Where the error is the difference between the measured and the predicted void fractions given by;

Table 4.1: Root Mean Square (RMS) in (%) of Empirical Correlation for the Horizontal and Vertical pipes

Correlations	Vertical	Horizontal
Hassan &Kabir 1988	18	6
Nicklin et al 1962	18	6
Kokal &Stanislav 1989	18	6
Clark& Femmer 1985	20	6
Hassan 1995	21	6
Cai et al 1997	21	6
Hughmark 1962	28	14
Greskovich &Cooper 1975	44	33

This comparison was based on their respective root mean square (RMS) errors to select the best correlation. It is interesting to note that, the RMS error increased with increase in the inclination angle for all the models considered. This is clearly shown in **Table 4.1** and **Figure 4.11**. The best correlations include Hassan and Kabir (1988), Nicklin et al. (1962) and Kokal and Stanislav (1989). The prediction from Greskovich and Cooper gave the highest error.

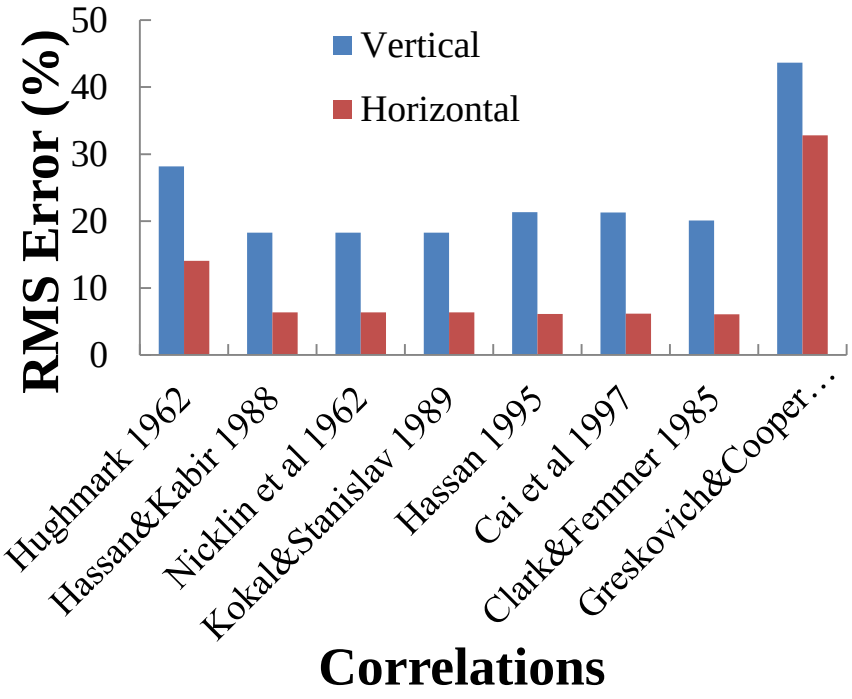

Figure 4.11: RMS of Empirical Correlation

4.6 Flow Regime Identification using Flow Pattern Map

From the flow pattern maps generated for the vertical and horizontal pipes shown in **Figure 4.12** and **4.13** respectively, it is easily seen that only two flow regimes were identified. The regimes were identified using the Shoham's map for the flow in the vertical pipe, whilst for the horizontal pipe, only one point was observed in the stratified wavy section with the dominant flow regime being slug flow. However, the visual observation gave three flow regimes. This was so because the model is a mechanistic model.

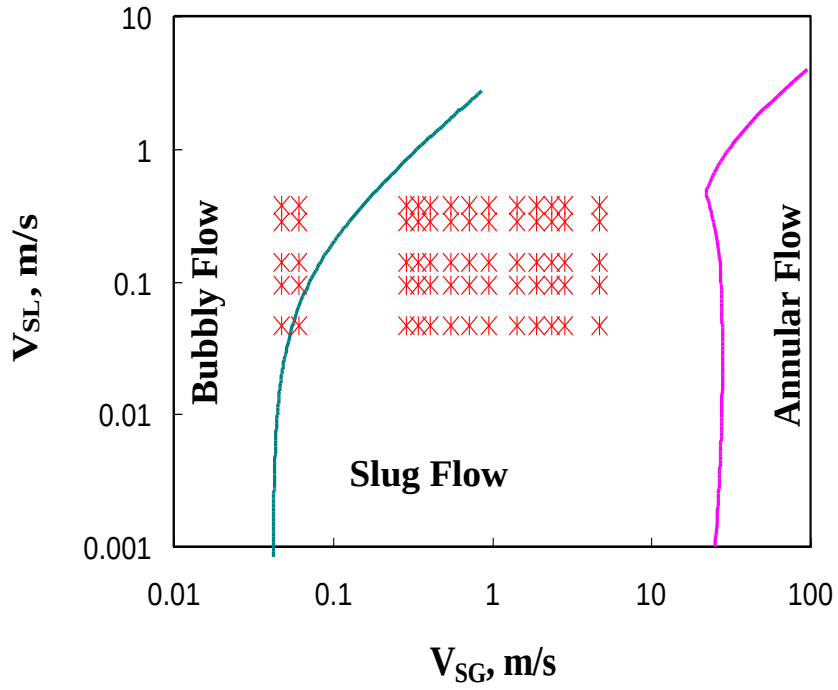

Figure 4.12: Shoham's flow pattern map for experimental dataset for Vertical Pipe

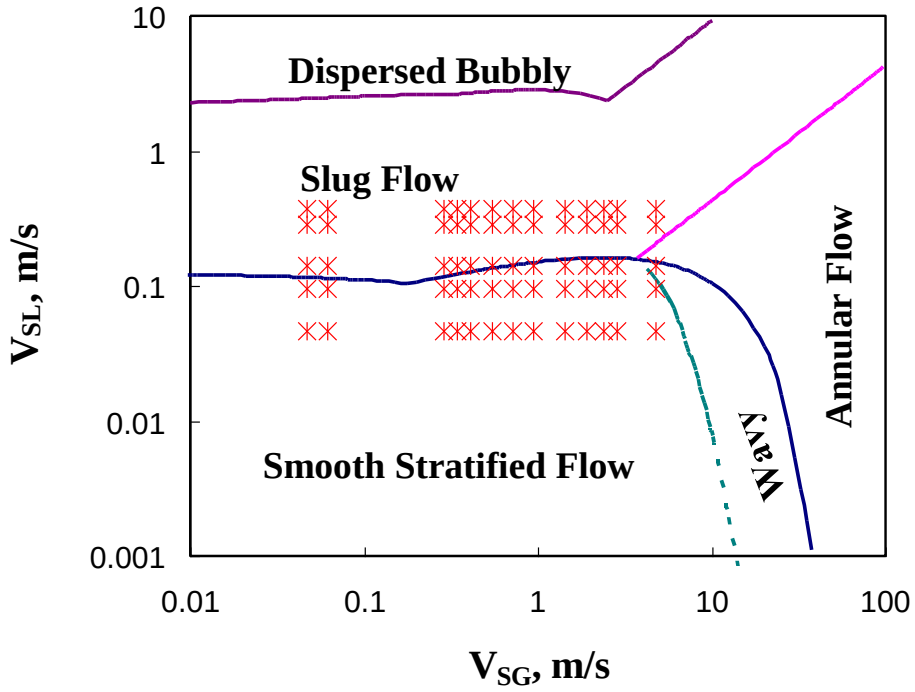

Figure 4.13: Shoham's flow pattern map for experimental dataset for Horizontal Pipe

4.7 Drift Flux Model

A plot of gas velocity against the mixture superficial velocity was made (**Figure 4.14-4.19**). A linear function was obtained with a good correlations coefficient. The C_o and the V_d were determined as the slope and intercept respectively. The values obtained from the various flow regimes were used to generate the model. The data used was compared to various drift-flux models available in literature. The comparison was done to determine the distribution parameter and drift velocity that best fits the data set available.

4.7.1 Drift-Flux Model in Different Flow Patterns

Results from these plots are shown in **Table 3** below, with their correlation coefficients as well as the C_o and V_d obtained. This was because there were different conditions governing the existence of the flow regimes. This observation can be attributed to the concentration profiles in the various flow regimes because of the liquid continuum in the cap bubble, the non-uniform effect which tends to be much stronger than the others.

However, because of the Taylor bubbles and liquid slugs appearing simultaneously in slug flow, the non-uniform effects are stronger, resulting in the C_o value obtained, likewise in the churn flow. We can therefore conclude that, the non-uniform effect in the flow increases with increase in the liquid phase, thereby increasing the C_o value. **Table 4.2** gives a summary of the parameters obtained for the various flow regimes.

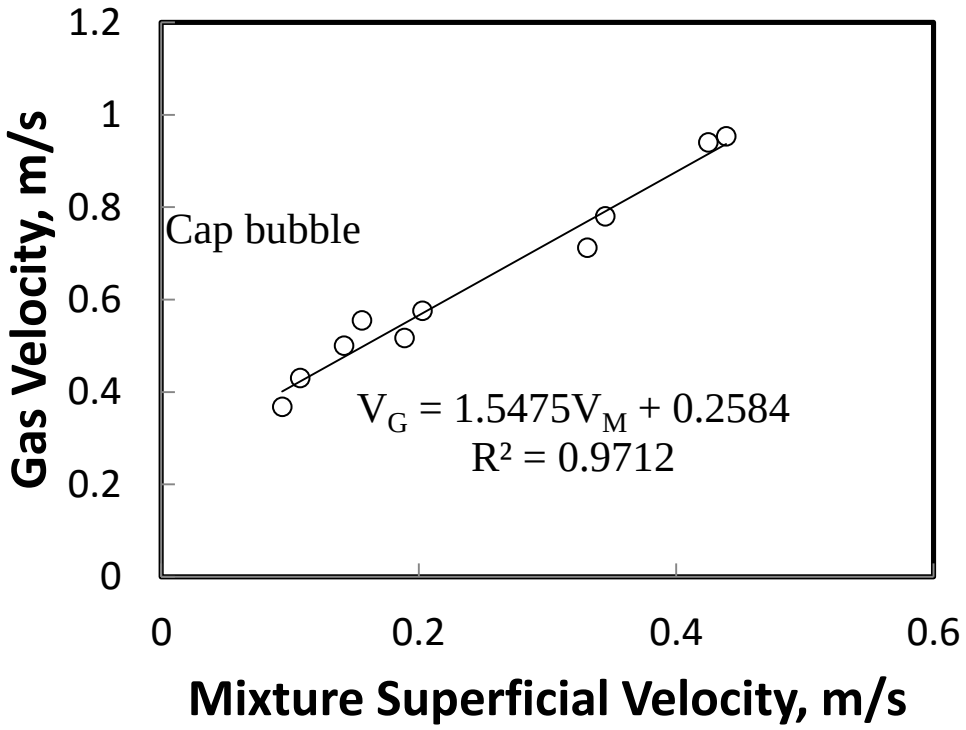

Figure 4.14: Drift-flux Model for Cap Bubble Flow in Vertical Pipe

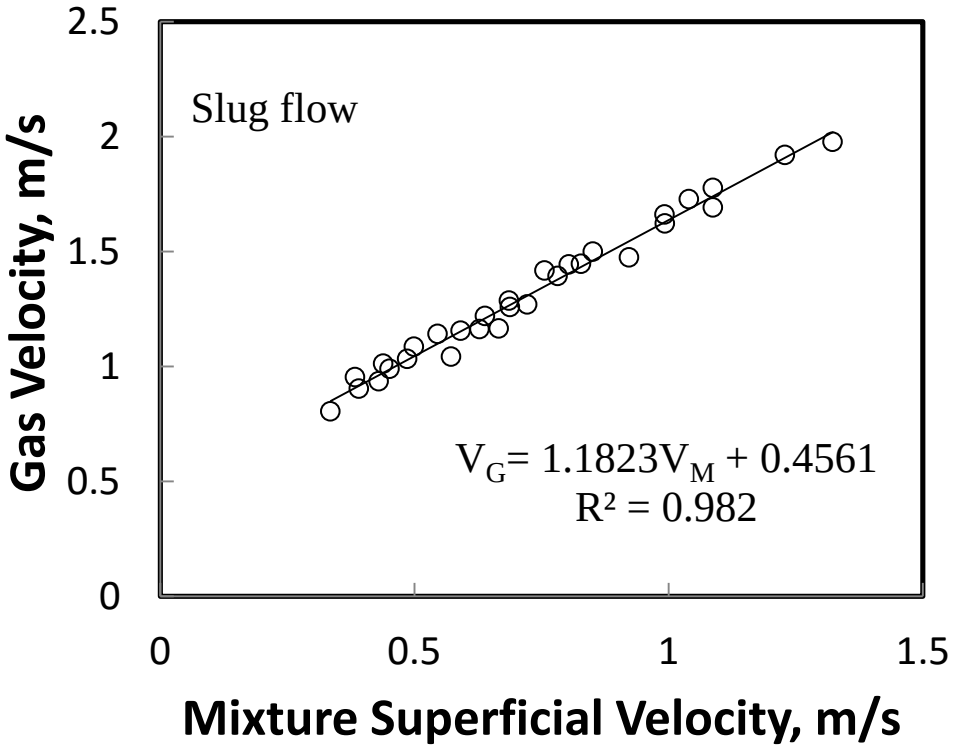

Figure 4.15: Drift-flux Model for Slug Flow in Vertical Pipe

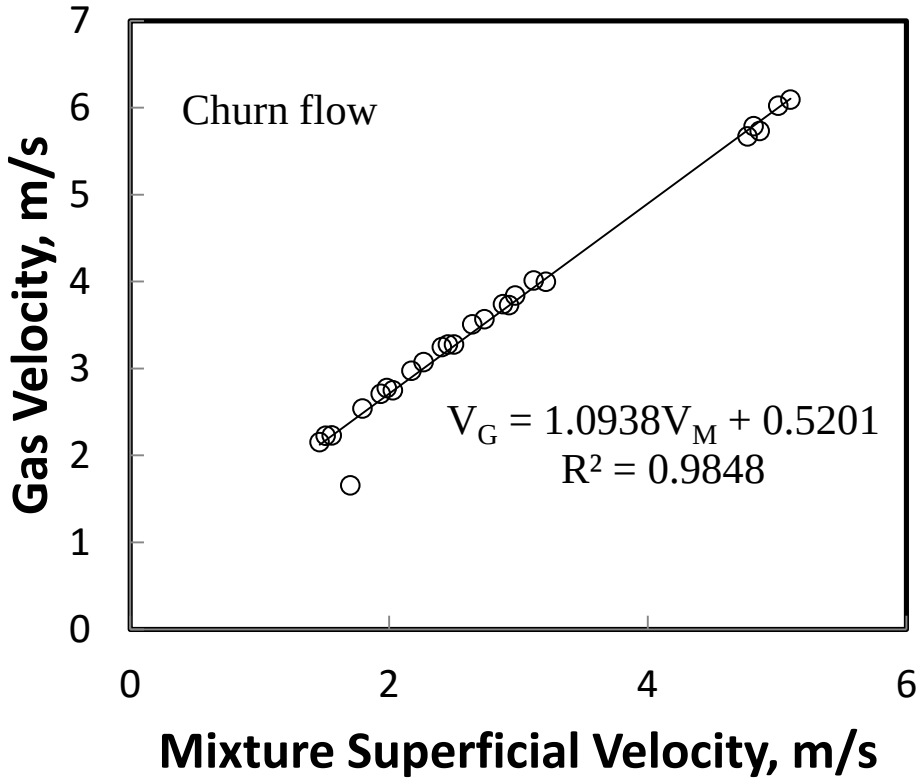

Figure 4.16: Drift-flux Model for Churn Flow in Vertical Pipe

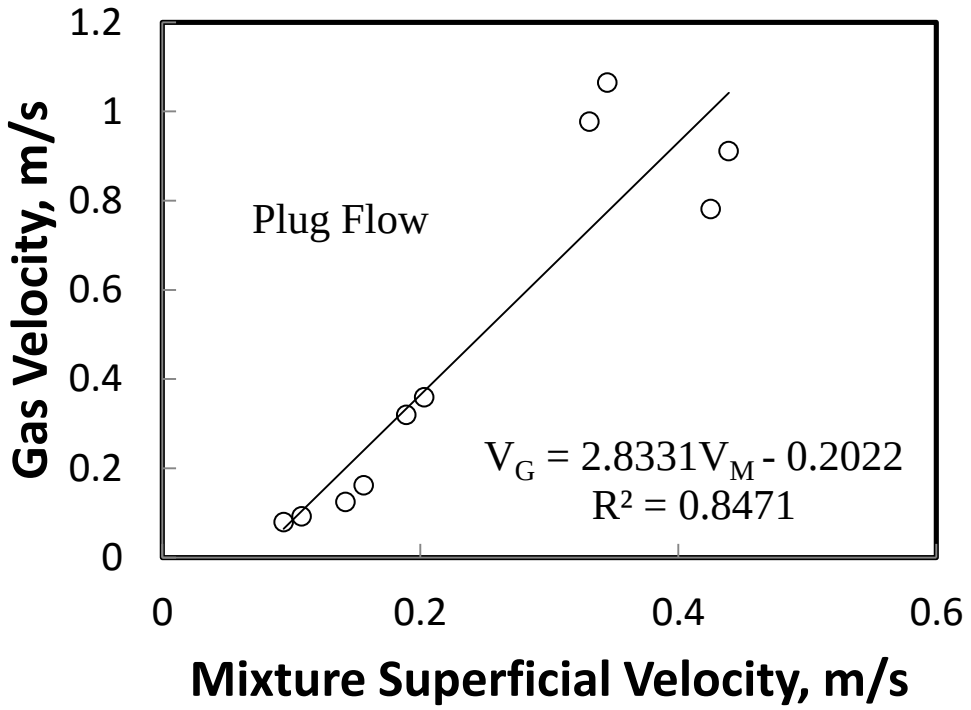

Figure 4.17: Drift-flux Model for Plug Flow in Horizontal Pipe

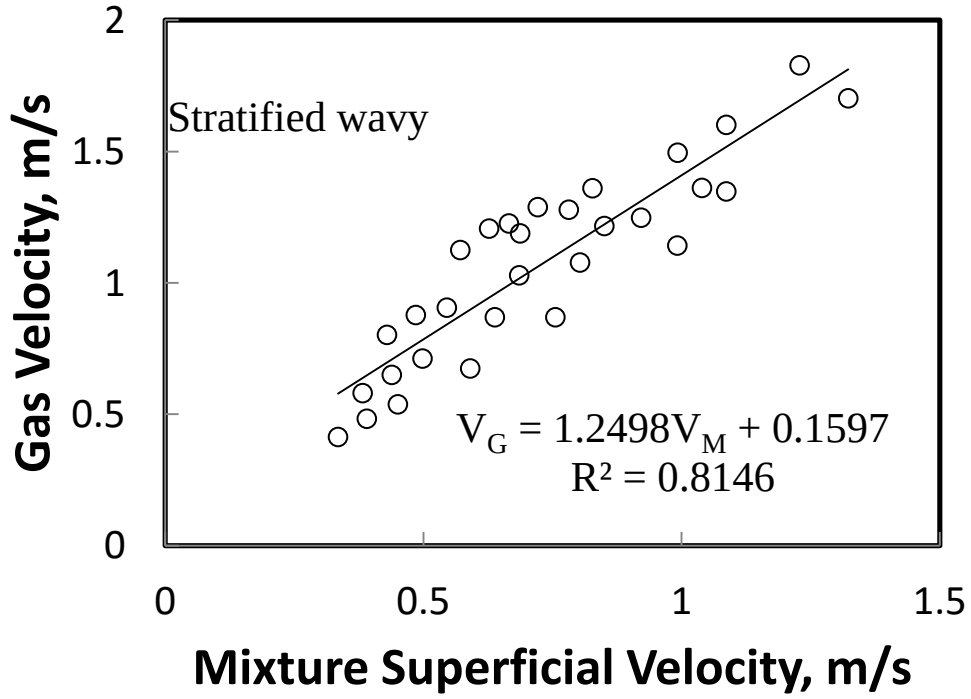

Figure 4.18: Drift-flux Model for Stratified Wavy Flow in Horizontal Pipe

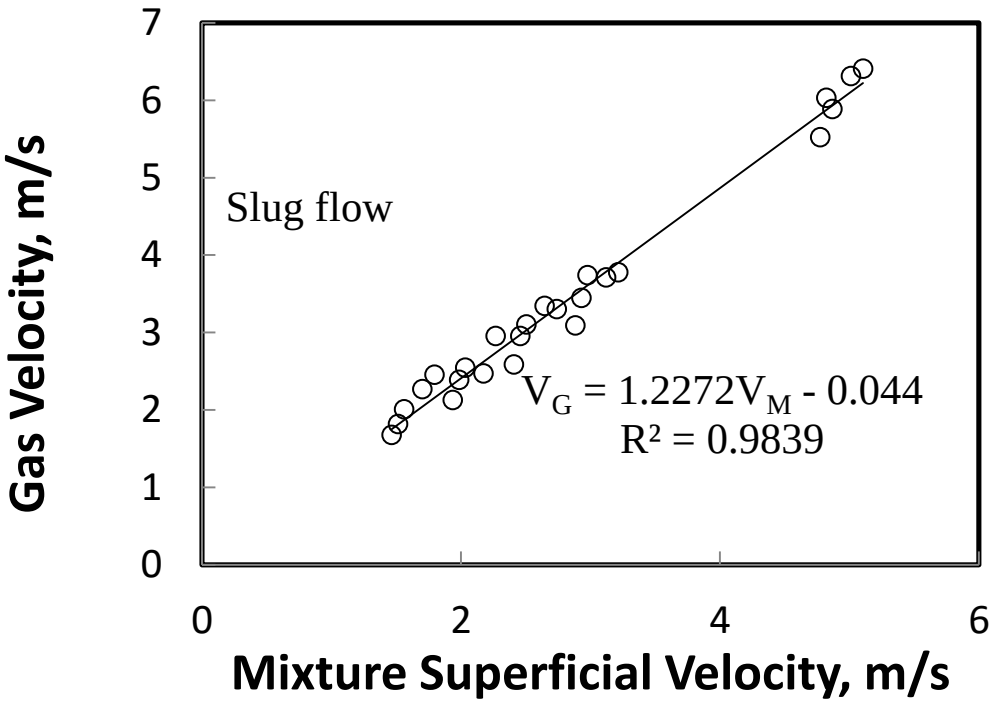

Figure 4.19: Drift-Flux Model for Slug Flow in Horizontal Pipe

Table 4.2: Drift Flux Obtained for the Proposed Model and that of the Existing Correlations

Distribution Parameter, Co	Drift Velocity, Vd	Flow Pattern
1.5475	0.2584	Cap
1.1823	0.4561	Slug
1.0938	0.5201	Churn
2.8331	-0.2022	Plug flow
1.2498	0.1597	Stratified wavy
1.2272	- 0.044	Slug flow
2.27	0.0246	Choi (2012)
1.2	0.0618	Zuber and Findlay (1965)
1	0.3868	Bestion (1990)

1.3	0.7	Mattar and Gregory (1974)
1.08	0.45	Toshiba (1989)

4.7.2 Distribution Parameter and Drift Velocity

Figure 4.20 and **4.21** present the plots made for the distribution parameter and drift velocity against void fraction. There are significant differences in the values of C_o and V_d among the various flow patterns. The general trend observed in these plots is a decrease in Co as void fraction increases whiles, V_d increases with an increase in void fraction. **Figure 4.22** and **4.23** presents the contribution of the void fraction to the formation of a particular flow regime as presented on a flow pattern map with the coordinates of V_M verse α_G. The various flow regimes are differentiated from each other with colours. Considering the vertical flow, at low α_G and V_M, cap bubble is observed. As α_G and V_M increases, slug flow is observed and finally churn flow. In analysing the horizontal flow, plug flow was identified as well as stratified wavy and slug flow.

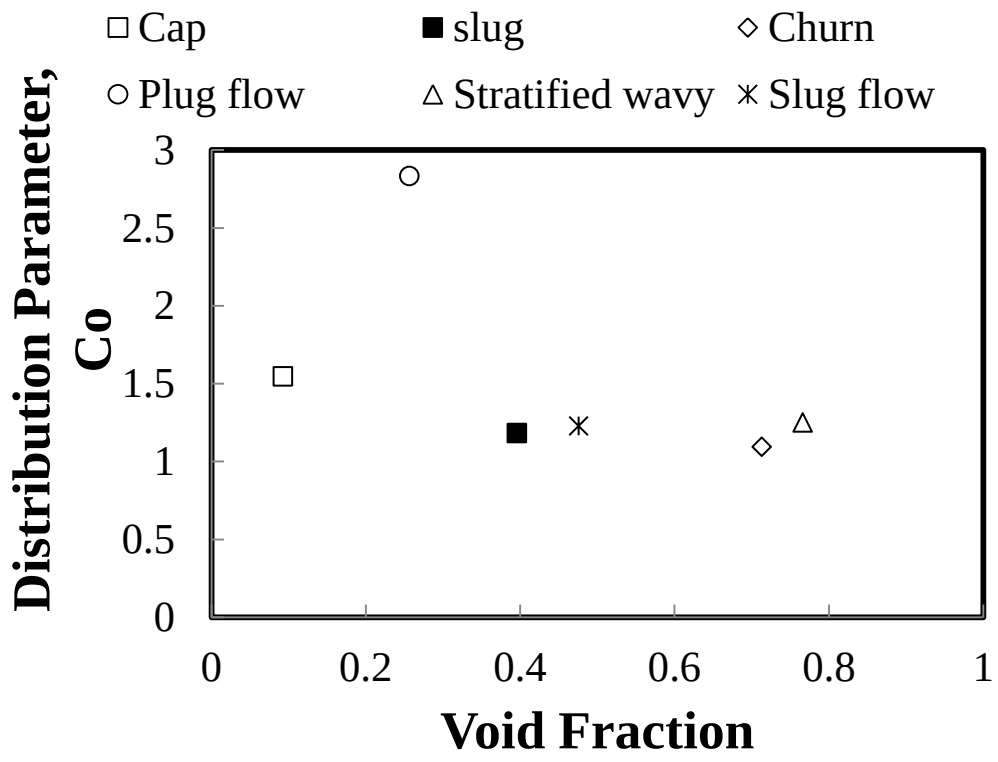

Figure 4.20: Values of Co in different patterns for both Horizontal and Vertical Pipes flow

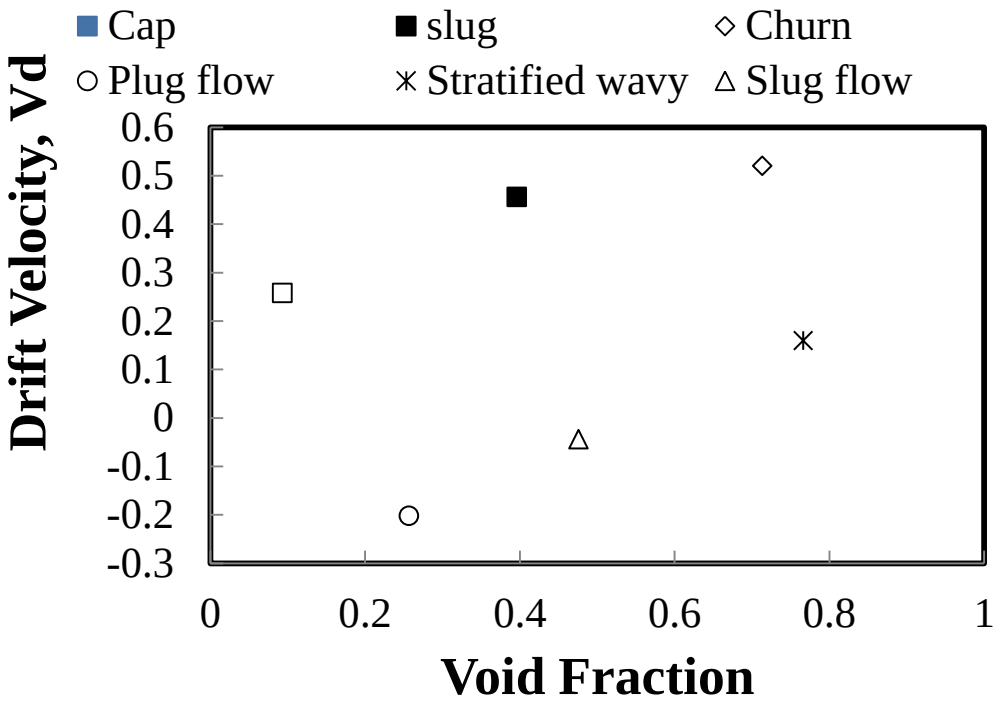

Figure 4.21: Values of Vd in different flow patterns for both Horizontal and Vertical Pipes

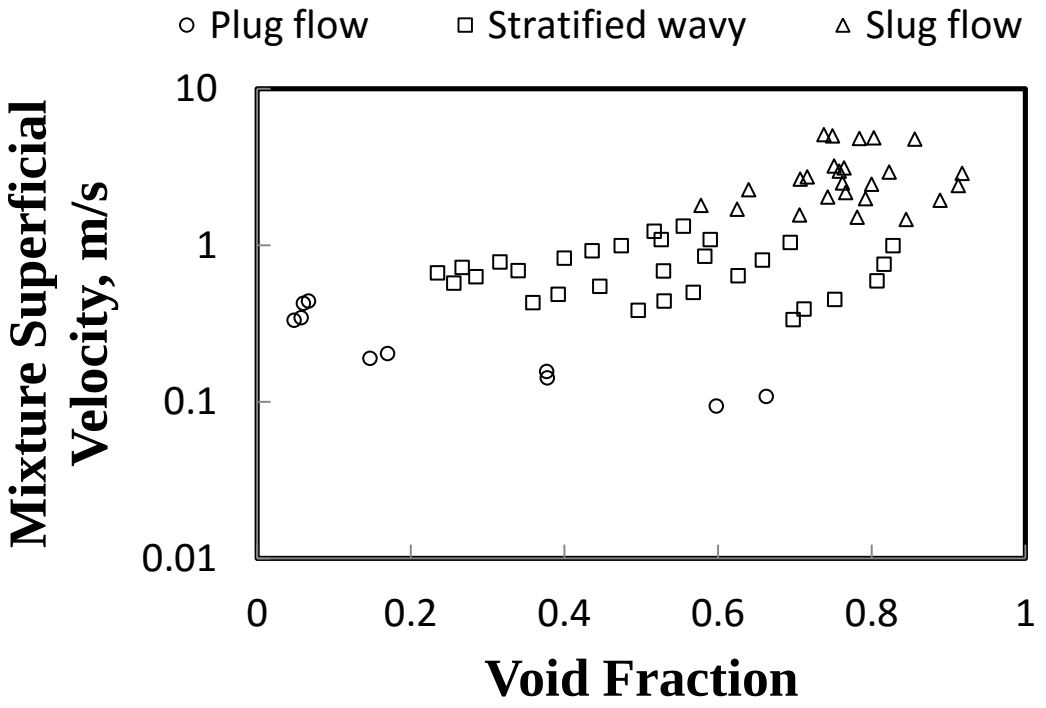

Figure 4.22: Flow pattern map in Coordinates of V_M verse α_G Air-Silicon Oil System, Horizontal Flow

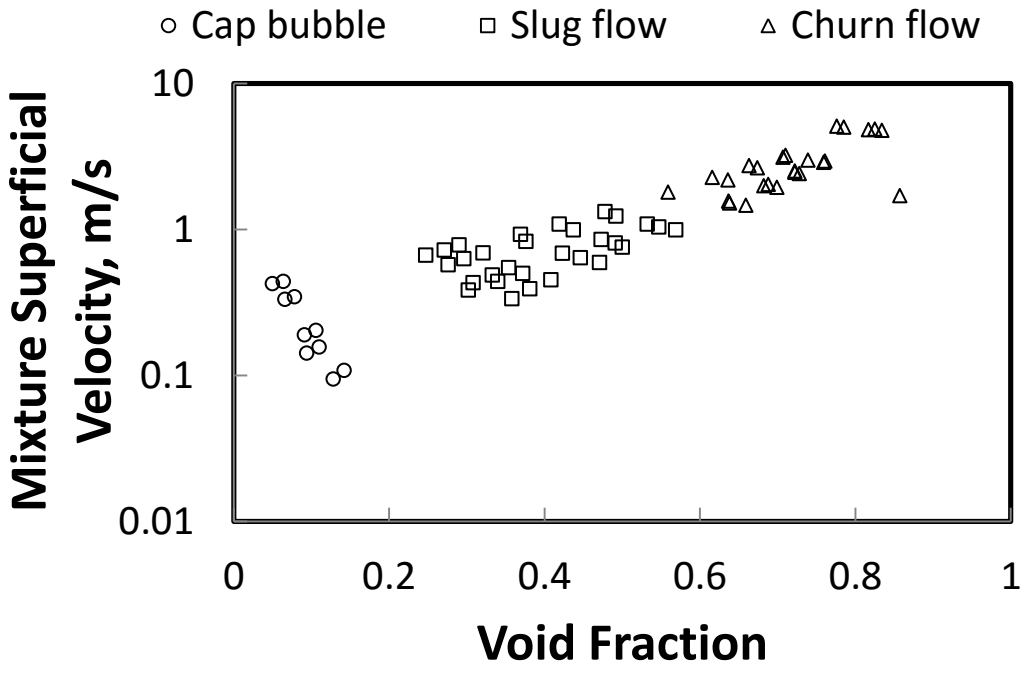

Figure 4.23: Flow Pattern Map in Coordinates of V_M vs. α_G Air-Silicon Oil System, Vertical Flow

4.7.3 Model Validation

The model generated was compared with the experimental data as well as five other existing correlations. The parameter used for the error estimation between the experimental data and the existing correlations is the root mean square error calculated as, the absolute value of the difference between the calculated void fraction and the experimental void fraction. The first step to assess the predictability of the model was to evaluate its performance against the other models available in literature. This is because each model developed is limited under the conditions which the experiment was performed. The void fraction was calculated for five existing models (Choi (2012), Bestion (1990), Zuber Findlay (1965), Mattar and Gregory (1974) and Toshiba (1989), as well as the proposed model. The values were then compared with the experimental data, and their RMSE calculated as shown in **Table 4.3**. The results were then presented on a bar chart. From the plot in **Figure 4.24**, it can be seen that the void fraction calculated from the proposed model had the least RMS error for both pipes. Considering the vertical flow, the next correlation that performed well is Toshiba's model. Zuber and Findlay's model had the highest RMSE, thus it had the poorest performance relative to other correlations. It is therefore not advisable to apply this model to this flow condition.

Table 4.3: Relative error for Proposed and Empirical Correlations

Correlations	RMS Error		Mean	Standard Deviation
	Vertical Pipe	Horizontal Pipe		
Choi	33	42	0.322495	0.108704
Zuber and Findlay	49	30	0.582099	0.026206
Bestion	15	26	0.538593	0.262309
Proposed	3	15	0.471312	0.231684
Mattar &Gregory (1974)	22	39	0.385417	0.196291
Toshiba (1989)	9	27	0.496205	0.238798

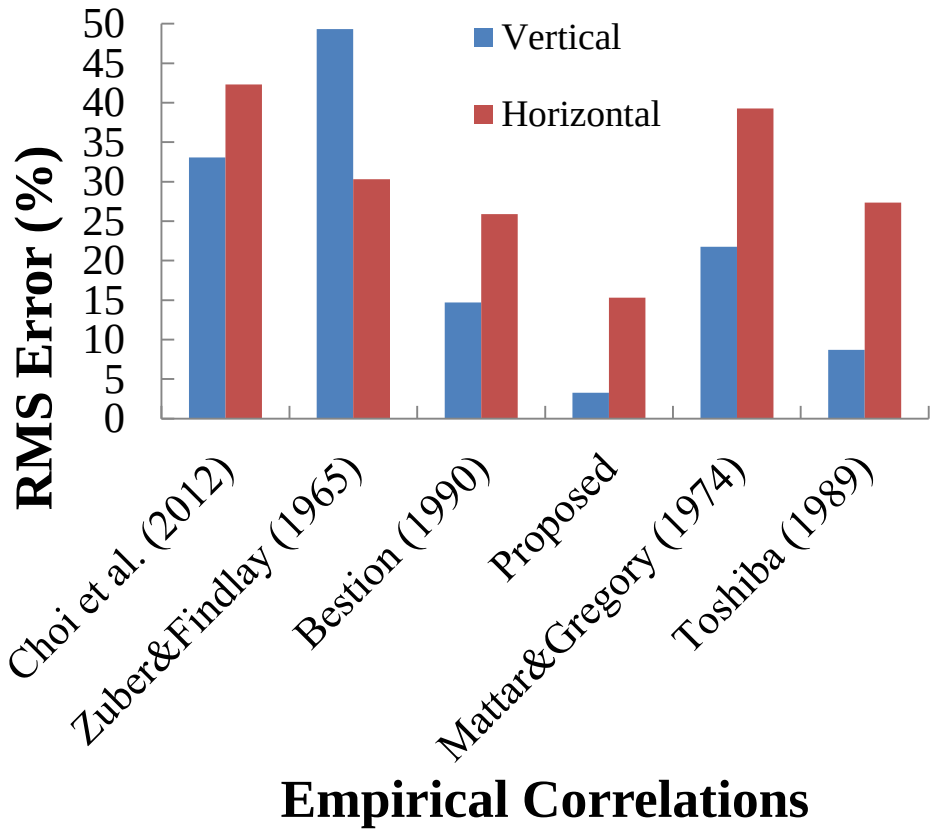

Figure 4.24: RMS Error for proposed model and Empirical Correlations

Also, the plot for the horizontal flow shows that Bestion's model was the next model that performed well relative to others with an RMSE of 26 %. In this case, Choi's model was noted to have the highest RMSE of 42 %, thus having the poorest performance and is not suitable for the horizontal flow for the condition considered.

Figures 4.25-4.36 are a cross-correlation between the experimental data and the models. From **Figure 4.25-4.30**, the proposed model was in perfect agreement with the experimental data. Zuber and Findlay's model agreed with the dataset at high void fraction around 0.8, Bestion's correlation was in agreement at a very low void fraction of about 0.15, whilst over predicting the other points. Choi's model was in agreement at a void fraction of about 0.3-0.4, after which the other points were under-predicted. Mattar and Gregory's model under predicted the dataset within a 20% deviation. Finally, Toshiba's model was also in good agreement with the dataset.

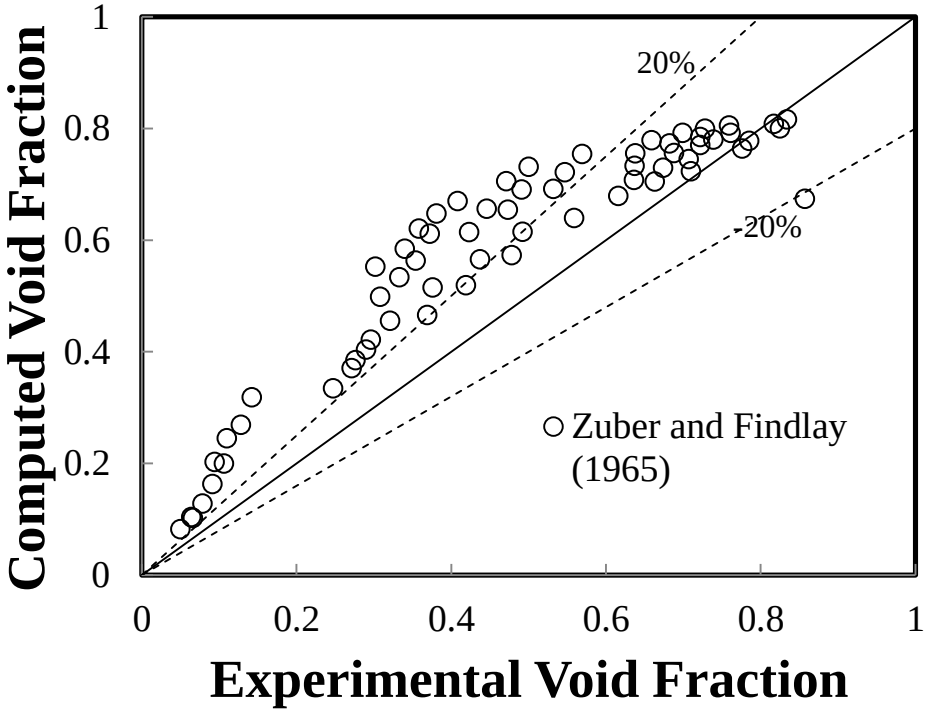

Figure 4.25: Comparison between Experimental Data and Zuber & Findlay (1965) for Vertical Flow

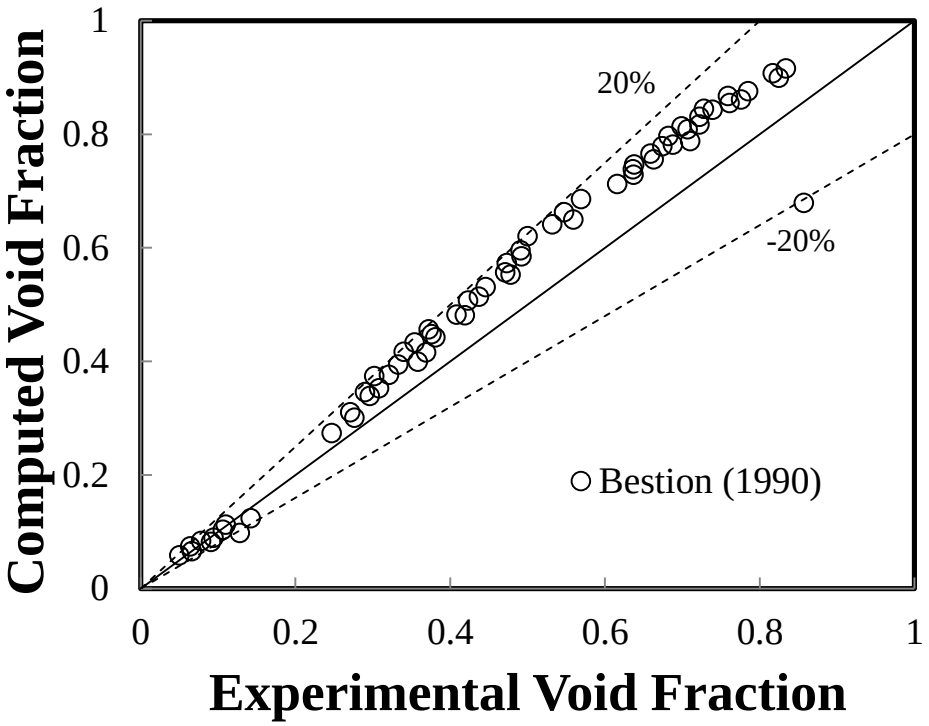

Figure 4.26: Comparison between Experimental Data and Bestion (1990) for Vertical Flow

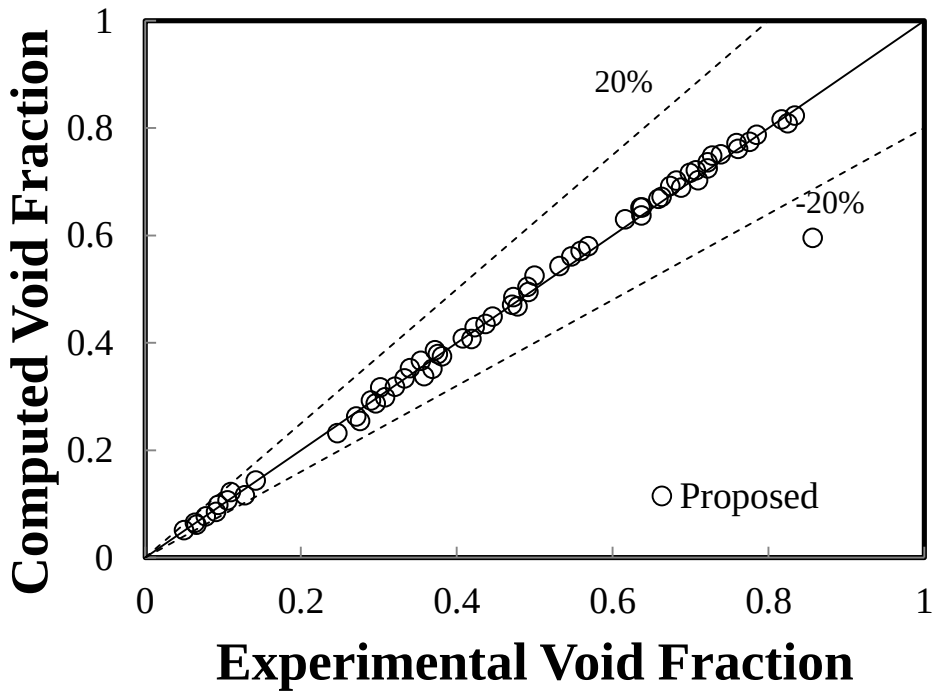

Figure 4.27: Comparison between Experimental Data and Proposed Model for Vertical Flow

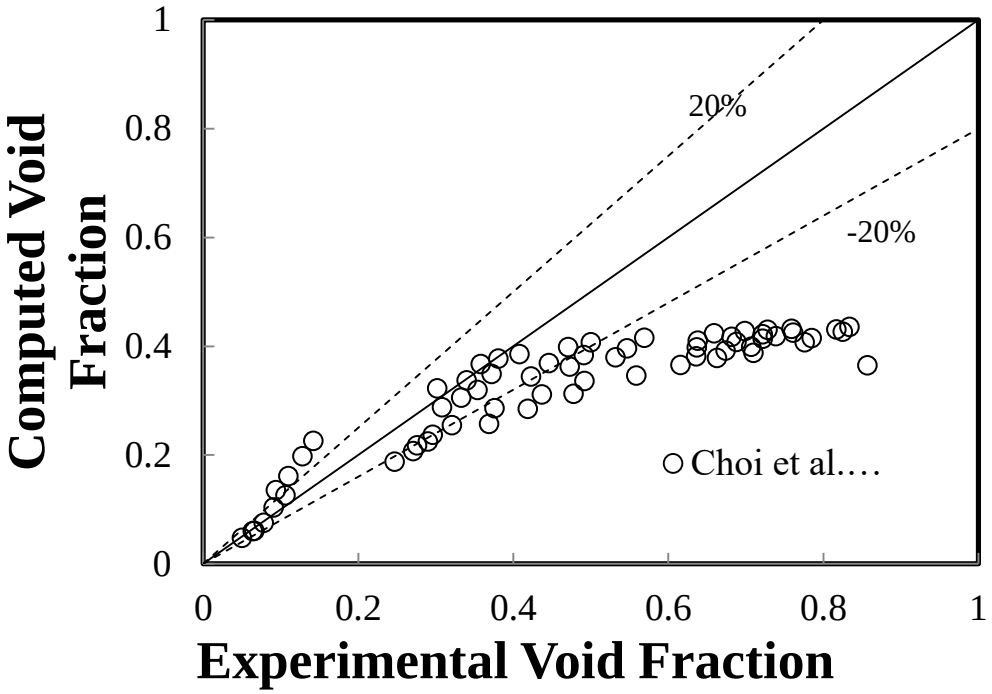

Figure 4.28: Comparison between Experimental Data and Choi (2012) for Vertical Flow

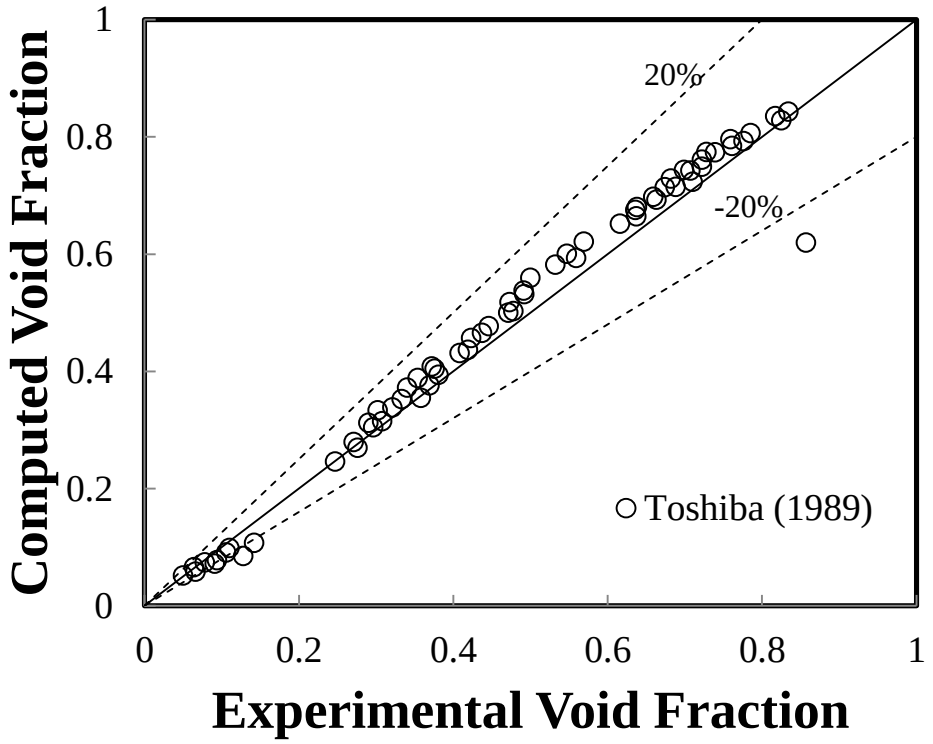

Figure 4.29: Comparison between Experimental Data and Toshiba (1989) for Vertical Flow

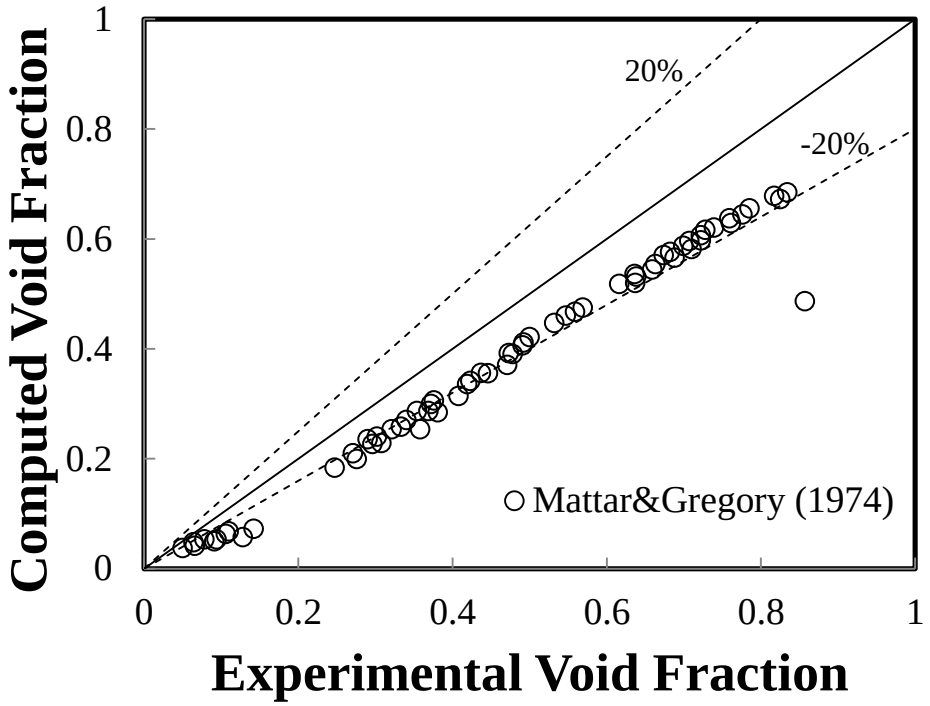

Figure 4.30: Comparison between Experimental Data and Mattar&Gregory (1974) for Vertical Flow

Figure 4.31-4.36 shows a scatter between the existing correlations and the proposed models, yet the proposed model was quite in agreement with the experimental data as compared to the existing correlations. Bestion's correlation was next in agreement, followed by Zuber and Findlay's correlations which agreed well with the dataset at a void fraction of 0.65-0.8. Toshiba's model showed a massive scatter with an error deviation of $\pm$ 20 %. In this case, Mattar and Gregory, as well as Choi's model under predicted the experimental data.

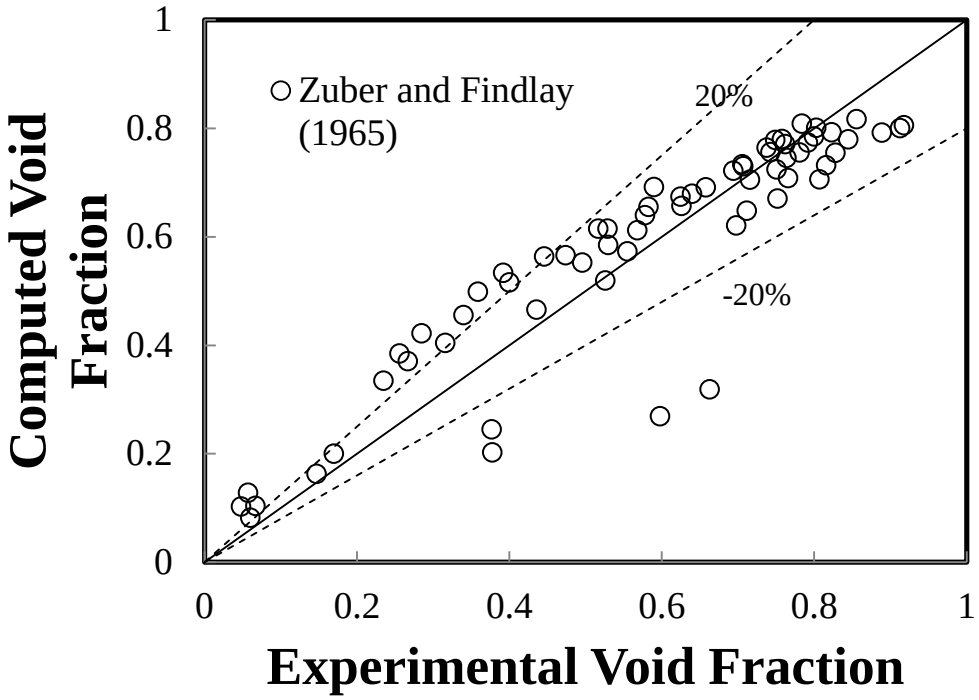

Figure 4.31: Comparison between Experimental Data and Zuber & Findlay (1965) for Horizontal Flow

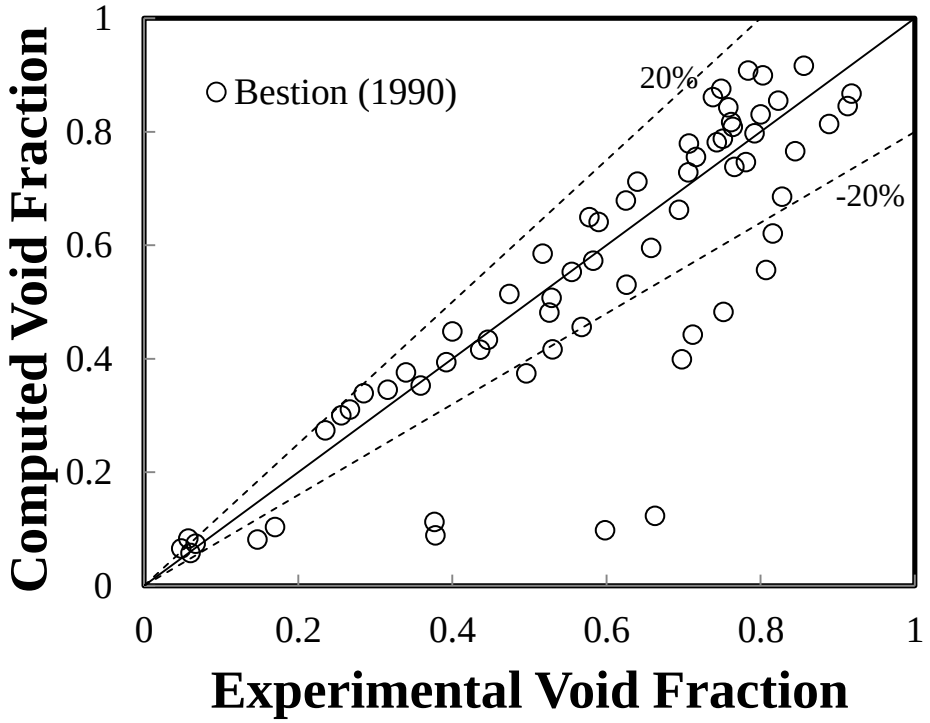

Figure 4.32: Comparison between Experimental Data and Bestion (1990) for Horizontal Flow

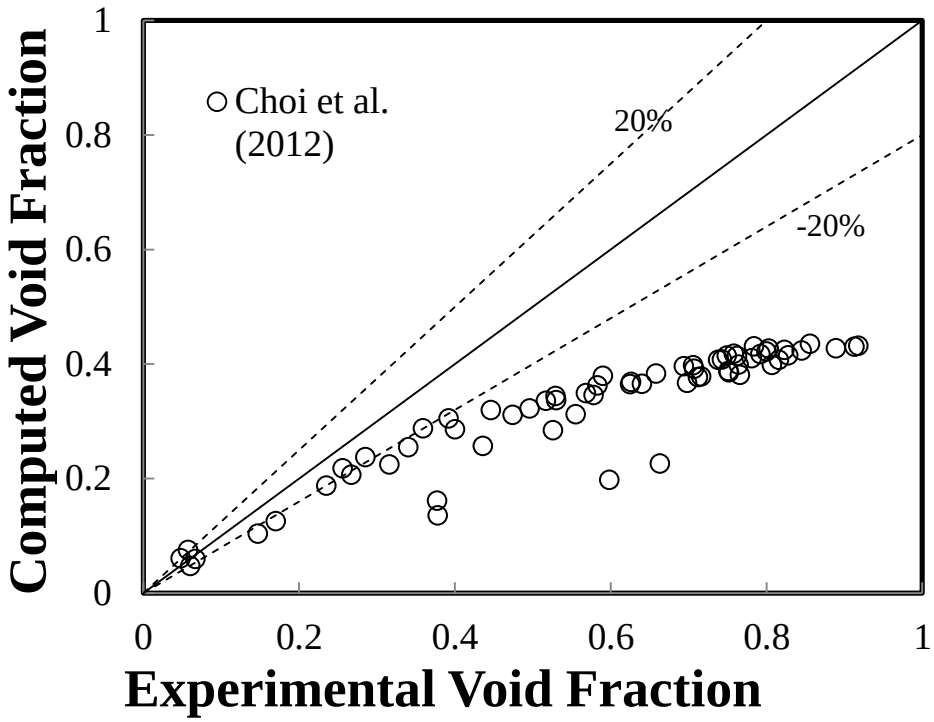

Figure 4.33: Comparison between Experimental Data and Choi (2012) for Horizontal Flow

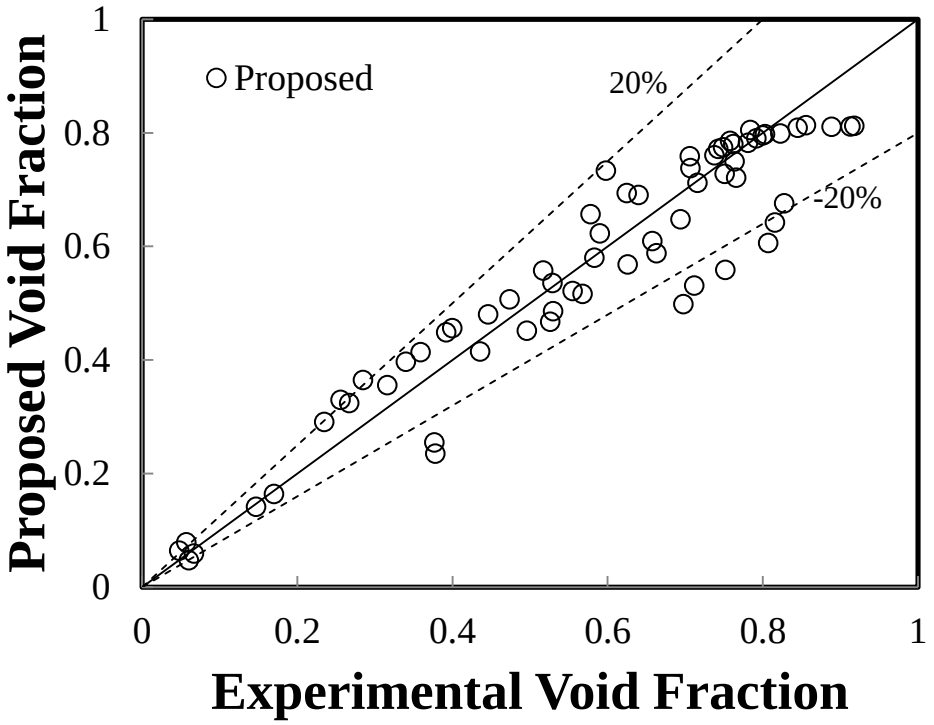

Figure 4.34: Comparison between Experimental Data and Proposed Model for Horizontal Flow

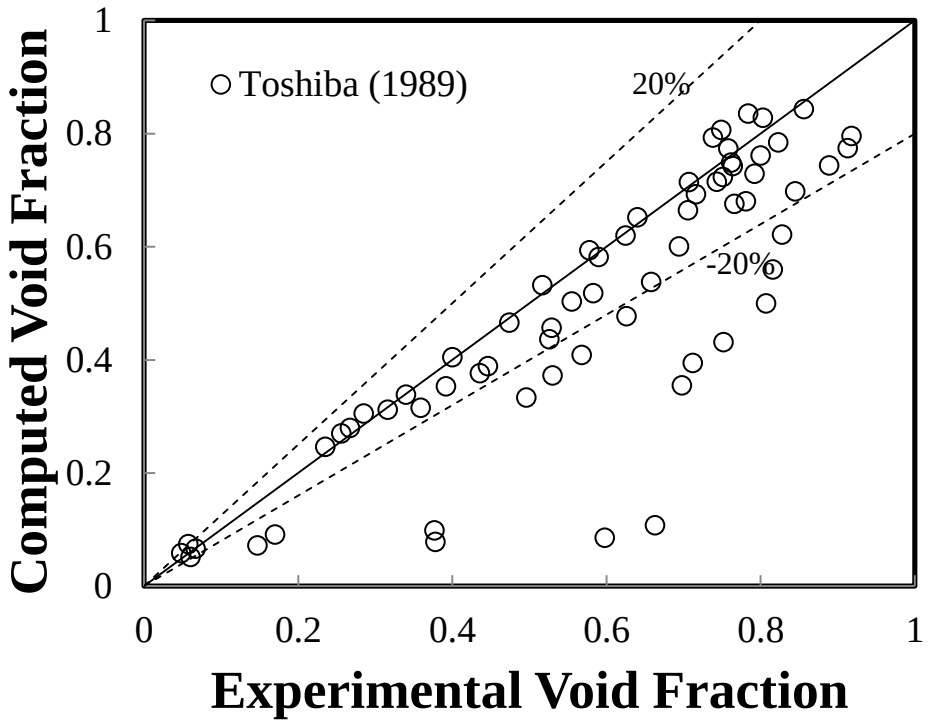

Figure 4.35: Comparison between Experimental Data and Toshiba (1989) for Horizontal Flow

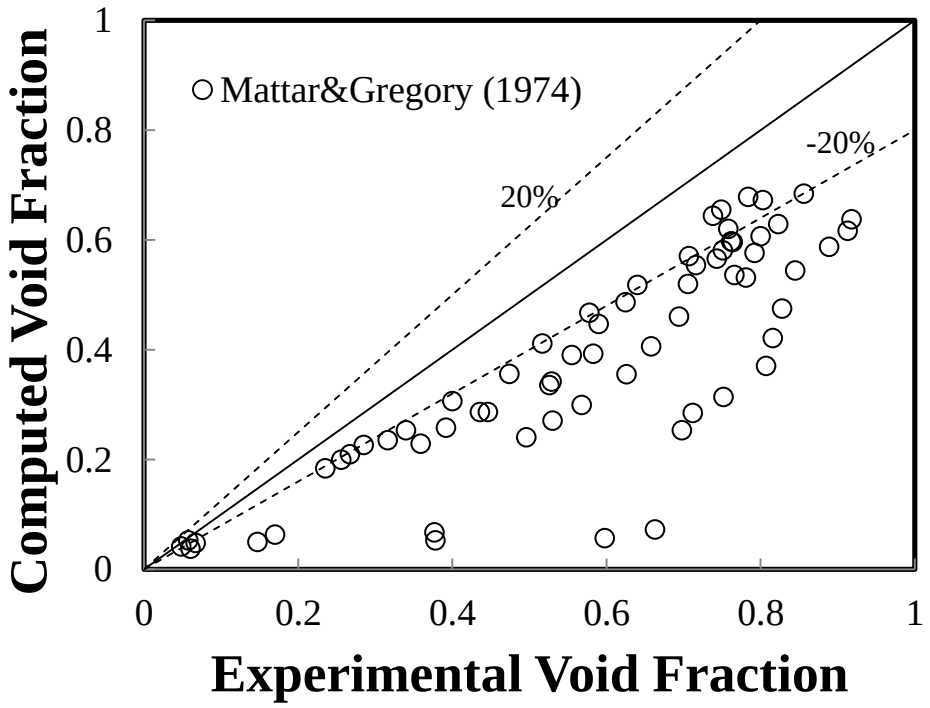

Figure 4.36: Comparison between Experimental Data and Mattar and Gregory (1974) for Horizontal Flow

CHAPTER 5

CONCLUSIONS AND RECOMMENDATIONS

5.1 Conclusions

Based on this study, the following conclusions were made:

- The void fraction of a multiphase system increases with an increase in gas superficial velocity and reduces with an increase in liquid superficial velocity.
- It was also established that void fraction reduces with the increasing inclination angle of the pipe.
- The general trend of radial phase distribution for the vertical and horizontal pipes indicate a higher void fraction at the center of the pipe and a lowest void fraction at the walls of the pipe.
- Comparison of the existing correlations based on the RMSE suggested that the best correlations include: Hassan and Kabir (1988), Nicklin et al. (1962), and Kokal and Stanislav (1989) correlations all having 18 % and 6 % for the vertical and horizontal pipes respectively, based on the dataset investigated.
- For the dataset considered, Shoham's flow pattern map suggested two regimes namely: bubbly and slug flow for the vertical pipe and three flow regimes namely: smooth stratified flow, wavy flow, and slug flow for the horizontal pipe.
- The driftflux model of different flow pattern possesses unique correlation coefficient which represents the fingerprint of each flow regime.
- The distribution parameters obtained for the drift flux model were 1.5475, 1.1823 and 1.0938 for the cap bubble, slug and churn flows respectively, whereas the drift velocity obtained were 0.2584, 0.4561 and 0.5201 for cap bubble, slug, and churn respectively.
- It was also observed that the distribution parameter (Co) which accounts for the non-uniformity decreases with increasing void fraction.
- The model generated performed better in comparison to existing models with an RMSE of 3 and 15 % for vertical and horizontal pipes respectively
- .

5.2 Recommendations

- Since the accurate identification of flow regimes is important to the oil, chemical and nuclear industries, the drift-flux model needs to be further assessed for downward and other inclinations.
- To mimic what exists in real life, much heavier fluids of higher viscosities should also be considered.

NOMENCLATURE

+A = Pipe Cross Sectional Area

C_o = Distribution Parameter

D = Pipe Internal Diameter

g = Gravitational Acceleration

Q = Volumetric Flow Rate

Re = Reynolds Number

V_d = Drift Velocity of Gas

V_G = Actual Gas Velocity

V_L = Actual Liquid Velocity

V_{SG} = Superficial Gas Velocity

V_{SL} = Superficial Liquid Velocity

V_M = Volumetric Flux of the Mixture

H_L = Liquid Holdup

α/ε = Void Fraction

ρ_f = Liquid Density

ρ_g = Gas Density

σ = Interfacial Tension/Surface Tension

$\boldsymbol{\mu}_L$ = Liquid viscosity

$\boldsymbol{\mu}_G$ = Gas Viscosity

D_h = Hydraulic diameter

Le = Effective Length

RMSE = Root Mean Square Error

RMS = Root Mean Square

Subscription

G = Gas phase

L = Liquid phase

* = Dimensionless

REFERENCES

1. Abdulkadir, M. Hernandez-Perez, V., Sharaf, S., Lowndes, I. S. and Azzopardi, B. J. (2010), "Experimental Investigation of Phase Distributions of Two-phase Air-silicone Oil Flow in a Vertical Pipe", World Academy of Science, Engineering and Technology, International Journal of Chemical, Molecular, Nuclear, Materials and Metallurgical Engineering Vol:4, No:1.
2. Abdulkadir, M., (2011), "Experimental and computational fluid dynamics (CFD) studies of gas-liquid flow in bends", PhD thesis, University of Nottingham, UK.
3. Abdulkadir, M., Hernandez-Perez, V., Sharaf, S., Lowndes, I. S. and Azzopardi, B. J. (2015), "Phase Distribution of an Air-Silicone Oil Mixture in a Vertical Riser", 7th International Conference on Heat Transfer, Fluid Mechanics and Thermodynamics, 19-21 July 2010, Antalya, Turkey.
4. Abdulkadir, M., (2015), "Multiphase Flow in Pipes", Lecture notes, African University of Science and Technology, Nigeria.
5. Abolore, A. (2014), "Investigating the effect of liquid viscosity on two-phase gas-liquid flows", Ph.D. thesis, University of Nottingham.
6. Agrawal, A. (2010), "Two-Phase Flow Patterns and Flow Maps", Indo –German Winter Academy, Indian Institute of Technology, Delhi.
7. Anon, (2016), "Oil and Gas Flow Assurance", Institute for Energy Technology, Date Accessed: 29/02/16.
8. Arthur, F. G., Nakayama, A. E., Cozin, C., Barbuto, F. A. A. and Morales, R. E. M., (2013), "Slug to Churn Transition Analysis In Upward Vertical Two-Phase Flow", Proceedings of ENCIT, 14th Brazilian Congress of Thermal Sciences and Engineering.
9. Azzopardi, B.J., (2015), "Chemical Engineering and Chemical Process Technology", Vol. I - Multiphase Flow.
10. Bhagwat, S. M. (2011), "Study of Flow Patterns and Void Fraction in Vertical Downward Two-Phase Flow", MSc thesis, Oklahoma State University, USA.
11. Bulk, F. P. (2012), "An Experimental Study on Cross-Flow Mixing in a Rod-Bundle Geometry using a Wire-Mesh", MSc thesis, Delft University of Technology, Netherlands.
12. Cheng, L. and Mewes, D. (2012), "Advances in Multiphase Flow and Heat Transfer", Volume 3, pp. 159-160.

13. Choi, J., Pereyra, E., Sarica, C., Park, C. and Kang, J. M., (2012), "An Efficient Drift-Flux Closure Relationship to Estimate Liquid Holdups of Gas-Liquid Two-Phase Flow in Pipes", *Energies* 2012, *5*, 5294-5306; doi:10.3390/en5125294, ISSN 1996-1073, www.mdpi.com/journal/energies.
14. Da Silva, J., Hampel, M., Arruda, U., L. V. R. and Morales, R. E. M. (2011), "Experimental Investigation of Horizontal Gas-Liquid Slug Flow by Means of Wire-Mesh Sensor", Special Issue 2011, Vol. XXXIII / 237.
15. Garaev, D. (2012), "Multiphase flow in large diameter pipes", MSc thesis, University of Nottingham, UK.
16. Ghajar, A. J. and Tang, C. C. (2010), "Void Fraction and Flow Patterns of Two-Phase Gas-Liquid Flow in Various Pipe Inclinations", 7th International Conference on Heat Transfer, Fluid Mechanics and Thermodynamics, Antalya, Turkey.
17. Ghiaasiaan, S. M. (2008), "Two-Phase Flow, Boiling and Condensation in Conventional and Miniature Systems".
18. Grace, J. R., Knowlton, T. M. and Avidan, A. A. (2012), "Circulating Fluidized Beds".
19. Hasan, A.R., Kabir, C.S. and Sayarpour, M., (2010), "Simplified two-phase flow modeling in wellbores", Journal of Petroleum Science and Engineering, 72(1–2):42 – 49, ISSN 0920-4105. doi: http://dx.doi.org/10.1016/j.petrol.2010.02.007. URL http://www.sciencedirect.com/science/article/pii/S0920410510000458.
20. Hernández-Pérez, V., Abdulkareem, L. A. and Azzopardi, B. J. (2009), "Effects of physical properties on the behaviour of Taylor bubbles", Computational Methods in Multiphase Flow, Vol. 355.
21. Hewitt, G. F. and Jayanti, S. (1993), "To Churn or Not To Churn", Int. J. Multiphase Flow Vol. 19, No. 3, pp. 527-529.
22. Hibiki, T. and Mishima, K. (2001), "Flow regime transition criteria for upward two-phase flow in vertical narrow rectangular channels", Nuclear Engineering and Design 203 (2001) 117–131.
23. Hibiki T. and Ishii, M., (2002), "Distribution Parameter and Drift Velocity of Drift-Flux Model in Bubbly Flow", International Journal of Heat and Mass Transfer, 45(4):707 – 721, 2002. ISSN 0017-9310, doi:http://dx.doi.org/10.1016/S001793-10(01)00195-8, URLhttp://www.sciencedirect.com/science/article/pii/S001793-1001001958.

24. Hong, S., Kim, J., Song, J. H. and Hong, S. (2005), “A Preliminary Design of a Wire Mesh Sensor for Measuring a Void Fraction”, Transactions of the Korean Nuclear Society Autumn Meeting Busan, Korea.
25. Ishii, M., (1977), “One-dimensional Drift–Flux Model and Constitutive Equations for Relative Motion between Phases in Various Two-Phase Flow Regimes”.
26. Inkum, H. (2014), “Analysis of Void Fraction Phase Distribution of Gas-Liquid Flow In A Horizontal Pipe Using Wire Mesh Sensor Data”, MSc thesis, African University of Science and Technology, Nigeria.
27. Kumar, R. (2010), “Two Phase Flow Patterns and Flow Maps”, Lecture notes, Indian Institute of Technology, Delhi.
28. Lemoine, R. O. (2005), “Hydrodynamics Mass Transfer and Modelling of the Toluene Oxidation Process”, Ph.D. thesis, University of Pittsburgh.
29. Malekzadeh, R. (2012), “Severe Slugging in gas-liquid two-phase pipe flow”, Msc thesis, Geboren te Ghaemshahr, Iran.
30. Matsubara, H., and Naito, K. (2011) “Effect of liquid viscosity on flow patterns of gas–liquid two-phase flow in a horizontal pipe”, International Journal of Multiphase Flow 37 (2011) 1277–1281.
31. Mao, Z. S. and Dukler, A. E. (1992), “The Myth of Churn Flow?”, Int. J. Multiphase Flow Vol. 19, No. 2, pp. 377-383.
32. Marco Jose da Silva, M.S.E.E. (2008), “Impedance Sensors for Fast Multiphase Flow Measurement and Imaging”, Ph.D. thesis, Dresden University of Technology, Germany.
33. McCready, M. J., (1998), “Demonstration of the effect of flow regime on pressure drop”, Lecture notes, the University of Notre Dame, IN 46556 USA.
34. McQuillan, K.W., and Whalley, P.B., (1985), “Flow patterns in vertical two-phase flow”, International Journal of Multiphase Flow 11, 161-175.
35. Mishima, K. and Ishii, M. (1985), “Flow Regime Transition Criteria for Upward Two-Phase Flow in Vertical Tubes”, Int. J. Multiphase Flow, Vol. 27. No. 5, pp. 123-731.
36. Murai, Y., Oiwa, H., Sasaki, T., Kondou, K., Yoshikawa, S. and Yamamoto F., (2005), “Backlight Imaging Tomography for Gas–Liquid Two-Phase Flow in a Helically Coiled Tube”, Institute of Physics Publishing, Meas. Sci. Technol. 16 (2005) 1459–1468 doi:10.1088/0957-0233/16/7/008.

37. Oteng, B. (2014), “Effect of Pipe Inclination Angle on Gas–Liquid Flow Using Electrical Capacitance Tomography (Ect) Data”, MSc thesis, African University of Science and Technology, Nigeria.
38. Pieter, V. G., (2012), “Churn-annular gas-liquid flows in large diameter vertical pipes”, Ph.D. thesis, University of Nottingham.
39. Pompilio, R., (2013), “Experimental analysis of air-water two-phase flow in vertical large pipes and development of drift-flux models”, MSc. thesis, Polytechnic University of Milan, Italy.
40. Schlegel, J., Hibiki, T. and Ishii, M., (2010), “Development of a Comprehensive Set of Drift-Flux Constitutive Models for Pipes of Various Hydraulic Diameters”, Progress in Nuclear Energy, 52(7):666 – 677, 2010. ISSN 01491970. doi:http://dx.doi.org/10.1016/j.pnucene.2010.03.007. URL http://www.sciencedirect.com/science/article/pii/S0149197010000600.
41. Shaikh, A. and Al-Dahhan, M. H. (2007), “A Review on Flow Regime Transition in Bubble Columns” International Journal Of Chemical Reactor Engineering, Vol. 5.
42. Sharaf, S. (2012), “Testing and application of wire mesh sensors in vertical gas liquid two-phase flow”, Ph.D. thesis, University of Nottingham, UK.
43. Sharaf, S., Van der Meulen, P., Agunjika, E. O. and Azzopardi, B.J. (2015), “Structures in Gas-Liquid Churn Flow in a Large Diameter Vertical Pipe”, International Journal of Multiphase Flow 78 (2016) 88-103.
44. Shen, X., Schlegel, J. P., Chen, S., Rassame, S., Griffiths, M. J., Hibiki, T. and Ishii, M. (2014), “Flow Characteristics and Void Fraction Prediction in Large Diameter Pipes”, L. Cheng (ed.), Frontiers and Progress in Multiphase Flow I, Frontiers and Progress in Multiphase Flow, DOI: 10.1007/978-3-319-04358-6_2, Springer International Publishing Switzerland.
45. Tengesdal, J.Ø., Kaya, A.S., and Sarica C. (1998), “A New Unified Model for Slug-Churn transition Based on Drift Flux Approach”, The University of Tulsa, SPE 50000.
46. Thome, J. R., (2010), “Engineering Data Book III”, Copyright 2004-2010 by Wolverine Tube, Inc.
47. Tzotzi, C., Bontozoglou, V. and Andritsos, N. (2011), “Effect of Fluid Properties on Flow Patterns in Two-Phase Gas-Liquid Flow in Horizontal and Downward Pipes”, Ind. Eng. Chem. Res., Vol. 50, No. 2.

48. Weerin, W., Yuichi, M., Steffen, R., Hiroshige, K., Masanori A. and Kazuhiko Y. (2003), "Intrusive Effect of Wire Mesh Tomography on Gas-liquid Flow Measurement", Journal of Nuclear Science and Technology, 40:11, 932-940.
49. Yuguang, C. (2001), "Modelling Gas-Liquid Flow in Pipes: Flow Pattern Transitions and Drift-Flux Modeling", MSc thesis, Stanford University.
50. Zhu, W., (2003), "An Investigation of Two-Phase Flow Regime Transition in Large Diameter Pipes", MSc thesis, McMaster University.

APPENDIX

Appendix A Comparison between experimental gas velocity and Proposed Model

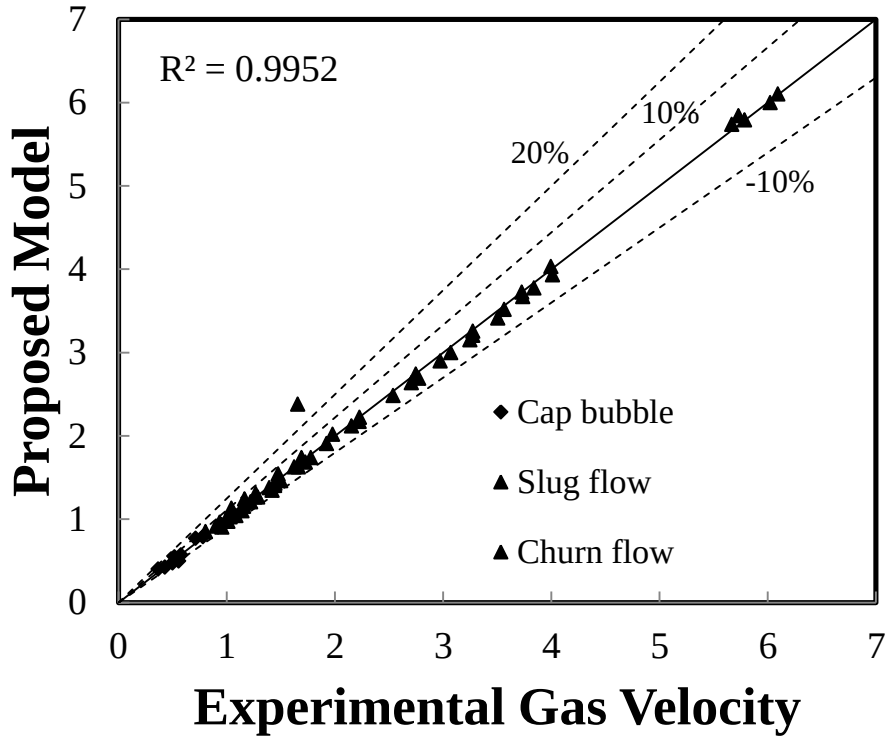

Figure A 1: A Graph of Predicted Gas Velocity Verse Experimental Velocity for Vertical Pipe

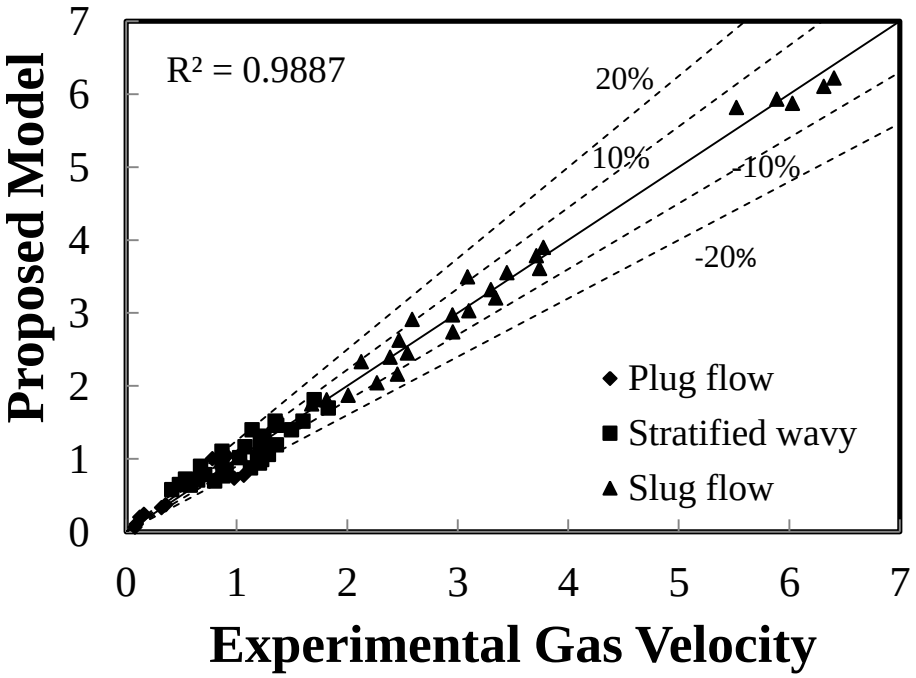

Figure A 2: A Graph of Predicted Gas Velocity Verse Experimental Velocity for Horizontal Pipe

Appendix B Comparison between experimental void fraction and proposed model

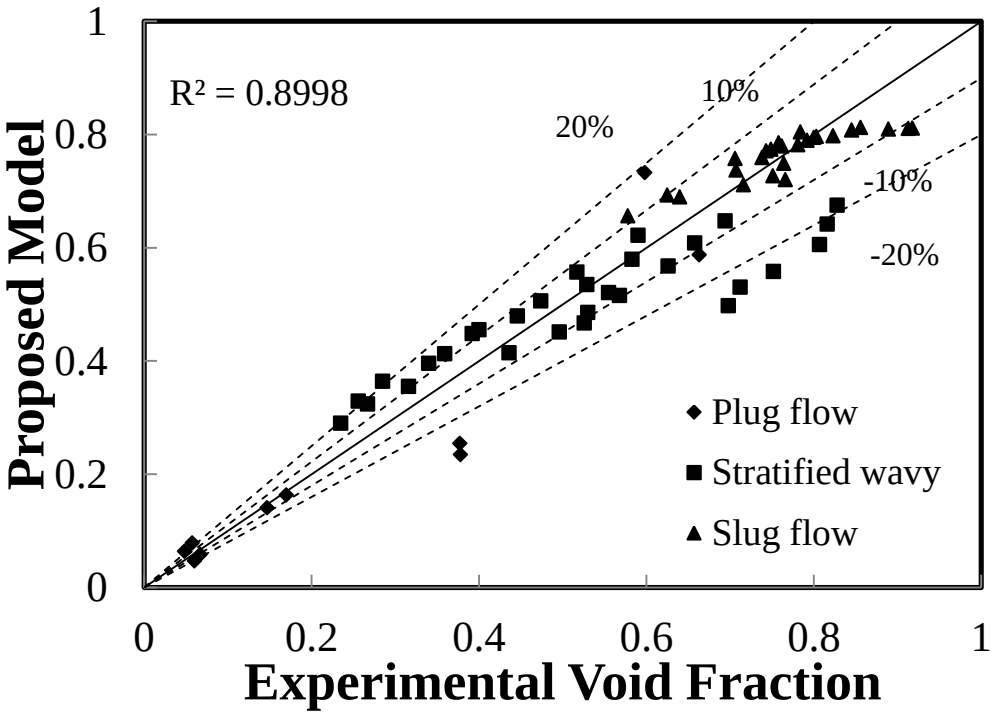

Figure B 1: A Graph of Predicted Gas Void Fraction Verse Experimental Void Fraction for Horizontal Pipe

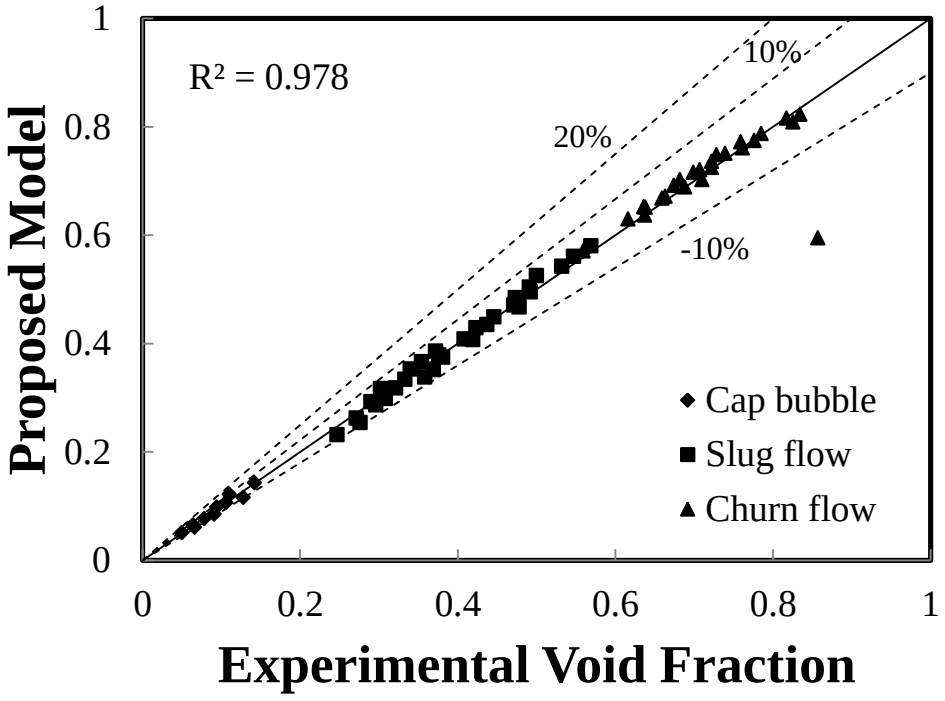

Figure B 2: A Graph of Predicted Void Fraction Verse Experimental Void Fraction for Vertical Pipe

Appendix C Comparison between experimental void fraction and Computed void fraction

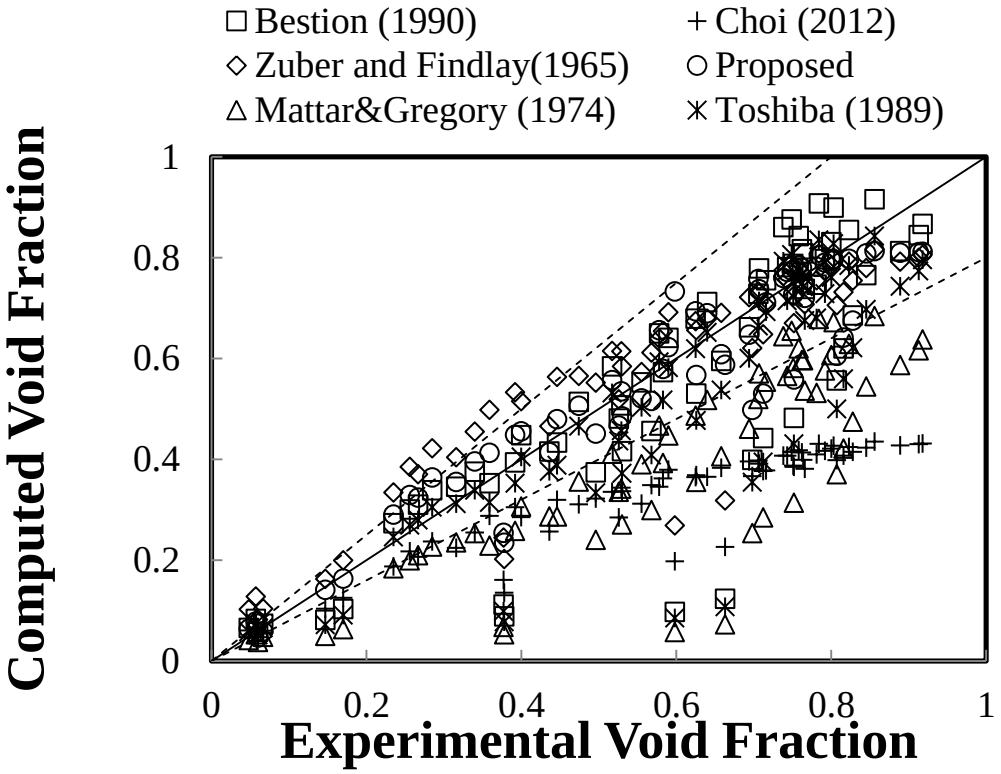

Figure C 1: Experimental Data against Computed Void Fraction for Horizontal Pipe

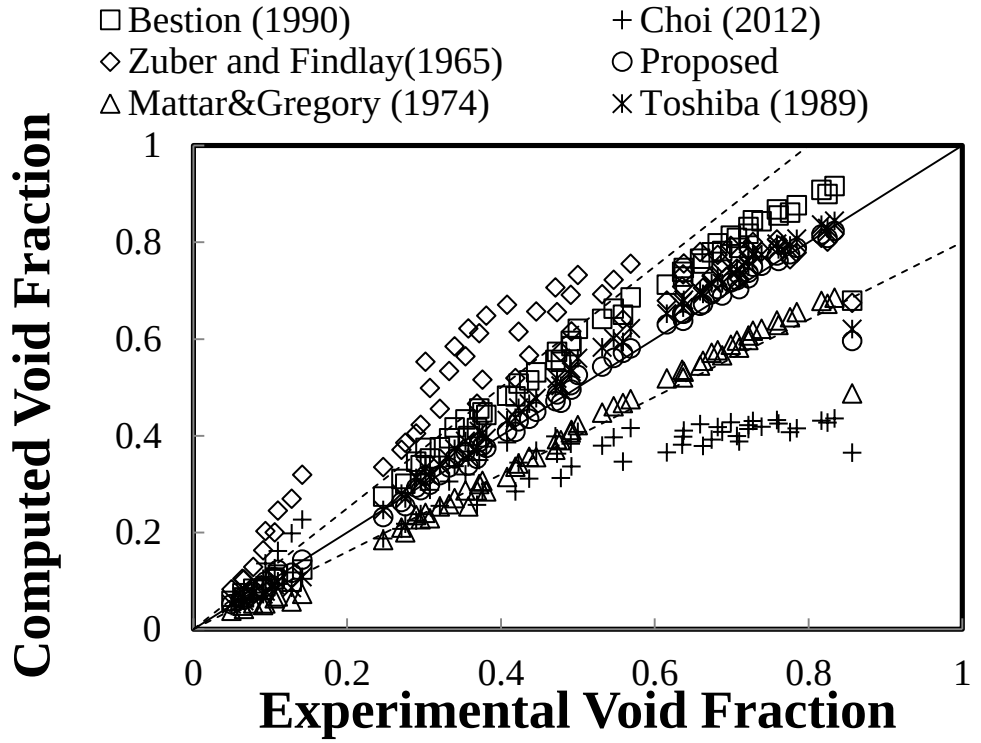

Figure C 2: Experimental Data against Computed Void Fraction for Vertical Pipe